Two-Higgs-doublet-plus-pseudoscalar model: Collider, dark matter, and gravitational wave signals

Giorgio Arcadi,[1] Nico Benincasa[,2] Abdelhak Djouadi[,2,3] and Kristjan Kannike[2]

[1]*Dipartimento di Scienze Matematiche e Informatiche, Scienze Fisiche e Scienze della Terra,
Universita degli Studi di Messina, Via Ferdinando Stagno d'Alcontres 31, I-98166 Messina, Italy*
[2]*NICPB, Rävala puiestee 10, 10143 Tallinn, Estonia*
[3]*CAFPE and Departamento de Fisica Teórica y del Cosmos, Universidad de Granada,
E-18071 Granada, Spain*

We perform a comprehensive study of a model in which the Higgs sector is extended to contain two Higgs doublet fields, with the four types of possibilities to couple to standard fermions, as well as an additional light pseudoscalar Higgs boson which mixes with the one of the two doublets. This two-Higgs-doublet-plus-pseudoscalar model includes also a stable isosinglet massive fermion that has the correct thermal relic abundance to account for the dark matter in the Universe. We summarize the theoretical constraints to which the model is subject and then perform a detailed study of the phenomenological constraints. In particular, we discuss the bounds from the LHC in the search for light and heavy scalar resonances and invisible states and those from high-precision measurements in the Higgs, electroweak, and flavor sectors, addressing the possibility of explaining the deviation from the standard expectation of the anomalous magnetic moment of the muon and the W-boson mass recently observed at Fermilab. We also summarize the astrophysical constraints from direct and indirect detection dark matter experiments. We finally conduct a thorough analysis of the cosmic phase transitions and the gravitational wave spectrum that are implied by the model and identify the parameter space in which the electroweak vacuum is reached after single and multiple phase transitions. We then discuss the prospects for observing the signal of such gravitational waves in near-future experiments such as the Laser Interferometer Space Antenna, Big Bang Observer, or Deci-hertz Interferometer Gravitational wave Observatory.

DOI: 10.1103/PhysRevD.108.055010

I. INTRODUCTION

The discovery of a new type of particle at the LHC a decade ago, the scalar Higgs boson with a mass of 125 GeV [1,2], has completed the spectrum of the Standard Model (SM) of particle physics and established it as a correct description of three of nature's fundamental interactions at present energies [3]. It opened and even encouraged the possibility that additional Higgs particles may also exist. Such extensions of the SM Higgs sector, with its unique doublet of complex scalar fields to spontaneously break the electroweak symmetry [4], are, in fact, predicted in a plethora of new physics extensions. This is particularly the case of supersymmetric theories in which the most economical version, the minimal supersymmetric SM (MSSM) [5], requires the existence of two Higgs doublet fields that lead to five Higgs states in the particle spectrum: two CP-even h and H, a CP-odd or pseudoscalar A, and two charged $H^{\pm}$ states [6,7]. But, in fact, two-Higgs-doublet models (2HDM), independently of supersymmetry, have been intensively discussed in the literature and their phenomenology studied in great detail; see, e.g., Ref. [8] for a comprehensive review. Other extensions have also been considered in which the Higgs sector involves additional scalar multiplets, from singlet to several doublets, to triplet Higgs fields [6].

The original motivation of the extension of the SM Higgs sector to include two doublets of complex scalar fields and a singlet pseudoscalar field was to alleviate the strong constraints on the particle physics candidates for dark matter (DM) [9–11] that is expected to form about 25% of the energy budget of the Universe [12]. Indeed, this model [13–18] offers the possibility to induce a direct coupling of the singlet pseudoscalar state to an isosinglet fermionic DM particle, as well as a coupling between this singlet and the SM fermions, via the mixing of the new pseudoscalar a with the pseudoscalar state of the two-Higgs-doublet model. This allows for an efficient annihilation of

the DM state into pairs of fermions in order for it to have the correct cosmological relic density. At the same time, the absence of couplings between the DM state and the two CP-even Higgs bosons of the model, including the SM-like one, forbids tree-level spin-independent interactions for the DM, allowing it to evade the stringent constraints from direct detection in astroparticle physics experiments.

The model with two Higgs doublets and a pseudoscalar a field, that we call here the $2HD + a$ model (also known as 2HDMa in the literature), has a very rich phenomenology. In particular, the presence of a possibly light a boson has far-reaching consequences. First, as it should substantially couple to SM fermions in order to generate the correct DM relic density, it could be produced and detected in collider experiments. In particular, searches for such a state have been performed at the Large Hadron Collider (LHC) and even earlier, and some constraints have been set on its mass and couplings; see, for instance, Refs. [19,20]. On the other hand, a light a state could address and resolve some anomalies that have been observed in recent experimental data, in particular, the significant discrepancy from the standard expectation of the anomalous magnetic moment of the muon recently measured at Fermilab [21]. Indeed, for a range of masses and couplings of the new light pseudoscalar and the fermionic states, it has been shown that the DM problem and the Fermilab value of the $(g - 2)_\mu$ could be simultaneously explained while satisfying all other constraints from astroparticle physics and collider searches, including the constraints from flavor physics [22]. Furthermore, another recent puzzling feature could also be simply addressed in the context of this $2HD + a$ model [23]: the large deviation from the SM of the W boson mass recently observed by the CDF experiment at the Tevatron [24]. Hence, the scenario has multiple advantages, addresses several issues, and is, thus, a good option for physics beyond the SM.

The model requires further scrutiny, and, in particular, one should simultaneously apply and update all the constraints to which it is subject. This is the case of the ones that apply on the heavy 2HDM and the possibly light pseudoscalar a bosons from the LHC searches, especially now that the ATLAS and CMS experiments have recently released their updated results with the full dataset collected at an energy of 13 TeV [25,26]. This is the first purpose of the present paper, to perform a comprehensive analysis of all the possible constraints on the $2HD + a$ model, from the high-precision measurements of the electroweak observables including the W-boson mass and of the couplings of the SM-like Higgs boson at the LHC, the constraints from flavor physics, in particular, the muon $(g - 2)$ and B-meson sector observables, and those from the search for the heavy and the possibly light Higgs bosons in the various channels to which they lead at the LHC and other colliders. We will also confront these constraints with the updated ones that come from astroparticle physics

searches, in particular, the very recent results from the LZ direct detection experiment [27].

We will show that, depending on the configuration or type of the couplings of the 2HDM states to the SM fermions, the so-called type I, II, X, and Y scenarios that allow for the absence of flavor-changing neutral currents at tree level, the various constraints can be either very strong as is, for instance, the case of the type II scenario which occurs in supersymmetric models and in which one doublet field couples to isospin down-type quarks and leptons and the other to up-type quarks, or rather weak, as is the case in the type I scenario, when both the Higgs doublets couple to isospin up-type and down-type quarks and charged leptons. For each type of scenario, including the X and Y configurations, we will delineate the parameter space of the $2HD + a$ scenario that is still allowed by collider and astrophysical data and, eventually, the one in which the $(g - 2)_\mu$ and the M_W anomalies could be resolved.

Another aspect, which has not been discussed before and that we address in this paper in a comprehensive manner, is the one connected to the cosmological phase transitions related to the dynamics of electroweak symmetry breaking and its link to gravitational waves (GWs) [28]. Given the properties of its extended Higgs sector, the $2HD + a$ model can easily admit first-order phase transitions resulting in a stochastic GW background, contrary to the SM, which predicts a phase transition that is a smooth crossover [29] and does not generate observable GW signals. Following a recent analysis for a pure 2HDM [30], we perform a random scan over the $2HD + a$ parameter space and determine the phase transition pattern in the plane formed by the two CP-even Higgs states. We show that a certain number of points, which incidentally also address the new measurement of the W-boson mass at the Tevatron, yields a GW signal that could be within the reach of future space-based GW observatories such as the Laser Interferometer Space Antenna (LISA) [31], Big Bang Observer (BBO) [32], Taiji [33], TianQuin [34], or Deci-hertz Interferometer Gravitational wave Observatory (DECIGO) [35].

The rest of the paper is organized as follows. In the next section, we will introduce the $2HD + a$ model, including the DM aspect, and briefly summarize the theoretical constraints to which it is subject. In Sec. III, we discuss the various phenomenological and experimental constraints from collider experiments, in particular, the ones from the high-precision measurements in the electroweak, B-meson, muon, and Higgs sectors and the ones from direct searches of additional Higgs bosons at the LHC and elsewhere as well as invisible states. We then present in Sec. IV the salient features which make the model, when it incorporates a fermionic stable particle, lead to the correct relic density while passing the bounds from direct and indirect detection experiments and combine all these constraints with the collider bounds. Section V will be devoted to the discussion of the cosmic phase transitions and the gravitational wave

spectrum, as well as the prospects for observing the signal of such waves in future experiments. A short conclusion is given in Sec. VI.

II. THEORETICAL ASPECTS OF THE 2HDMa

In this section, we present the 2HD + a model enlarged with a fermionic dark matter candidate and its salient theoretical features. We first introduce our constrained two-Higgs-doublet model with the four allowed types of couplings to standard fermions. We then discuss the consequences of including a possibly light pseudoscalar Higgs field. The theoretical constraints on the model, mainly from the perturbativity of the scalar quartic couplings and the stability of the electroweak vacuum, are then summarized.

A. The two-Higgs-doublet model

In a 2HDM, the scalar sector consists of two doublets of complex scalar fields Φ_1 and Φ_2 which, when invariance under CP symmetry is assumed, can be described by the following scalar potential [8]:

$$
\begin{aligned}
V_{2\mathrm{HDM}} &= m_{11}^2 \Phi_1^\dagger \Phi_1 + m_{22}^2 \Phi_2^\dagger \Phi_2 - m_{12}^2 (\Phi_1^\dagger \Phi_2 + \mathrm{H.c.}) \\
&\quad + \frac{1}{2} \lambda_1 (\Phi_1^\dagger \Phi_1)^2 + \frac{1}{2} \lambda_2 (\Phi_2^\dagger \Phi_2)^2 \\
&\quad + \lambda_3 (\Phi_1^\dagger \Phi_1)(\Phi_2^\dagger \Phi_2) + \lambda_4 (\Phi_1^\dagger \Phi_2)(\Phi_2^\dagger \Phi_1) \\
&\quad + \frac{1}{2} \lambda_5 [(\Phi_1^\dagger \Phi_2)^2 + \mathrm{H.c.}].
\end{aligned} \tag{1}
$$

From the very beginning, we assume the presence of a discrete symmetry[1] [36] which forbids the introduction of two additional couplings[2] λ_6 and λ_7. Electroweak symmetry breaking is achieved when the fields Φ_1 and Φ_2 acquire the vacuum expectation values (VEVs) v_1 and v_2, respectively. These VEVs have to satisfy the relation $\sqrt{v_1^2 + v_2^2} = v$, with $v \simeq 246$ GeV being the standard one, and their ratio defines the very important parameter $\tan\beta = v_2/v_1$. After symmetry breaking, one obtains five physical states in the spectrum: two CP-even h and H bosons, a CP-odd A^0, and two charged Higgs bosons $H^\pm$.

In addition to the four Higgs boson masses M_h, M_H, M_{A^0}, and $M_{H^\pm}$ and the angle β defined above, at least another input parameter is needed to entirely characterize the model: the angle α which describes the mixing between the two CP-even h, H bosons. The h state will be identified

---

[1]The fields transform under the discrete symmetry as $\phi_1 \to \phi_1$ and $\phi_2 \to -\phi_2$; note, however, that we have allowed for the operator $\phi_1^\dagger \phi_2 + \mathrm{H.c.}$, which softly breaks this symmetry.

[2]CP violation in a 2HDM would impact the dynamics of the phase transitions to be discussed later only very weakly [37]; it will be ignored here, as we need to distinguish between scalar and pseudoscalar states.

---

by convention to be the scalar particle with a 125 GeV mass observed at the LHC, and the H boson will be considered to be heavier, $M_H > M_h$ (we ignore the unlikely reverse possibility discussed, e.g., in Refs. [38,39]). The five quartic couplings λ_i of the scalar potential above can be more conveniently expressed in terms of the physical state masses and the angles α and β introduced above. The five couplings would read

$$
\begin{aligned}
\lambda_1 v^2 &= -M^2 \tan^2\beta + \frac{\sin^2\alpha}{\cos^2\beta} M_h^2 + \frac{\cos^2\alpha}{\cos^2\beta} M_H^2, \\
\lambda_2 v^2 &= -\frac{M^2}{\tan^2\beta} + \frac{\cos^2\alpha}{\sin^2\beta} M_h^2 + \frac{\sin^2\alpha}{\sin^2\beta} M_H^2, \\
\lambda_3 v^2 &= -M^2 + 2M_{H^\pm}^2 + \frac{\sin 2\alpha}{\sin 2\beta}(M_H^2 - M_h^2), \\
\lambda_4 v^2 &= M^2 + M_{A^0}^2 - 2M_{H^\pm}^2, \qquad \lambda_5 v^2 = M^2 - M_{A^0}^2, \tag{2}
\end{aligned}
$$

when using the abbreviation (with M being possibly positive or negative)

$$
M^2 \equiv m_{12}^2 / (\sin\beta \cos\beta). \tag{3}
$$

The additional parameter m_{12} will enter only in the trilinear and quartic couplings among the physical Higgs states, and, as we will see shortly, it can be ignored in most of the present discussion together with the mass parameters m_{11} and m_{22}.

The mixing between the neutral CP-even Higgs bosons of the model makes h and H share the coupling of the standard Higgs particle H^0 to the massive gauge bosons $V = W, Z$:

$$
\begin{aligned}
g_{hVV} &= g_{hVV}^{2\mathrm{HDM}} / g_{H^0 VV}^{\mathrm{SM}} = \sin(\beta - \alpha), \\
g_{HVV} &= g_{HVV}^{2\mathrm{HDM}} / g_{H^0 VV}^{\mathrm{SM}} = \cos(\beta - \alpha). \tag{4}
\end{aligned}
$$

As a result of CP invariance, there is no coupling of the CP-odd A^0 state to the massive W, Z bosons, $g_{A^0 VV} = 0$. The couplings between two Higgs bosons and a massive vector boson V are complementary to the previous ones. Up to normalization factors, one has, for instance,

$$
\begin{aligned}
g_{hA^0 Z} &= g_{hH^\pm W} = \cos(\beta - \alpha), \\
g_{HA^0 Z} &= g_{HH^\pm W} = \sin(\beta - \alpha). \tag{5}
\end{aligned}
$$

There are also couplings of the charged Higgs boson to gauge bosons which simply read

$$
\begin{aligned}
g_{A^0 H^\pm W} &= 1, \qquad g_{H^+ H^- \gamma} = -e, \\
g_{H^+ H^- Z} &= -e \cos 2\theta_W / (\sin\theta_W \cos\theta_W). \tag{6}
\end{aligned}
$$

Finally, there are couplings of the various Higgs bosons to the standard fermions. They are slightly more involved

TABLE I.   Couplings of the 2HDM Higgs bosons to third-generation fermions, normalized to the SM-Higgs ones, as a function of the angles α and β for the four types of 2HDM scenarios. For the CP-even h, H states, the values in the alignment limit $\alpha \to \beta - \frac{\pi}{2}$ are also shown.

	Type I	Type II	Type X	Type Y
g_{htt}	$\frac{\cos\alpha}{\sin\beta} \to 1$	$\frac{\cos\alpha}{\sin\beta} \to 1$	$\frac{\cos\alpha}{\sin\beta} \to 1$	$\frac{\cos\alpha}{\sin\beta} \to 1$
g_{hbb}	$\frac{\cos\alpha}{\sin\beta} \to 1$	$-\frac{\sin\alpha}{\cos\beta} \to 1$	$\frac{\cos\alpha}{\sin\beta} \to 1$	$-\frac{\sin\alpha}{\cos\beta} \to 1$
$g_{h\tau\tau}$	$\frac{\cos\alpha}{\sin\beta} \to 1$	$-\frac{\sin\alpha}{\cos\beta} \to 1$	$-\frac{\sin\alpha}{\cos\beta} \to 1$	$\frac{\cos\alpha}{\sin\beta} \to 1$
g_{Htt}	$\frac{\sin\alpha}{\sin\beta} \to -\frac{1}{\tan\beta}$	$\frac{\sin\alpha}{\sin\beta} \to -\frac{1}{\tan\beta}$	$\frac{\sin\alpha}{\sin\beta} \to -\frac{1}{\tan\beta}$	$\frac{\sin\alpha}{\sin\beta} \to -\frac{1}{\tan\beta}$
g_{Hbb}	$\frac{\sin\alpha}{\sin\beta} \to -\frac{1}{\tan\beta}$	$\frac{\cos\alpha}{\cos\beta} \to \tan\beta$	$\frac{\sin\alpha}{\sin\beta} \to -\frac{1}{\tan\beta}$	$\frac{\cos\alpha}{\cos\beta} \to \tan\beta$
$g_{H\tau\tau}$	$\frac{\sin\alpha}{\sin\beta} \to -\frac{1}{\tan\beta}$	$\frac{\cos\alpha}{\cos\beta} \to \tan\beta$	$\frac{\cos\alpha}{\cos\beta} \to \tan\beta$	$\frac{\sin\alpha}{\sin\beta} \to -\frac{1}{\tan\beta}$
$g_{A^0 tt}$	$\frac{1}{\tan\beta}$	$\frac{1}{\tan\beta}$	$\frac{1}{\tan\beta}$	$\frac{1}{\tan\beta}$
$g_{A^0 bb}$	$-\frac{1}{\tan\beta}$	$\tan\beta$	$-\frac{1}{\tan\beta}$	$\tan\beta$
$g_{A^0 \tau\tau}$	$-\frac{1}{\tan\beta}$	$\tan\beta$	$\tan\beta$	$-\frac{1}{\tan\beta}$

and can be described by the following Yukawa-type Lagrangian:

$$
\begin{aligned}
-\mathcal{L}^{\mathrm{SM}}_{\mathrm{Yuk}} = &\sum_{f=t,b,\tau} \frac{m_f}{v} \left(g_{hff}\bar{f}fh + g_{Hff}\bar{f}fH - ig_{A^0 ff}\bar{f}\gamma_5 fA^0 \right) \\
&- \frac{\sqrt{2}}{v} \left(\bar{t}(m_t g_{A^0 tt}P_L + m_b g_{A^0 bb}P_R)bH^+ \right. \\
&\left. + m_\tau g_{A^0 \tau\tau}\bar{\nu}_\tau P_R \tau H^+ + \mathrm{H.c.} \right),
\end{aligned} \tag{7}
$$

with the usual projectors $P_{L/R} = \frac{1}{2}(1 \mp \gamma_5)$. $g_{\phi ff}$ are the reduced couplings of the ϕ boson to quarks and leptons, and we will take into account here only those of the third generation which are the only relevant ones (except in the case of the muon $g-2$ as will be seen later). They have been normalized to the couplings of the SM H^0 boson, $g_{\phi ff} = g^{\mathrm{2HDM}}_{\phi ff}/g^{\mathrm{SM}}_{H^0 ff}$.

In the 2HDM with a discrete symmetry that we are considering here, the absence of flavor-changing neutral currents (FCNCs), which are experimentally constrained to be very small, is enforced by coupling in a specific manner the original Φ_1 and Φ_2 fields to isospin up-type quarks and isospin down-type quarks and charged leptons. There are four configurations or types [40]. The most discussed ones [8] are the so-called type II model, in which the field Φ_1 couples to isospin down-type quarks and leptons and Φ_2 to up-type quarks, and the type I model, in which the field Φ_2 couples to both isospin up- and down-type fermions. To be more general, we will also study the two additional options in which the charged leptons will have a different coupling compared to down-type quarks, namely, the type X or lepton-specific model, in which the Higgs couplings to quarks are as in the type I case but those to leptons are as in type II, and the type Y or flipped model, in which the Higgs couplings are as in the previous model but with the type I and type II couplings reversed.

The neutral Higgs couplings to fermions in these four flavor-conserving types of 2HDMs, as functions of the angles β and α, are listed in Table I. The couplings of the charged Higgs bosons follow those of the pseudoscalar A^0 state. In the case of the CP-even h and H bosons, we also give for completeness the values of these couplings in the alignment limit in which the h state is SM-like. This alignment limit is strongly favored by LHC Higgs data as will be seen in the next section and is achieved by simply setting $\alpha = \beta - \frac{\pi}{2}$.

B. The pseudoscalar sector of the 2HD + a scenario

In our study, we will consider the extension of the 2HDM previously introduced by an additional singlet pseudoscalar Higgs field a^0 [13–17]. The most general scalar potential for such a 2HD + a scenario is given by[3] [17]

$$
\begin{aligned}
V_{\mathrm{2HD+a}} = &V_{\mathrm{2HDM}} + \frac{1}{2}m^2_{a^0}(a^0)^2 + \frac{\lambda_a}{4}(a^0)^4 \\
&+ \left(i\kappa a^0 \Phi_1^\dagger \Phi_2 + \mathrm{H.c.} \right) \\
&+ \left(\lambda_{1P}(a^0)^2 \Phi_1^\dagger \Phi_1 + \lambda_{2P}(a^0)^2 \Phi_2^\dagger \Phi_2 \right), \quad (8)
\end{aligned}
$$

where V_{2HDM} is the 2HDM potential given in Eq. (1) and κ, λ_{1P}, and λ_{2P} are the new trilinear couplings between the two Higgs doublets and the pseudoscalar a^0 state and λ_a the quartic a^0 coupling (we assume that κ is real for simplicity).

After electroweak symmetry breaking, the physical content of the Higgs sector of the theory will consist of again two CP-even h, H states, two charged $H^\pm$ bosons, but two CP-odd a^0 and A^0 states which could mix. Hence, in addition to the usual mixing angles α and β of a 2HDM, there will be an extra mixing angle θ which allows one to

---

[3]This additional scalar potential would also softly break the Z_2 symmetry.

transform the (A^0, a^0) current eigenstates to the (A, a) physical CP-odd eigenstates

$$\begin{pmatrix} A^0 \\ a^0 \end{pmatrix} = \begin{pmatrix} \cos\theta & \sin\theta \\ -\sin\theta & \cos\theta \end{pmatrix} \begin{pmatrix} A \\ a \end{pmatrix}. \tag{9}$$

This mixing angle is given, in terms of κ and the physical masses M_a and M_A, by

$$\tan 2\theta = \frac{2\kappa v}{M_A^2 - M_a^2}. \tag{10}$$

The CP-odd mixing will modify two of the quartic couplings of the 2HDM given in Eq. (2) when the replacement $A^0 = \cos\theta A + \sin\theta a$ is made. More explicitly, one would have

$$\lambda_4 v^2 = M^2 + M_A^2 \cos^2\theta + M_a^2 \sin^2\theta - 2M_{H^\pm}^2,$$
$$\lambda_5 v^2 = M^2 - M_A^2 \cos^2\theta - M_a^2 \sin^2\theta. \tag{11}$$

In the case of the Higgs couplings to fermions, one can consider simply those discussed in the context of the 2HDM with the four configurations, type I, II, X, and Y, but modify the neutral Higgs sector to introduce the additional pseudoscalar Higgs state. The neutral current part of the Lagrangian $\mathcal{L}_{\mathrm{Yuk}}$ which contains the Yukawa

interactions with the SM fermions will then read

$$\mathcal{L}_{\mathrm{Yuk}} = \sum_f \frac{m_f}{v} \Big[g_{hff} h\bar{f}f + g_{Hff} H\bar{f}f - i g_{Aff} A\bar{f}\gamma_5 f$$
$$- i g_{aff} a\bar{f}\gamma_5 f \Big], \tag{12}$$

where the couplings $g_{\phi ff}$ of the 2HDM CP-even h, H (as well as implicitly those of the charged Higgs bosons $H^\pm$) are given in Table I in the four types of configurations, while the Yukawa couplings of the pseudoscalar Higgs bosons will be given by

$$g_{Aff} = \cos\theta g_{A^0 ff}, \qquad g_{aff} = \sin\theta g_{A^0 ff}, \tag{13}$$

with the reduced couplings $g_{A^0 ff}$ again given in Table I in the four 2HDM configurations.

Finally, there are also trilinear interactions between the Higgs states which could be relevant. Here, we will be interested only in the interactions of the SM-like h boson whose couplings to two pseudoscalar fields are given by the Lagrangian $\mathcal{L}_{\mathrm{scal}}$:

$$\mathcal{L}_{\mathrm{scal}} = \lambda_{haa} haa + \lambda_{haA} haA + \lambda_{hAA} hAA, \tag{14}$$

where, using the abbreviations $s_X, c_X = \sin(X), \cos(X)$ and $t_\beta = \tan\beta$, one would have

$$\lambda_{haa} = -\frac{2M_a^2}{v} s_{\beta-\alpha} s_\theta^2 - \frac{M_h^2}{v} s_\theta^2 \frac{s_{\beta-\alpha} t_\beta + c_{\beta-\alpha}(1 - t_\beta^2)}{t_\beta} + \frac{M^2}{v} s_\theta^2 \frac{2 s_{\beta-\alpha} t_\beta + c_{\beta-\alpha}(1 - t_\beta^2)}{t_\beta}$$
$$- 2\lambda_{1P} v c_\theta^2 \frac{s_{\beta-\alpha} - c_{\beta-\alpha} t_\beta}{1 + t_\beta^2} - 2\lambda_{2P} v c_\theta^2 \frac{t_\beta(s_{\beta-\alpha} t_\beta + c_{\beta-\alpha})}{1 + t_\beta^2},$$

$$\lambda_{haA} = \frac{M_A^2}{2v} s_{\beta-\alpha}^2 s_{2\theta} + \frac{M_a^2}{2v} s_{\beta-\alpha} s_{2\theta} + \frac{M_h^2}{2v} s_{2\theta} \frac{s_{\beta-\alpha} t_\beta + c_{\beta-\alpha}(1 - t_\beta^2)}{t_\beta} - \lambda_{1P} v s_{2\theta} \frac{s_{\beta-\alpha} - c_{\beta-\alpha} t_\beta}{1 + t_\beta^2}$$
$$- \lambda_{2P} v s_{2\theta} \frac{t_\beta(s_{\beta-\alpha} t_\beta + c_{\beta-\alpha})}{1 + t_\beta^2} - \frac{M^2}{2v} s_{2\theta} \frac{2 s_{\beta-\alpha} t_\beta + c_{\beta-\alpha}(1 - t_\beta^2)}{t_\beta},$$

$$\lambda_{hAA} = -\frac{2M_A^2}{v} s_{\beta-\alpha} c_\theta^2 - \frac{M_h^2}{v} c_\theta^2 \frac{s_{\beta-\alpha} t_\beta + c_{\beta-\alpha}(1 - t_\beta^2)}{t_\beta} + \frac{M^2}{v} c_\theta^2 \frac{s_{\beta-\alpha} t_\beta - c_{\beta-\alpha}(1 - t_\beta^2)}{t_\beta}$$
$$- 2\lambda_{1P} v s_\theta^2 \frac{s_{\beta-\alpha} - c_{\beta-\alpha} t_\beta}{1 + t_\beta^2} - 2\lambda_{2P} v s_\theta^2 \frac{t_\beta(s_{\beta-\alpha} t_\beta + c_{\beta-\alpha})}{1 + t_\beta^2}. \tag{15}$$

In the following, we will show the results of several parameter scans. For the latter, we have adopted the following set of free parameters:

  (i) the physical masses of the Higgs states, M_H, M_A, M_a, and $M_{H^\pm}$;

  (ii) the mixing angles α [possibly traded against $\cos(\beta - \alpha)$, β (we will mostly use $\tan\beta$), and θ (we will mostly use $\sin\theta$)]; and

  (iii) the scalar couplings $\lambda_{1,2P}$ and λ_3, with the latter replaced by M in some cases.

C. Theoretical constraints on the model

We now summarize the theoretical constraints that one can impose on the 2HD + a model. These generally apply on the quartic couplings of the scalar potential which can be

translated into bounds on the Higgs masses M_a, M_A, M_H, and $M_{H^\pm}$ as functions of the angles α and β, using, for instance, Eqs. (2) and (11). The most relevant bounds can be obtained following those derived in the context of a 2HDM only [41–43] assuming λ_{P1}, $\lambda_{P2} > 0$.

There is first the requirement of perturbative unitarity which leads to the following bounds on the combinations of the couplings λ_i:

$$|x_i| < 8\pi, \qquad |\lambda_{1,2P}| < 4\pi, \qquad |\lambda_3 \pm \lambda_4| < 4\pi,$$

$$\left| \frac{1}{2} \left(\lambda_1 + \lambda_2 \pm \sqrt{(\lambda_1 - \lambda_2)^2 + 4\lambda_k^2} \right) \right| < 8\pi, \quad k = 4, 5,$$

$$|\lambda_3 + 2\lambda_4 \pm 3\lambda_5| < 8\pi, \qquad |\lambda_3 \pm \lambda_5| < 8\pi, \qquad (16)$$

where the x_i's are the solutions of the equation

$$0 = x^3 - 3(\lambda_a + \lambda_1 + \lambda_2)x^2 + (9\lambda_1\lambda_a + 9\lambda_2\lambda_a - 4\lambda_{1P}^2 - 4\lambda_{2P}^2 - 4\lambda_3^2 - 4\lambda_3\lambda_4 - \lambda_4^2 + 9\lambda_1\lambda_2)x$$
$$+ 12\lambda_{2P}^2\lambda_1 + 12\lambda_{1P}^2\lambda_2 - 16\lambda_{1P}\lambda_{2P}\lambda_3 - 8\lambda_{1P}\lambda_{2P}\lambda_4 + (-27\lambda_1\lambda_2 + 12\lambda_3^2 + 12\lambda_3\lambda_4 + 3\lambda_4^2)\lambda_a. \qquad (17)$$

In addition, there is the requirement that the scalar potential should be bounded from below, which leads to the following constraints on the scalar quartic couplings (with the assumption λ_{P1}, $\lambda_{P2} > 0$, the last two lines are always satisfied) [44]:

$$\lambda_1 > 0, \qquad \lambda_2 > 0, \qquad \lambda_a > 0,$$

$$\bar{\lambda}_{12} \equiv \sqrt{\lambda_1\lambda_2} + \lambda_3 + \min(0, \lambda_4 - |\lambda_5|) > 0,$$

$$\bar{\lambda}_{1P} \equiv \sqrt{\frac{\lambda_1\lambda_a}{2}} + \lambda_{1P} > 0, \qquad \bar{\lambda}_{2P} \equiv \sqrt{\frac{\lambda_2\lambda_a}{2}} + \lambda_{2P} > 0,$$

$$\sqrt{\frac{\lambda_1\lambda_2\lambda_a}{2}} + \lambda_{1P}\sqrt{\lambda_2} + \lambda_{2P}\sqrt{\lambda_1} + [\lambda_3 + \min(0, \lambda_4 - |\lambda_5|)]\sqrt{\frac{\lambda_a}{2}} + \sqrt{2}\sqrt{\bar{\lambda}_{12}\bar{\lambda}_{1P}\bar{\lambda}_{2P}} > 0. \qquad (18)$$

It is interesting to further discuss this requirements for the specific case of the coupling λ_3. Defining the SM Higgs self-coupling as $\lambda = M_h^2/(2v^2)$, one has $\lambda_3 > 2\lambda$, and under the assumption $M_A \gg M_a$, which will be intensively used later on, one would have

$$\lambda_3 > \frac{M_A^2 - M_a^2}{v^2} \sin^2\theta - 2\lambda \cot^2 2\beta \qquad (19)$$

from unitarity constraints. When combining this equation with the perturbativity requirement $\lambda_3 < 4\pi$, one realizes that it is not possible to have an arbitrary mass splitting between the a and A bosons when mixing is present, i.e., $\sin\theta \neq 0$.

III. COLLIDER CONSTRAINTS

A. Higgs signal strengths

We come now to the phenomenological constraints on the 2HD + a and first discuss the ones that emanate from the high-precision measurements of the properties of the 125 GeV Higgs state performed at the LHC. Indeed, precise measurements of the h boson production and decay rates strongly constrain its couplings to massive gauge bosons g_{hVV} and fermions g_{hff} given in the upper part of Table I and, hence, the values of the angles α and β.

It has become now customary to study these h couplings by looking at their deviation from the SM expectation, which is achieved when considering a specific search channel X, by

means of the signal strength modifier μ_{XX} [3,45]. This quantity characterizes the h production cross section times its decay branching ratio into the X states, normalized to the expected SM values. One would then have, in the narrow width approximation, the relation

$$\mu_{XX} = \frac{\sigma(pp \to h \to XX)}{\sigma(pp \to H^0 \to XX)|_{\mathrm{SM}}}$$

$$= \frac{\sigma(pp \to h) \times \mathrm{BR}(h \to XX)}{\sigma(pp \to H^0)|_{\mathrm{SM}} \times \mathrm{BR}(H^0 \to XX)|_{\mathrm{SM}}} \qquad (20)$$

with H^0 representing the SM 125 GeV Higgs boson; note that $M_h = M_{H^0}$ has been assumed.

For instance, assuming that the h boson is produced in the by far dominant gluon-gluon fusion process $gg \to h$ and focusing on the $h \to XX$ decay channel, one can relate the signal strength μ_{XX} to the coupling modifier κ_X^2 which measures the deviations of the h coupling to the particle X, g_{hXX}, from its value as predicted in the SM:

$$\kappa_X^2 = \frac{\Gamma(h \to XX)}{\Gamma(H^0 \to XX)|_{\mathrm{SM}}} \simeq \frac{g_{hXX}^2}{g_{H^0XX}^2|_{\mathrm{SM}}}. \qquad (21)$$

The measurements of the various h couplings have been recently updated by the ATLAS and CMS Collaborations for the tenth anniversary of the Higgs discovery, using the full available set of data, about 139 fb^{-1}, collected at the energy of 13 TeV [25,26]. The corresponding signal strengths

TABLE II.   Summary of the values of the signal strengths of the 125 GeV Higgs boson assumed to be the h state as measured by ATLAS [25] and CMS [26] using the full set of available data in the various possible decay channels; the quoted uncertainties are the total ones.

Signal strength	ATLAS	CMS
$\mu_{\gamma\gamma}$	$1.04^{+0.10}_{-0.09}$	1.13 ± 0.09
μ_{ZZ}	1.01 ± 0.11	$0.97^{+0.12}_{-0.11}$
μ_{WW}	1.09 ± 0.11	0.97 ± 0.09
μ_{bb}	$1.02^{+0.12}_{-0.11}$	$1.05^{+0.22}_{-0.21}$
$\mu_{\tau\tau}$	$0.93^{+0.13}_{-0.12}$	0.85 ± 0.10
$\mu_{gg \to h}$	1.00 ± 0.05	$0.97^{+0.08}_{-0.07}$

measured by ATLAS and CMS are summarized in Table II in the case of Higgs decays into gauge boson ($\mu_{\gamma\gamma}, \mu_{WW}, \mu_{ZZ}$) as well as bottom quark and tau lepton ($\mu_{bb}, \mu_{\tau\tau}$) final states. Together with the central values, the total (theoretical, statistical, and systematical) uncertainties as estimated by the Collaborations are also shown. In the last line, we also give the measured signal strength from the cross section for h production in the dominant production channel, the gluon-fusion process $gg \to h$, which is dominantly mediated by top quark loops and is, thus, directly related to the h coupling to top quarks.

The table shows that h has been found to have SM-like properties with an accuracy of about 10% or less. In particular, it should have an almost SM-like coupling to $V = W, Z$ bosons which, assuming the custodial SU(2) symmetry to which the SM as well as our model obey, are equal $g_{hWW} = g_{hZZ} \equiv g_{hVV}$. This provides the most stringent test of the departure from the SM expectation or the alignment limit, $\cos^2(\beta - \alpha) \equiv 1 - g_{hVV}^2 = 0$. One can thus turn these measurements into constraints on the angles α and β of our 2HD + a scenario.

To avoid the risk of combining the ATLAS and CMS results given in Table II, we consider only the ATLAS results (those of CMS are rather similar); we show in Fig. 1 the regions in the $[\cos(\beta - \alpha), \tan\beta]$ plane which are allowed at the 95% confidence level (C.L.) by the combined constraints on the Higgs couplings to gauge bosons and fermions in the context of a 2HDM in their four specific realizations, namely, type I and II (upper row) and X and Y (lower row). As we are considering only the CP-even state h whose couplings are not altered by the presence of the additional pseudoscalar Higgs boson, the results shown in the figure are also valid in our 2HD + a scenario.[4]

---

[4]Such an analysis has been performed in a complete and sophisticated way by the ATLAS Collaboration in the four 2HDM types; see Ref. [46] and its Fig. 20. Unfortunately, it cannot be used in our context, since, first, it involves experimental cuts (such as a rapidity cut $y_H < 2.5$) and, second, it does not consider values of $\tan\beta$ higher than 10. Nevertheless, we find a qualitative agreement with the figure.

One sees from the figure that, in the type II, type Y, and to some extent type X scenarios, $|\cos(\beta - \alpha)|$ is constrained to be small or close to zero, $|\cos(\beta - \alpha)| \lesssim 0.1$, for any value of $\tan\beta$ that we varied from a minimum of $\tan\beta = 0.3$ to a maximum of $\tan\beta = 50$ which are the values that allow for perturbative top and bottom quark Yukawa couplings in the type II and type Y scenarios.

The reason is that, in these three models, one of the Yukawa couplings to the b quark or τ lepton would be enhanced at large $\tan\beta$ values if one is not in the SM-like configuration $\cos(\beta - \alpha) \to 0$. This then forces the fermionic signal strengths μ_{bb} and/or $\mu_{\tau\tau}$ to depart from the unit values to which they are experimentally constrained to be close, as shown in Table II. In turn, in the type I model, no coupling to fermions is enhanced at high $\tan\beta$ and, thus, $\cos(\beta - \alpha)$ can significantly deviate from unity for all considered values of $\tan\beta \gtrsim 0.3$ without affecting too much the fermionic h signal strengths. Note that, at small $\tan\beta$, the deviations in g_{hff} can be larger, but the measured values are below the SM expectation, which forces g_{hVV} to be less than unity and, hence, $\cos(\beta - \alpha) \neq 0$.

Another comment to be made is that in earlier analyses of these three models (see, e.g., Ref. [11]) there were narrow "arms" at $\cos(\beta - \alpha) \gtrsim +0.1$ which corresponded to the so-called "wrong-sign" Yukawa regime [47] in which the h couplings to down-type quarks and/or leptons are equal in magnitude to those of the SM Higgs boson for $\cos(\beta - \alpha) = 0$ but opposite in sign. These regions have been substantially reduced by the recent and more precise measurements, and only a few such points are left in our scan.

In any case, all these constraints from the h signal strengths can be simultaneously satisfied in the so-called alignment limit, $\alpha = \beta - \frac{\pi}{2}$ [48–51]. In this case, the couplings of the CP-even h and H states to gauge bosons are by construction such that $g_{hVV} = 1$ as for the SM Higgs and $g_{HVV} = 0$ as is the case for the pseudoscalar A in our CP-conserving model. The Higgs couplings to fermions in the alignment limit, also given in Table I, are such that $g_{htt} = g_{hbb} = g_{h\tau\tau} \to 1$ again as for the SM Higgs and $g_{Hff} \to g_{A^0 ff}$ which means that all couplings of the heavier CP-even H reduce to those of the 2HDM pseudoscalar A^0.

Finally, let us note that, for the couplings between two Higgs and one gauge boson, those involving h vanish in the alignment limit, $g_{hAZ} = g_{hH^\pm W^\mp} = 0$, while those involving H become maximal, $g_{HAZ} = g_{HH^\pm W^\mp} = 1$.

B. Constraints from flavor physics

Let us now turn to the constraints that come from flavor physics, focusing first on the heavier 2HDM Higgs bosons in the four considered configurations, type I, II, X, and Y. While these scenarios are free from tree-level FCNCs by construction, they are nevertheless induced at the loop level. Severe constraints come from processes in which there are $b \to s$ transitions at the basic level, which have
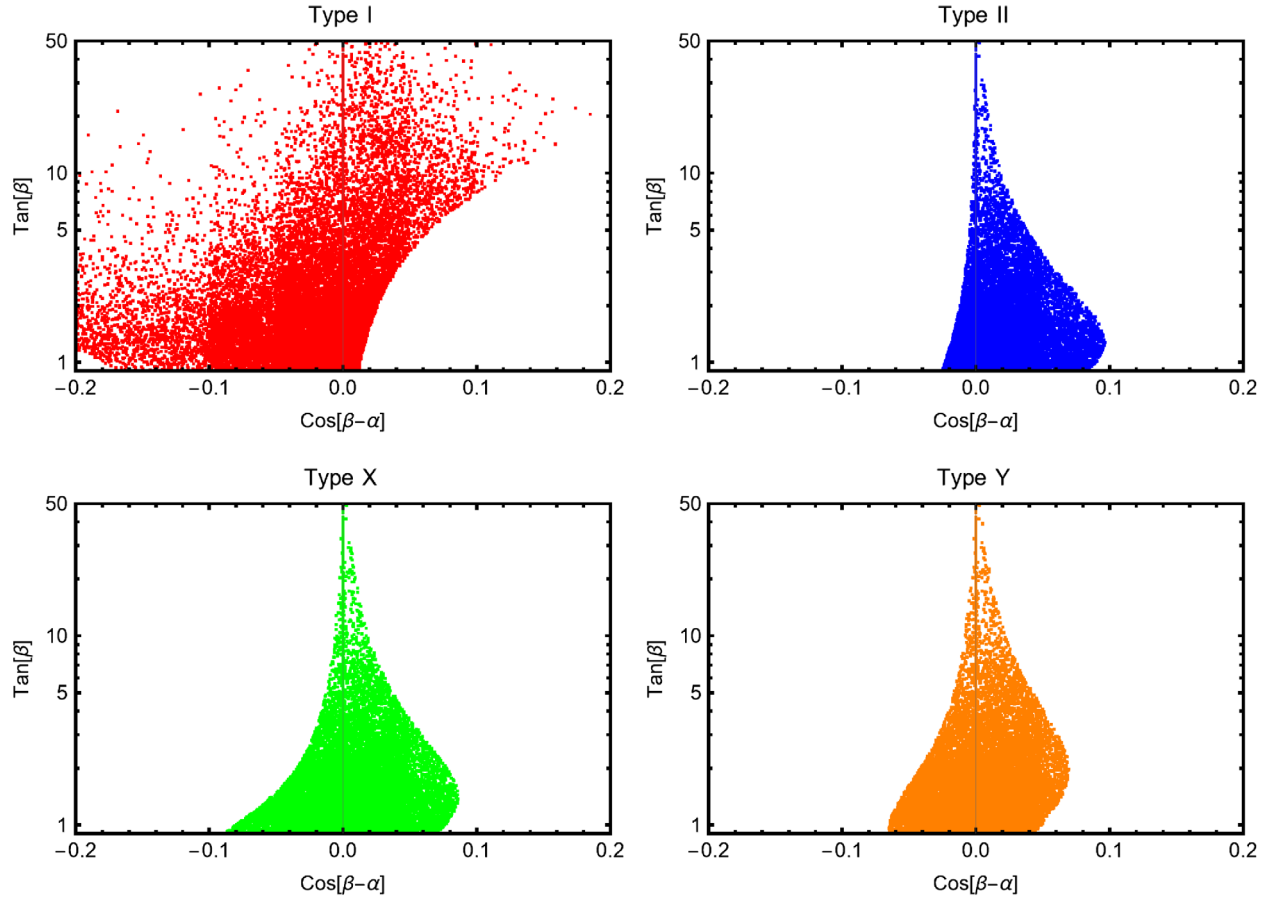
FIG. 1.   Allowed regions in the plane $[\cos(\beta - \alpha), \tan \beta]$ for the h signal strengths measured at the LHC in the four types of 2HD + a configurations that do not induce tree-level FCNCs.

rates that are essentially sensitive to the parameters entering the charged Higgs sector, namely, $M_{H^\pm}$ and $\tan \beta$. The type II and Y models are the ones that are most affected, as they involve the $H^\pm$ coupling component to bottom quarks g_{Abb} that is proportional to $\tan \beta$ and which can be strongly enhanced at large $\tan \beta$ values. In the configurations II and X with enhanced Higgs couplings to muons, additional constraints come from B-meson decays such as $B_s \to \mu^+ \mu^-$ and $B \to K \mu^+ \mu^-$ [52].

Nevertheless, the most stringent constraints are due to the loop-induced decay process $B \to X_s \gamma$. Indeed, at the fundamental level, the radiative decay $b \to s \gamma$ proceeds in a 2HDM or 2HD + a through a triangular loop involving W and $H^\pm$ bosons along with top quarks. At leading order, the contribution of the $H^\pm$ states to the amplitude is proportional to the two combinations of couplings g_{Auu}^2 and $g_{Auu} g_{Add}$, and, hence, in the four 2HDM configurations one has contributions that are proportional to $\tan^2 \beta$ as in type II and type Y scenarios or are proportional to $\cot^2 \beta$ as in type I and type X scenarios. As a result, and taking into account the most up-to-date value of the branching fraction BR$(B \to X_s \gamma) = (3.43 \pm 0.21 \pm 0.07) \times 10^{-6}$ [53,54] and the most precise calculation performed at next-to-next-to-leading

order in Refs. [55,56], one obtains the following constraints, depending on the considered 2HDM type:

$$
\begin{aligned}
\text{Type II or Y}: M_{H^\pm} &\gtrsim 800 \text{ GeV} \quad \text{for any } \tan \beta, \\
\text{Type I or X}: M_{H^\pm} &\gtrsim 500 \text{ GeV} \quad \text{for } \tan \beta \lesssim 1.
\end{aligned}
\tag{22}
$$

As can be seen, these bounds are rather severe. Only in models of type I and X and for $\tan \beta \gtrsim 2$ that one has the loose bound $M_{H^\pm} \gtrsim 80$ GeV from LEP searches (see later).

Turning now to the case of a possibly very light pseudoscalar particle, it can affect a large variety of low-energy processes, especially those involving b quarks which have enhanced couplings to a at high $\tan \beta$ in type II and Y scenarios. This is, for instance, the case of the decay rates of B and K mesons which can be substantially modified by the emission of a very light a state [57]. At high $\tan \beta$ values and, again in the type II scenario, very constraining processes are the decays $\Upsilon \to a \gamma, B_s \to \mu^+ \mu^-$, and $B \to K \mu^+ \mu^-$. In particular, the mode $B_s \to \mu^+ \mu^-$ can potentially receive large contributions from the exchange of a light a state if it has large couplings to b quarks and muons as is the case in the type II model. In the case of the type X configuration, constraints as severe as in the type II

case could be derived from the searches of a light leptophilic scalar boson which have been performed rather recently by the *BABAR* Collaboration [58]. The corresponding limits on the mass of a (even if it cannot be emitted on shell) are included in our numerical analysis via a procedure discussed in Ref. [59], to which we refer for details. Note that there are also constraints from violation of lepton universality in the decays of the Z boson and the τ lepton [60].

All constraints of this type can be fulfilled at this early stage (further stronger constraints from direct LHC searches of the pseudoscalar a boson will be discussed in Sec. III.5), by adopting a lower bound of 10 GeV on the mass of the a state.

C. Constraints from electroweak precision measurements

Another set of strong constraints on the 2HD + a scenario emerges from electroweak high-precision measurements, in particular, the one of the effective electroweak mixing angle $\sin^2 \theta_W$ and of the W boson mass M_W. The by far dominant set of radiative corrections to these two quantities is the one that affects the so-called ρ parameter, which measures the strength of the neutral to charged currents ratio at zero-momentum transfer [61]. It is defined by

$$\Delta\rho = \Pi_{WW}(0)/M_W^2 - \Pi_{ZZ}(0)/M_Z^2, \qquad (23)$$

where Π_{VV} are the transverse parts of the $V = W, Z$ boson two-point functions or self-energies. This parameter strongly constrains the mass splitting between particles that belong to the same SU(2) isodoublet, as they give contributions that are quadratically dependent on the masses. In a 2HDM scenario, for instance, they force the masses of the additional heavy A^0, H, and $H^\pm$ states to be very close in mass, $M_{A^0} \approx M_H \approx M_{H^\pm}$ [62,63]. Note that the SM-like h boson also contributes to the ρ parameter, but the contribution is only logarithmic and it is already included in the fit of the SM data in the limit where h is SM-like, i.e., in the alignment limit discussed previously.

In our 2HD + a model, there are not only contributions from the 2HDM extra A^0, H, and $H^\pm$ bosons but also additional contributions due to the extra pseudoscalar Higgs boson a^0 which mixes with the 2HDM pseudoscalar state with an angle θ. Outside the alignment limit that we will consider from time to time, the full contribution to the ρ parameter is given by

$$
\begin{aligned}
\Delta\rho = {} & \frac{\alpha_{\text{QED}}(M_Z^2)}{16\pi^2 M_W^2 (1 - M_W^2/M_Z^2)} \Big\{ \sin^2(\beta - \alpha)[f(M_{H\pm}^2, M_H^2) + \cos^2\theta f(M_{H\pm}^2, M_A^2) + \sin^2\theta f(M_{H\pm}^2, M_a^2) \\
& - \cos^2\theta f(M_A^2, M_H^2) - \sin^2\theta f(M_a^2, M_H^2)] + \cos^2(\beta - \alpha)[f(M_{H\pm}^2, M_h^2) + \cos^2\theta f(M_{H\pm}^2, M_A^2) \\
& + \sin^2\theta f(M_{H\pm}^2, M_a^2) - \cos^2\theta f(M_A^2, M_h^2) - \sin^2\theta f(M_a^2, M_h^2)] \Big\},
\end{aligned}
\qquad (24)
$$

where α_{QED} is the fine structure constant evaluated at M_Z and the loop function f reads

$$f(x, y) = x + y - \frac{2xy}{x - y} \log\frac{x}{y}. \qquad (25)$$

This quantity vanishes if the loop particles are mass degenerate, $f(x, x) = 0$, and, for a large splitting $x \gg y$, one would have $f(x, 0) = x$ and, hence, possibly large contributions.

One can also take into account the subleading contributions to the electroweak observables beyond the ρ parameter and, for instance, consider the ones of the Peskin-Takeuchi S, T, U parameters [64]. In this scheme, the largest contribution T is, in fact, simply the $\Delta\rho$ contribution $T \propto \Delta\rho - \Delta\rho|_{\text{SM}}$, while S and U describe new contributions to, respectively, neutral current processes at different energies and the W mass from new charged currents.

The central values for the three variables in the case of the SM are as follows [62,63]:

$$\mathcal{O}^{\text{SM}} = (S, T, U)^{\text{SM}} = (0.04, 0.09, -0.02). \qquad (26)$$

A global fit to all electroweak precision observables available before the new CDF measurement of the W mass to be discussed later has been made in Refs. [62,63] and leads to the following χ^2 as a function of the departure of the three variables from their SM values:

$$\chi^2 = \sum_{i,j} (\mathcal{O}_i - \mathcal{O}_i^{\text{SM}})(\sigma_i V_{ij} \sigma_j)^{-1}(\mathcal{O}_j - \mathcal{O}_j^{\text{SM}}), \qquad (27)$$

where the standard deviations and the covariance matrix are given by

$$\sigma = (0.11, 0.14, 0.11), \quad V = \begin{pmatrix} 1 & 0.92 & -0.68 \\ 0.92 & 1 & -0.87 \\ -0.68 & -0.87 & 1 \end{pmatrix}. \qquad (28)$$

For our numerical evaluation, we have performed a scan on the parameters of the 2HD + a model over the following ranges:

$$\tan\beta \in [1, 60], \qquad |\cos(\beta - \alpha)| < 0.2, \qquad \sin\theta \in [0.1, 0.8],$$

$$[M_H, M_A, M_{H^\pm}] \in [(125 \text{ GeV}, 90 \text{ GeV}, 80 \text{ GeV}), 1 \text{ TeV}], \qquad M_a \in [10, 400] \text{ GeV}, \qquad |\lambda_3, \lambda_{1P}, \lambda_{2P}| < 4\pi, \qquad (29)$$

where the 2HDM Higgs masses were taken to be such that $M_H > M_h$ (by construction) and $M_{H^\pm} \gtrsim M_W, M_A \gtrsim M_Z$ which are the limits obtained from the negative LEP2 searches as will be seen later. In addition, we have imposed the hierarchy $M_a < M_A$.

The model points which pass the theoretical constraints discussed before, as well as the bounds on the Higgs signal strengths and flavor physics, are displayed for the type I, II, X, and Y 2HD + a in Fig. 2 in the $[M_H - M_A, M_{H^\pm} - M_A]$ planes. The points passing all the constraints are the ones represented in blue in the different panels of the figure. In addition, we have highlighted the impact on the allowed parameter space, of the different types of constraints (namely, the ones from the theory
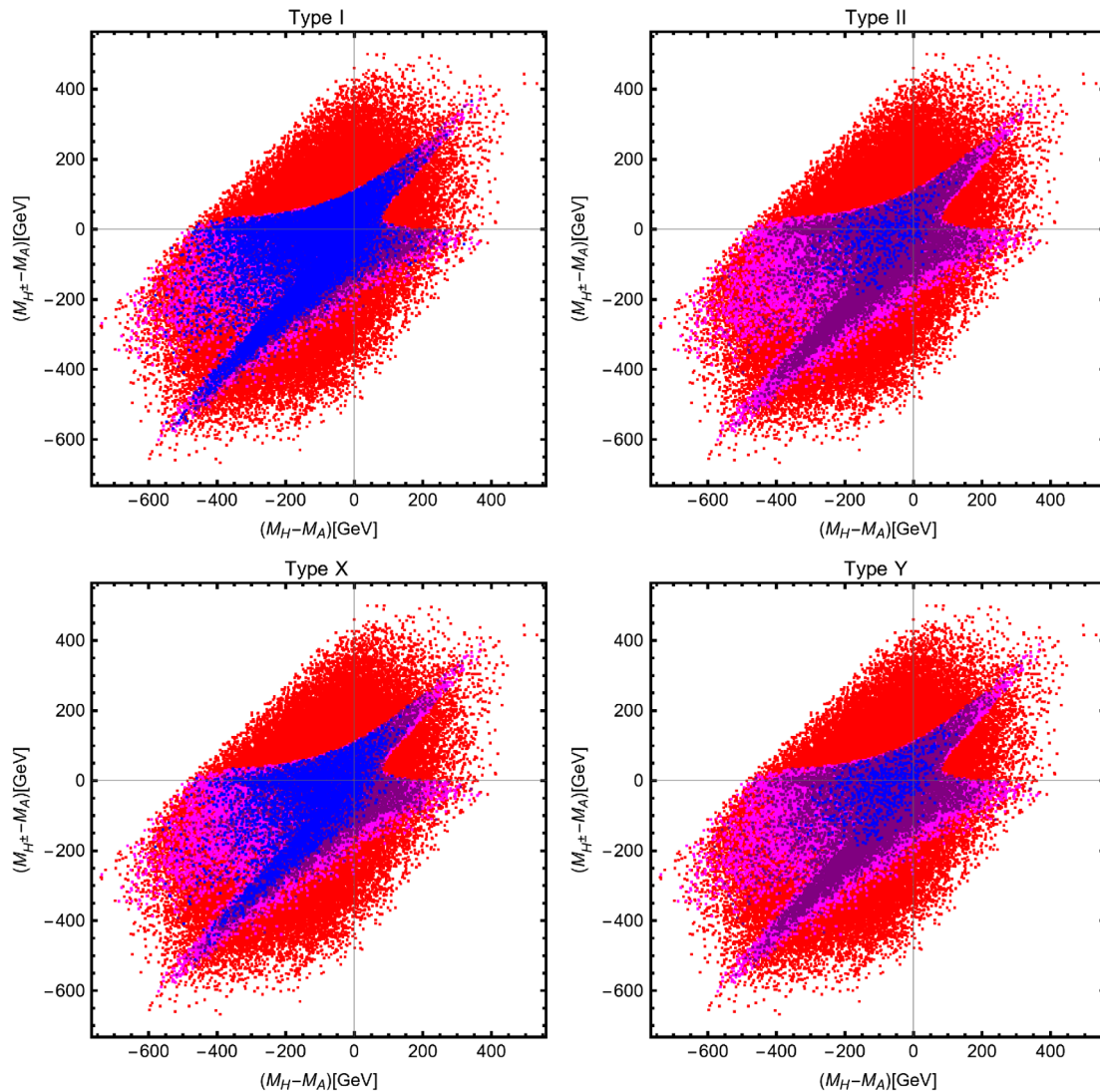
FIG. 2.   2HD + a model points in the $[M_H - M_A, M_{\tilde{H}}^\pm - M_A]$ plane in the four configurations I, II, X, and Y. In each panel, the red points represent the parameter space compatible with the theory constraints on the quartic Higgs couplings, the magenta points in addition comply within 95% C.L. with the constraints on electroweak precision data (using the SM fit for the W-boson mass), the purple points are compatible in addition with the constraints from the h signal strength, and, finally, the blue points represent the model points passing all constraints also including those from B-meson physics.
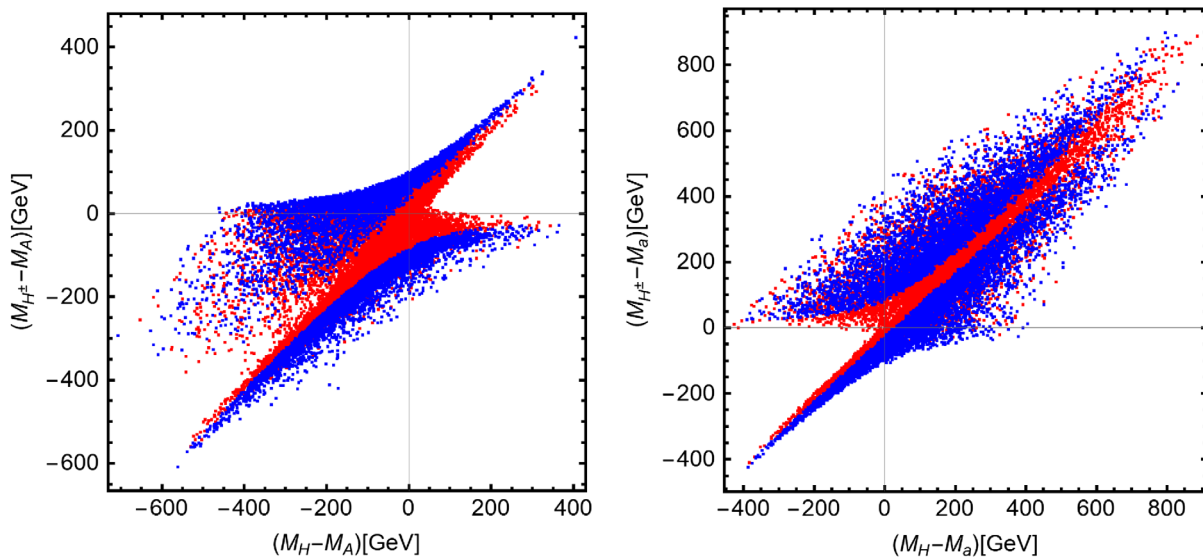
FIG. 3. The 2HD + a model points complying with theoretical and electroweak constraints assuming the SM fit (red points) or accounting for the new CDF M_W value (blue points); the left and right panels show the result of the scans in the $[M_H - M_{A/a}, M_{H^\pm} - M_{A/a}]$ planes.

requirements, the electroweak precision data, the h signal strengths, and B-physics constraints) using the different color codes indicated in the figure caption. As can be seen, a significant Higgs mass splitting is possible, in particular, in the type I and X scenarios. These two configurations give similar results, as is also the case for type II and Y scenarios.

Let us now briefly comment on the impact of the new M_W measurement performed by the CDF Collaboration [24] which turned out to be significantly different not only from the expectation in the SM, about 7σ, but also from other measurements performed in other experiments. In the context of the 2HDM and 2HD + a, this deviation could be explained simply by allowing for a larger splitting between the H, A, and $H^\pm$ masses. In Ref. [22], numerical examples have been given in the type II and type X scenarios to illustrate this possibility, and we extend the discussion here to the other two configurations.

We compare in Fig. 3 the outcome of scans of the 2HD + a, when varying the parameters in the same range of values as before assuming either a purely SM fit for M_W (as given by the red points) or those that allow for an explanation for the new CDF measurement[5] of M_W (given by the blue points). The two panels in the figure show the results in, respectively, the $[M_H - M_A, M_{H^\pm} - M_A]$ and $[M_H - M_a, M_{H^\pm} - M_a]$ planes. For definiteness, we have performed the parameter scan considering the type I configuration. For simplicity, only the theoretical bounds on the coupling of the scalar potential have been considered

in addition to the electroweak observables. These bounds are not sensitive to a specific Yukawa configuration. The main purpose of Fig. 3 is to show that the CDF W-boson mass anomaly could be easily explained in our 2HD + a scenario by simply allowing for a more significant splitting between the masses of the H, A, and $H^\pm$ states. Notice that Fig. 3 should be regarded simply as an illustration; in the rest of the paper we will strictly assume the SM fit for the electroweak data.

D. Impact of the muon $g - 2$

We come now to the constraint from the anomalous magnetic moment of the muon, $a_\mu = \frac{1}{2}(g - 2)_\mu$, which has been recently measured by the Muon $g - 2$ Collaboration at Fermilab [21] and which, when combined with a previous measurement at Brookhaven [66], gives [21]

$$a_\mu^{\text{EXP}} = (116592061 \pm 41) \times 10^{-11}. \qquad (30)$$

This results implies a 4.2σ deviation from the consensual SM value generally adopted by theorists [67]. It is tempting to attribute this discrepancy to new physics beyond the SM and, in particular, to the 2HD + a model that we are considering here, ignoring the possibility that it could partly or entirely be due to unknown uncertainties (as suggested by a debate triggered by a conflicting theoretical value obtained in a lattice calculation [68]).

The 2HD + a $\Phi = h, H, H^\pm, A, a$ bosons contribute to the $(g - 2)_\mu$ in two ways. There is first a one-loop contribution when they are exchanged between the two muon legs in the $\gamma\mu^+\mu^-$ vertex as is shown in the left-hand side in Fig. 4 (in the $H^\pm$ case, the initial photon couples to

---

[5]To account for the CDF measurement, we have replaced the set O_i^{SM} and the corresponding σ_i with the set dubbed "CDF" in Ref. [65] in Eq. (27).
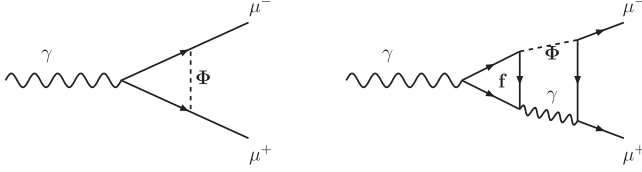
FIG. 4. Feynman diagrams for the one-loop (left) and two-loop (right) contributions of a Higgs boson $\Phi = h, H, H^\pm, A, a$ to the muon $(g-2)$.

the $H^+ H^-$ states and a ν_μ neutrino is exchanged between the two muon lines). Such diagrams give rise to contributions that scale like $m_\mu^4 / M_\Phi^2 \times g_{\Phi\mu\mu}^2$; we assume, of course, the universality of the Higgs couplings and, hence, $g_{\Phi\mu\mu} = g_{\Phi\tau\tau}$. As will be discussed later, such a contribution is sizable only for enhanced $g_{\Phi\mu\mu}$ couplings, hence favoring the type II and X scenarios, and light, namely, $M_\Phi \lesssim \mathcal{O}(100 \text{ GeV})$, exchanged neutral bosons. In our setup, only the pseudo-scalar a will be considered in this mass range. Within a good approximation, the one-loop contribution to $(g-2)_\mu$ can be written as [69,70]

$$\Delta a_\mu^{\text{1-loop}} = -\frac{\alpha_{\text{QED}}}{8\pi \sin^2\theta_W} \frac{m_\mu^4}{M_W^2 M_a^2} g_{a\mu\mu}^2 \left[\log\left(\frac{M_a^2}{m_\mu^2}\right) - \frac{11}{6}\right]. \quad (31)$$

A comparable or even larger contribution to the one discussed above comes from Barr-Zee-type diagrams [71–74], a representative example of which is shown in the right panel in Fig. 4. Their contribution is enhanced with respect to $\Delta a_\mu^{1-\text{loop}}$ by a factor m_f^2 / m_μ^2, compensating the higher α_{QED} power suppression. The two-loop contribution to Δa_μ, restricting for simplicity to the exchange of a, can be written as [72–74]

$$\Delta a_\mu^{\text{2-loop}} = \frac{\alpha_{\text{QED}}^2}{8\pi^2 \sin^2\theta_W} \frac{m_\mu^2}{M_W^2} g_{a\mu\mu} \sum_f g_{aff} N_c^f Q_f \frac{m_f^2}{M_a^2} F\left(\frac{m_f^2}{M_a^2}\right),$$
$$(32)$$

where F is the loop function of the mass ratio $a = m_f^2 / M_a^2$ and it is defined by

$$F(r) = \int_0^1 dx \frac{\log(r) - \log[x(1-x)]}{r - x(1-r)}. \quad (33)$$

Notice that the analytical expressions provided above serve just as an illustration of the leading contributions. The numerical results illustrated below are based on a more detailed computation, adapting to the 2HD + a case the complete expressions provided in Ref. [74], and including all the additional Higgs bosons running in the loops.

Figure 5 shows the value of Δa_μ as a function of M_a for model points obtained by making a parameter scan, according to the ranges listed in Eq. (29), with the exception of M_a for which the upper bound $M_a \leq 200$ GeV is used. This is due to the fact that the low-M_a regime is the most relevant for $(g-2)_\mu$. These points comply with theoretical constraints on the parameters of the scalar potential and with electroweak data (assuming the SM fit).

The four panels of the figure consider individually the four different Yukawa configurations, namely, type I (red points), II (blue points), X (green points), and Y (orange points). The results are compared to the 1σ (2σ) region of the Fermilab measurement drawn in green (yellow). As can be seen, the type I and type Y models, featuring $\tan\beta$ suppressed interactions of the neutral Higgs bosons with the muon, provide a too small contribution to the $(g-2)_\mu$ anomaly, far below the experimental bands.

Hence, a sufficiently large contribution to a_μ can be achieved only in the type II case when the mass of a is less than a few 10 GeV, while the contribution in the type I and type Y scenarios is far too small. In the type X model, on the contrary, the contribution can get close to the experimental sensitivity but falls short to reach the experimental bands. The reason for such a behavior is that, in type II, it is the b-quark loop contribution that is enhanced by $\tan\beta$ (both g_{abb} and $g_{a\mu\mu}$ are proportional to $\tan\beta$) while, in type X, only the loop involving τ leptons (which has a lower mass and no color factor compared to b quarks) contributes significantly since only $g_{a\ell\ell} \propto \tan\beta$. As already discussed in Ref. [22], the a contribution can be made sufficiently large in the type X case as to explain the $(g-2)_\mu$ excess by invoking extremely large $\tan\beta$ values, $\tan\beta \approx 80$. While they lead to a nonperturbative b Yukawa coupling in the type II scenario, these $\tan\beta$ values are acceptable in type X, as the coupling g_{abb} is not enhanced and the τ-lepton coupling is still perturbative as a result of the smaller mass. Such extreme assignment of the value of $\tan\beta$ has not been considered in our present study, as we assume $\tan\beta \leq 60$ in all cases. For this reason, contrary to Refs. [22,23], no model points are present in the experimentally favored bands.

E. Constraints from direct Higgs searches

The most stringent constraints on some of the 2HD + a configurations come from the direct searches at colliders of the additional Higgs bosons compared to the already observed h state. As already mentioned before, bounds were already available on the 2HDM states from negative LEP2 searches at a c.m. energy up to $\sqrt{s} = 209$ GeV [60]: $M_A \gtrsim 90$ GeV in the associated production process $e^+ e^- \to hA$ and $M_{H^\pm} \gtrsim 80$ GeV in the pair production process $e^+ e^- \to H^+ H^-$. These bounds are independent of the value of $\tan\beta$ and, to a large extent, of the value of the angle α as there is some complementarity between various
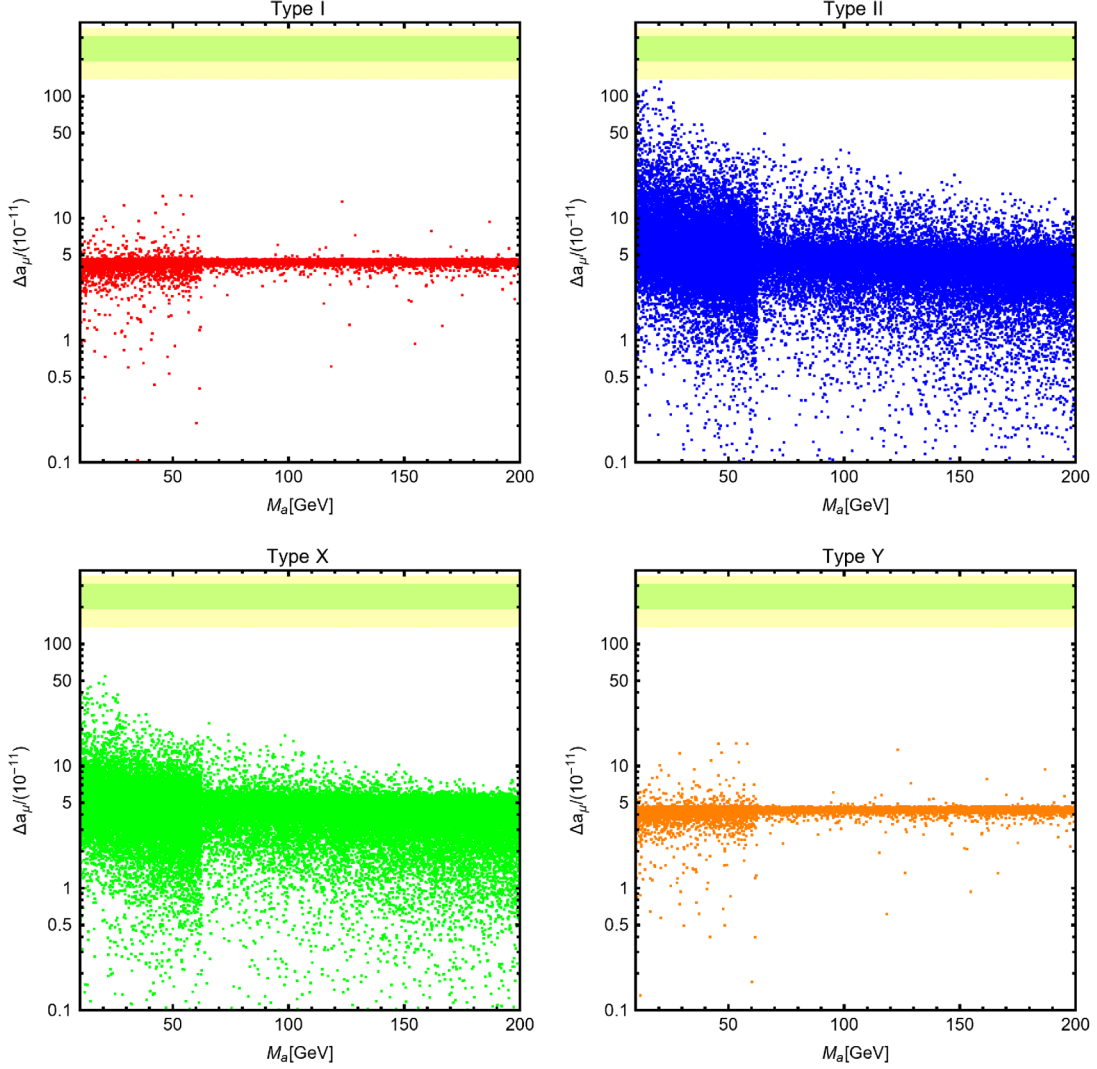
FIG. 5.   Values of Δa_μ in units of 10^{-11} as a function of M_a for the four 2HD + a model types. The colored points are obtained from a scan of the parameters discussed in the text.

processes. Added to that, one has the *ad hoc* assumption of $M_H > M_h = 125$ GeV that we have introduced from the start and which is also favored by LEP2 and present data.[6]

In the case of a light pseudoscalar a with $M_a = \mathcal{O}$ (a few 10 GeV), there are constraints from LEP1 at high $\tan\beta$ for the type II and X models via searches of associated production $e^+e^- \to b\bar{b}a$ and $e^+e^- \to \tau^+\tau^-a$ [75,76]. In addition, besides constraints from searches of exotic $Z \to a\gamma$ decays induced by heavy fermion or Higgs boson loops at LEP1 [76], there must also be a constraint from the associated production process $e^+e^- \to ha$ at LEP2 when there is significant Aa mixing and one is outside

the alignment limit as to make the coupling $g_{haZ} \approx \sin\theta\cos(\beta - \alpha)$ nonzero, as is particularly the case in the type I scenario; see Fig. 1.

More significant portions of the parameter space of the 2HD + a model have been probed by direct Higgs searches at the LHC, in particular, at a c.m. energy of $\sqrt{s} = 13$ TeV with the full collected luminosity of 139 fb^{-1} [77–84] as will be summarized below.

1. Single production of the heavy H/A and $H^\pm$ states

At the LHC, the heavy 2HDM neutral bosons $\Phi = H, A$ can be searched for in several channels, the most important one being their production in the gluon-fusion process as single resonances via loops of heavy quarks and their decay into the clean $\tau^+\tau^-$ final states [77,78]:

$$pp \to gg \to \Phi = H/A \to \tau^+\tau^-. \tag{34}$$

---

[6]There is, though, still the possibility of a light Higgs with a mass $M_H \approx 96$ GeV [38,39] for which there was a slight excess of events at LEP2 and also more recently in CMS. We will not consider this possibility.

The experimental outcome strongly depends on the type of scenario and on the value of $\tan\beta$. Most of the ATLAS and CMS analyses have been performed in two benchmark scenarios of the MSSM (more precisely, the so-called hMSSM [85,86] and $M_h^{\max}$ [87] scenarios) which has a type II configuration with the additional constraint of being close to the decoupling regime that is similar to alignment, i.e., with $\alpha \simeq \beta - \frac{\pi}{2}$, making the Φ states have similar couplings, with the additional constraint of being almost degenerate in mass, $M_H \approx M_A$.

At high $\tan\beta$, that is, $\tan\beta \gtrsim 10$, the dominant contribution in $gg \to H/A$ production is due to loops of b quarks that have enhanced couplings, $g_{\Phi bb} \simeq \tan\beta$. In this case, the process is supplemented by contributions from initiated b-quark fusion, $b\bar{b} \to H/A$ which has a comparable rate. The Φ states mostly decay into b quarks and τ-lepton pairs with respective branching ratios $\mathrm{BR}(\Phi \to b\bar{b}) \approx 90\%$ and $\mathrm{BR}(\Phi \to \tau^+\tau^-) \approx 10\%$ as one also has $g_{\Phi\tau\tau} = \tan\beta$. All other decays are suppressed: The bosonic ones are absent in the alignment limit, and the decays into top quark pairs, for Φ masses above the $t\bar{t}$ threshold $M_\Phi \gtrsim 350$ GeV which is favored by constraints from flavor physics, have suppressed rates as $g_{\Phi tt} = 1/\tan\beta$.

At low $\tan\beta$, i.e., $\tan\beta \lesssim 3$, the $gg \to \Phi$ cross section is mostly generated by loops of top quarks which have couplings that are not strongly suppressed or are even enhanced for $\tan\beta < 1$; the yield of $b\bar{b}$ fusion becomes negligible in this case. At the decay end, the only relevant mode would be $\Phi \to t\bar{t}$ above the favored mass range of $M_\Phi > 2m_t$, with an almost unit branching ratio. One would, thus, have the partonic process

$$gg \to \Phi = H/A \to t\bar{t} \qquad (35)$$

for the Higgs signal. One then needs to consider the large QCD background from the process $gg \to t\bar{t}$ as well as its interference with the signal, as both have the same initial and final states, rendering the interpretation of the searches more problematic [88].

Some of these features are also present at intermediate $\tan\beta$ values, with $3 \lesssim \tan\beta \lesssim 10$, where the H/A couplings to b and t quarks are comparable and not strong enough. The production rates are not large, and there is a competition between the $b\bar{b}$ and $t\bar{t}$ decay modes even for H/A masses above the $2m_t$ threshold. Any new decay channel into particles that do not have suppressed couplings to the Higgs bosons could be important and even dominating. This would be the case of, for example, invisible decays of the A state into pairs of the DM particles, $A \to \chi\chi$, which is not detectable in this particular channel. Concerning the CP-even H state, there is the possibility of $H \to aa$ decays, if the coupling g_{Haa} is not too small, which would lead to complicated topologies with, e.g., $4b$, $2b2\tau$, and 4τ final states.

In the case of the charged Higgs state, besides the LEP bound $M_{H^\pm} \gtrsim 80$ GeV, there are searches at LHC (and the Tevatron) of top quark decays $t \to bH^+$ with the subsequent decay $H^- \to \tau\nu$ and eventually $H^- \to c\bar{s}$, leading to an exclusion of the mass range $M_{H^\pm} \lesssim m_t \approx 170$ GeV for any value of $\tan\beta$ [89]. For the larger $H^\pm$ masses that are still allowed by flavor constraints, the dominant process would be the associated production mechanism

$$gb \to tH^\pm \quad \text{with} \quad H^\pm \to tb, \tau\nu, \qquad (36)$$

at low $\tan\beta \lesssim 1$ or large $\tan\beta \gg 1$ values, for which either the t or the b component of the $g_{H^\pm tb}$ coupling is strong. In the former case, $H^\pm$ will decay into tb final states with almost 100% probability, while, in the second case, one would have the tb and $\tau\nu$ final states with branching ratios of $\mathrm{BR}(H^+ \to tb) \approx 90\%$ and $\mathrm{BR}(H^+ \to \tau\nu) \approx 10\%$. Both these topologies have been searched for at the LHC, but at present only loose constraints have been set at low $\tan\beta \lesssim 1$ and high $\tan\beta \gtrsim 50$ [89] which do not compete with the limits from $b \to s\gamma$.

Recently, an updated analysis of these constraints has been performed [90] in the context of the MSSM (and, more precisely, of the hMSSM in which the value $M_h = 125$ GeV is enforced) which has the following simplified features in the decoupling limit $\alpha \simeq \beta - \frac{\pi}{2}$ (which is reached as soon as $M_A \gtrsim 500$ GeV and it should be valid in order to cope with the h signal strengths): (i) the same Higgs couplings as in the type II 2HDM in the alignment limit, (ii) only values $1 \lesssim \tan\beta \lesssim 50$ are allowed, and (iii) the approximate mass degeneracy, $M_H \simeq M_A \simeq M_{H^\pm}$. Using the full LHC data of 139 fb^{-1} collected at an energy of 13 TeV, and considering the three main search channels of Eqs. (34)–(36), one obtains the excluded area at the 95% C.L. of the $[M_A, \tan\beta]$ plane shown in Fig. 13 in Ref. [90].

From this figure, one can see that the $pp \to H/A \to \tau^+\tau^-$ search is extremely efficient and excludes values of M_A below 1 TeV for the entire range $\tan\beta \gtrsim 10$. The exclusion extends to $\tan\beta \approx 5$ for $M_A \approx 700$ GeV and $\tan\beta \gtrsim 20$ for $M_A \approx 1.5$ TeV. The search in the $H/A \to t\bar{t}$ final state is much less constraining, as only values $M_A \lesssim 750$ GeV are excluded for $\tan\beta \lesssim 2$. The search for the charged Higgs boson in the mode $H^+ \to t\bar{b}$ excludes masses below $M_{H^\pm} \lesssim 700$ GeV at both low $\tan\beta \lesssim 2$ and high $\tan\beta \gtrsim 40$ values.

In our 2HD + a context, these limits can be overcome or loosened in the following cases:

One can first have a nondegenerate mass scenario, $M_H \neq M_A$, in such a way that, in the $pp \to H/A \to \tau^+\tau^-$ process, one looks for two resonances rather than a single one. This lowers the excluded values of $\tan\beta$ by approximately a factor $\sqrt{2}$. The mass nondegeneracy would also allow cascade decays, such as $H \to AZ$, $A \to HZ$, and

$H/A \rightarrow H^{\pm}W^{\mp}$ depending on the hierarchy of masses, which lead to lower $\tau\tau$ rates and, hence, looser bounds.

The cross section for A production is lowered by a factor $\cos^2\theta$ compared to the MSSM. In addition, as noted previously, one could have the additional decays $A \rightarrow \chi\chi$ as well as $H \rightarrow aa$ in the case of the CP-even Higgs (in addition to the cascade decays above) which would lead to less severe bounds, in particular, at intermediate $\tan\beta$ values.

Finally, in the charged Higgs case, one has the additional decay $H^{\pm} \rightarrow aW^{\pm}$ [91] which is always favored by phase space and which, for the sizable Aa mixing needed for DM issues, can compete with the $H^+ \rightarrow tb$ mode (in addition to the possible $H^{\pm} \rightarrow W + H/A$ decays).

All these features would make the LHC heavy Higgs searches less constraining in our model compared to the MSSM. Nevertheless, they still exclude a substantial area of the parameter space of the model as will be seen shortly when we move to our numerical analysis. Before that, let us first adapt all these discussions held for the type II scenario to the other 2HD + a model configurations, namely, type I, X, and Y.

First, in the type Y scenario, Φ production is the same as above, since the Higgs couplings to t and b quarks are as in type II. In turn, as the Higgs couplings to τ leptons are now $\propto 1/\tan\beta$, only the decay mode $H/A \rightarrow b\bar{b}$ is relevant at high $\tan\beta$, and it is subject to a large QCD background which makes it difficult to probe at the LHC. At low $\tan\beta$ values, the situation is similar as in type II, as only the channel $\Phi \rightarrow t\bar{t}$ is relevant. In the case of the $H^{\pm}$ state, the search channel $gb \rightarrow tH^{\pm} \rightarrow ttb$ is the only relevant one at low $\tan\beta$ but also at high $\tan\beta$, as the coupling $g_{A\tau\tau} \propto 1/\tan\beta$ is suppressed in this case.

In the type I scenario, the main process for H/A production is again gluon fusion, but it is generated by top quark loops which give large rates only at low $\tan\beta$ values, $\tan\beta \lesssim 3$ when $g_{\Phi tt} \propto 1/\tan\beta$ is strong. In the strict alignment limit, the dominant decay modes for $M_{\Phi} \gtrsim 350$ GeV are into top quarks with branching ratios of the order of 100% unless there are exotic decays. For the $H^{\pm}$ states, the only relevant production process would be again $gb \rightarrow tH^{\pm}$ with a large rate at low $\tan\beta$ where $H^+ \rightarrow t\bar{b}$ decays have a unit branching ratio.

Finally, in the type X scenario, neutral Higgs production is as in the type I case and is important only at low $\tan\beta$ values, with exclusive $\Phi \rightarrow t\bar{t}$ decays for Higgs masses above the $2m_t$ threshold. For the $H^{\pm}$ state, the production is also as in type I, but, at high $\tan\beta$, BR($H^+ \rightarrow \tau\nu$) will be dominant thanks to the enhanced $g_{H^{\pm}\tau\nu} \propto \tan\beta$ coupling.

An important remark to be made at this stage is that there is another source of H, A, and $H^{\pm}$ states at the LHC whose rates do not depend on $\tan\beta$ in the alignment, namely, production in pairs in the Drell-Yan processes $q\bar{q} \rightarrow H^+H^-, HA$ and $q\bar{q}' \rightarrow HH^{\pm}, AH^{\pm}$. These occur through virtual gauge boson exchange and have rates that are unsuppressed by the scalar-vector couplings g_{HAZ} and $g_{H^{\pm}HW}$ which are maximal in the alignment limit, Eq. (5). The production rates are limited only by phase space, but, as we have already the constraint $M_{H,A,H^{\pm}} \gtrsim 500$ GeV in most cases, they should be small and these channels, which have not yet been considered by the experiments, are or should not be very constraining.

In order to determine LHC limits for the scenario under scrutiny, we have computed the production cross sections of the neutral Higgs bosons using the package SuSHI [92,93] in the four flavor-preserving 2HDMs. The results have been then adapted to the corresponding 2HD + a case by applying suitable $\sin^2\theta$ and $\cos^2\theta$ factors.

We have again performed multiple scans, considering individually the different Yukawa configurations, over the ranges described in Eq. (29), applying together with theoretical, electroweak, flavor, and Higgs signal strengths, the following constraints.

Next we discuss the limits from the search in the process $pp \rightarrow H/A \rightarrow \tau^+\tau^-$ *as given in Ref.* [77].—As already pointed out, this is probably the most constraining search, impacting, in particular, our 2HD + a model. We have ignored the limits from the processes $gg \rightarrow H/A \rightarrow t\bar{t}$ and $gb \rightarrow H^-t \rightarrow tb, \tau\nu$, as these are sensitive only to small areas of the parameter space that are excluded by the previous channel and by B-physics constraints.

In order to consider also the region outside the alignment limit, which is not realized everywhere in particular in the type I scenario, we also include the limits from the two search channels $pp \rightarrow A \rightarrow Zh$ [94] and $pp \rightarrow H \rightarrow ZZ$ [95]. Both have rates that are suppressed by the factor $g_{HVV} = g_{hAZ} = \cos(\beta - \alpha)$ which vanishes in the alignment limit.

To cope with the possibility of a significant mass splitting between the masses of the heavy neutral Higgs bosons, $|M_H - M_A| \gtrsim M_Z$, we also include the search channels $pp \rightarrow A \rightarrow ZH$ [96] and $pp \rightarrow H \rightarrow ZA$ [97]. Again, in the alignment limit, the decays $H \rightarrow AZ$ or $A \rightarrow HZ$ depending on the mass hierarchy, are not suppressed since $g_{HAZ} = 1$.

As will be discussed in the next subsection, we will also include the possible decay $H \rightarrow Za$ which is always phase-space allowed in our context, since we assume $M_H \gg M_a$. This is done by considering one of the previous channels, $pp \rightarrow H \rightarrow ZA$ [97], formulated in the 2HDM with $M_H \gg M_A$, and adapting it to the case $pp \rightarrow H \rightarrow Za$.

Finally, we have considered again the $pp \rightarrow H \rightarrow Za(A)$ and $pp \rightarrow A \rightarrow ha$ processes in the specific case in which the final state pseudoscalar states decay dominantly into invisible DM pairs [98,99]. For these searches we have adopted the upper bounds on the production cross section times branching ratio determined in [18].

The constraints from the $pp \rightarrow H/A \rightarrow \tau^+\tau^-$ channel are shown in Fig. 6 in the $[M_A, \tan\beta]$ plane in the four configurations for some choices of the a parameters, $M_a = 100$ and 50 GeV and $\sin\theta = 1/\sqrt{2}$ or 0.1. In all cases, the
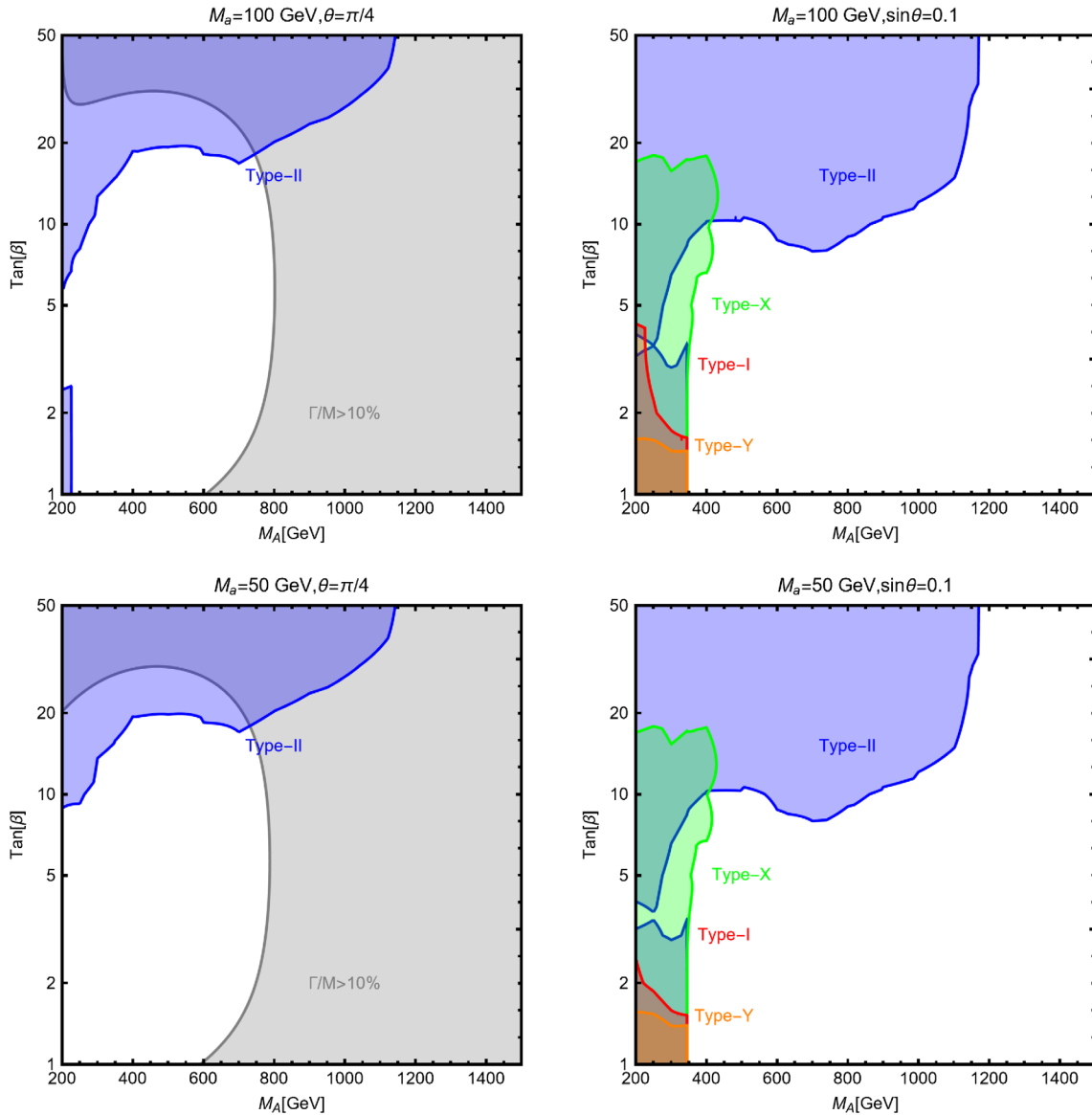
FIG. 6. LHC limits from searches in the $pp \to H/A \to \tau^+\tau^-$ channel in the $[M_A, \tan\beta]$ plane for different assignments of the $(M_a, \sin\theta)$ pair and assuming $M_H = M_A = M_{H^\pm} = |M|$. The different colored regions correspond to the exclusions for a given Yukawa configuration, namely, type I (red), type II (blue), type X (green), and type Y (orange). In the panels with $\theta = \frac{\pi}{4}$, the gray regions correspond to the case in which at least one between the H and A states has a total decay width that exceeds 10% of its mass.

equality $M_H = M_{H^\pm} = M_A$ has been assumed. As can be seen, while the constraint is strong in the type II case, it is less severe in the other configurations and only masses below the $t\bar{t}$ threshold, $M_A < 350$ GeV, are excluded for $\tan\beta$ values of the order of 20 in type X and 2 in type I and Y scenarios. In the left panels, we also show the regions (in gray) in which the total decay width of either the A or H states exceeds 10% of its mass. While this condition should not be strictly regarded as a constraint, it should, however, be noted that most of the bounds from resonance searches are given assuming the narrow width approximation. The gray regions, thus, require a dedicated study which is nevertheless beyond our scope here.

The model points passing all constraints are shown in Fig. 7, distinguishing as usual the four different Yukawa configurations. From the left to the right columns, displayed are the viable model points in the bidimensional planes[7] $[M_A, \tan\beta]$, $[M_H, \tan\beta]$, $[M_H^\pm, \tan\beta]$, and finally $[\cos(\beta - \alpha), \tan\beta]$.

As expected, the type II case appears to be the most constrained one, allowing only for values of M_A between

---

[7]The collider constraints discussed above have a negligible impact on the $\sin\theta$ parameter, at least for values within the range chosen for the scan. For this reason, we do not display plots as functions of $\sin\theta$.
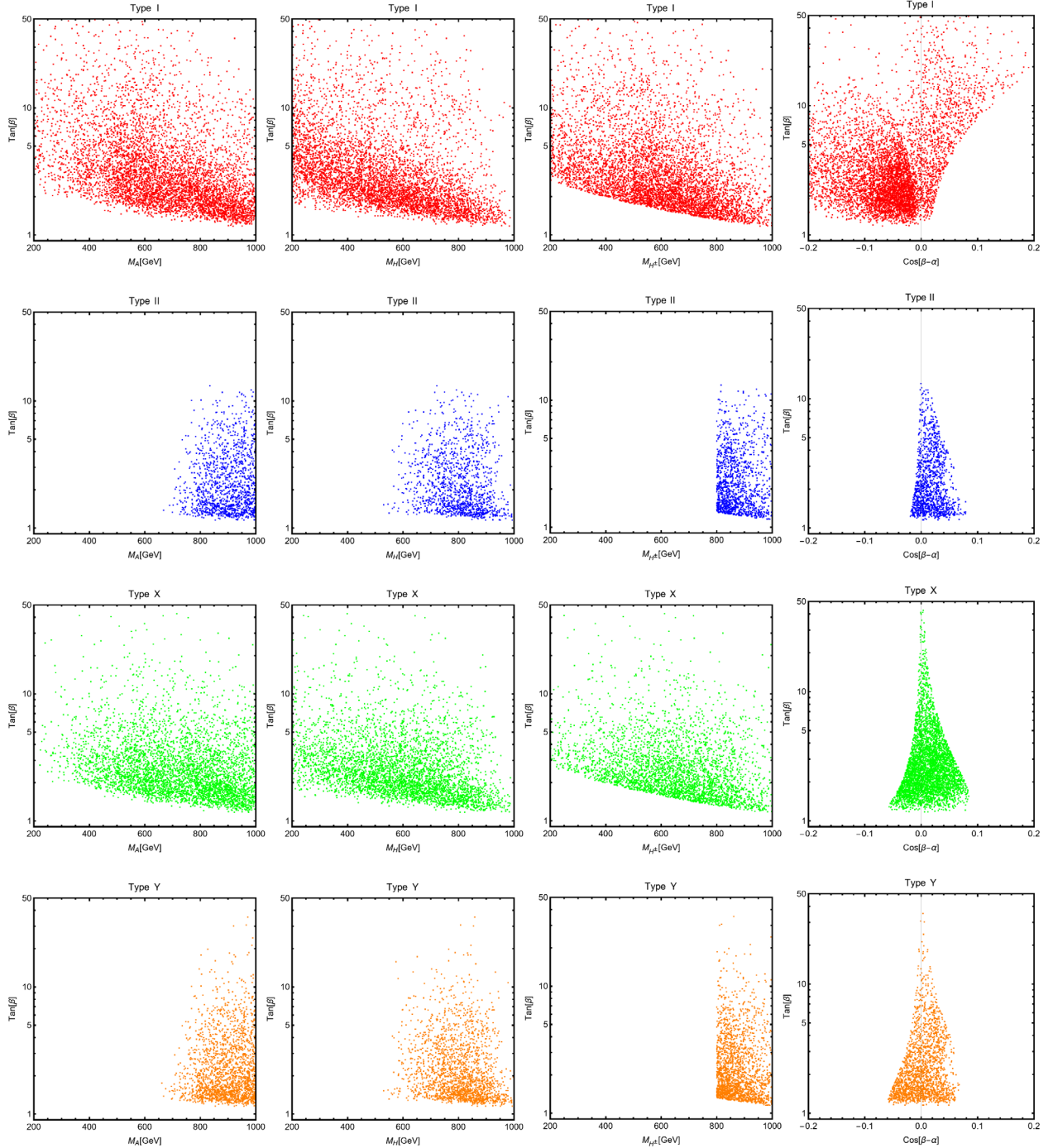
FIG. 7. Model points for the four flavor-preserving Yukawa configurations of the 2HD + a model, which comply with theoretical constraints, the bounds from flavor and Higgs signal strengths, and LHC searches of extra Higgs states (see the main text for details). The points which pass these constraints are shown from left to right, in the $[M_A, \tan\beta]$, $[M_H, \tan\beta]$, $[M_{H^\pm}, \tan\beta]$, and $[\cos(\beta-\alpha), \tan\beta]$ planes.

700 GeV and 1 TeV and limiting $\tan\beta$ to $2 \lesssim \tan\beta \lesssim 15$. The lower limit on M_A is essentially due to the bound from $b \to s\gamma$. While the latter strictly applies to the mass of the $H^\pm$ boson, it impacts also the other mass eigenstates, since theoretical and electroweak constraints do not allow for arbitrary mass splittings. The low $\tan\beta$ region is ruled out

by the constraints on the $B_s \to \mu^+\mu^-$ process, while high $\tan\beta$ values are disfavored by searches of neutral Higgs decaying into $\tau^+\tau^-$.

As already mentioned, the lower bound is weaker compared to the hMSSM case as a result of the suppression of the A production cross section as well as its reduced

decay branching fraction into τ pairs. The allowed parameter region is similarly small for the type Y model. The only difference is the absence of a lower bound on $\tan\beta$, since searches of $\tau^+\tau^-$ resonances are not effective in this case. The only constraint is represented by the Higgs signal strengths which require one to be close to the alignment limit for values $\tan\beta \gtrsim 10$.

The type I and X models are, on the contrary, very weakly affected by collider constraints. The most effective bound is the one on low $\tan\beta$ coming from $B_s \to \mu^+\mu^-$. It is also worth noticing that our analysis shows that searches for $Zh/ZH/ZA/ZZ$ events lead to weaker bounds than the ones obtained by the corresponding searches in the ordinary 2HDM [94–97]. This is due to the presence of additional decay channels such as $H \to aa, aA$ or $A \to ha$ which reduce the branching fractions of the considered signals. More dedicated experimental searches for the production of light pseudoscalars from the decays of heavy resonances are needed to efficiently probe the 2HD + a model, besides the type II.

2. Constraints on the light a boson

Turning to the case of the light pseudoscalar a boson, in addition to the pre-LHC bounds discussed in the beginning of this section, there is first a severe constraint from searches at the LHC in the decay $h \to aa$ of the SM-like Higgs boson for masses $M_a \lesssim 62$ GeV [14,16,19]. The partial decay width involves the λ_{haa} coupling of Eq. (15) and is given by

$$\Gamma(h \to aa) = \frac{|\lambda_{haa}|^2}{32\pi M_h}\sqrt{1 - 4M_a^2/M_h^2}. \qquad (37)$$

This process has been intensively searched for by the ATLAS and CMS Collaborations in various topologies, namely, $2b2\mu$, $2b2\tau$, $4b$, $jj\gamma\gamma$, $2\mu2\tau$, and 4τ, and is also constrained by the h invisible branching ratio which can be inferred from the Higgs signal strengths discussed earlier and which was measured to be BR($h \to$ inv) < 0.11 [100]. To evade this constraint, a very small coupling is required, $\lambda_{haa}/M_h \lesssim \mathcal{O}(10^{-3})$. Such a value is achieved by choosing for the parameters entering Eq. (15), e.g., $\sin\theta$ and $\lambda_{1P,2P}$, *ad hoc* values that lead to an almost vanishing coupling. Hence, one should rely on blind spots on the coupling, and we refer to Ref. [22] for a more detailed discussion that involves the possibility of including radiative corrections to λ_{haa} that are generated by loops of b and t quarks with enhanced couplings.

Searches of mono-Z and mono-h signatures, corresponding to $pp \to Za, ha$ with $a \to \chi\chi$, represent a very interesting tool for probing the 2HD + a model; see, e.g., Ref. [101]. These have been already discussed in the previous section.

The most severe constraints on a with a significant mixing with the heavier A comes from searches of light resonances decaying into muon pairs which have been revived recently [20]:

$$pp \to gg, \qquad b\bar{b} \to a \to \mu^+\mu^-. \qquad (38)$$

As in the case of H/A discussed above, the gluon-fusion process is mediated by t-quark loops at low and b-quark loops at high $\tan\beta$ in scenarios like type II and Y; in the high-$\tan\beta$ case, additional contributions from b-quark fusion should also be included. The decay branching ratio BR($a \to \mu^+\mu^-$) is important only in type II and X scenarios at high $\tan\beta$ when the coupling is $g_{a\ell\ell} = \sin\theta\tan\beta$.

Two recent searches have been conducted in this channel, one by CMS [102] and another one by the LHCb Collaboration [103]. The latter, which has been interpreted only in the type Y configuration when setting $\tan\beta = \frac{1}{2}$ and assuming $M_a \gtrsim 10$ GeV, is the strongest.

We have recast the resulting bound of this search in the $[M_a, \sin\theta]$ plane and for larger a masses up to $M_a = \frac{1}{2}M_h$. The production rate $\sigma(pp \to a)$ has been calculated using the programs HIGLU [104] and for the decay rate BR($a \to \mu^+\mu^-$) using the program HDECAY [105,106], and we have compared the obtained result with the corresponding one given by CMS [102]. The excluded regions in the $[M_a, \tan\beta]$ plane and for different assignments of $\sin\theta$ are shown in Fig. 8, in which the four panels correspond to the four Yukawa configurations, namely, type I, II, X, and Y. The mass M_a is varied from 10 to 62 GeV, while the CP-odd mixing angle was assigned the values $\sin\theta = 0.15, 0.25, 0.5$, and 0.7.

In agreement with the findings of Refs. [22,23], as well as in the earlier discussion in Ref. [20], the strongest constraint applies on the type II scenario in which both the production and decay rates are enhanced as $g_{abb} = g_{a\ell\ell} \propto \tan\beta$. In the absence of additional decays of the a state, it basically rules out, for $\sin\theta \geq 0.25$, the whole parameter space for which the considered searches have sensitivity. A weaker but still sizable constraint is obtained in the type X model, as a consequence of the $\tan\beta$ enhancement of the coupling of the a state with muons. Much weaker are the limits which apply in the type I and Y models, for which one obtains the lower bounds $\tan\beta \gtrsim 2$ (5) for $\sin\theta = 0.5$ (0.7).

Finally, let us note that, for a nonzero Aa mixing, one would also have the possibility of pair production of the H/A and $H^\pm$ states with a light pseudoscalar a, $q\bar{q} \to Ha$ and $q\bar{q}' \to H^\pm a$ which occur through virtual vector boson exchange. When $\theta = \frac{\pi}{2}$, the cross sections are maximal and the processes are favored by phase space, as we expect the a state to be much lighter than the A and $H^\pm$ bosons. They lead to interesting topologies with four fermions in the final states like $H \to b\bar{b}, t\bar{t}$ and $H^+ \to tb$ while one should have $a \to \tau\tau, b\bar{b}$ and even $a \to \mu^+\mu^-$ decays for the light a. Nevertheless, except for the Ha case which has been adapted from the 2HDM CMS search in the channel $pp \to AH$ [97] discussed before, these processes have not been

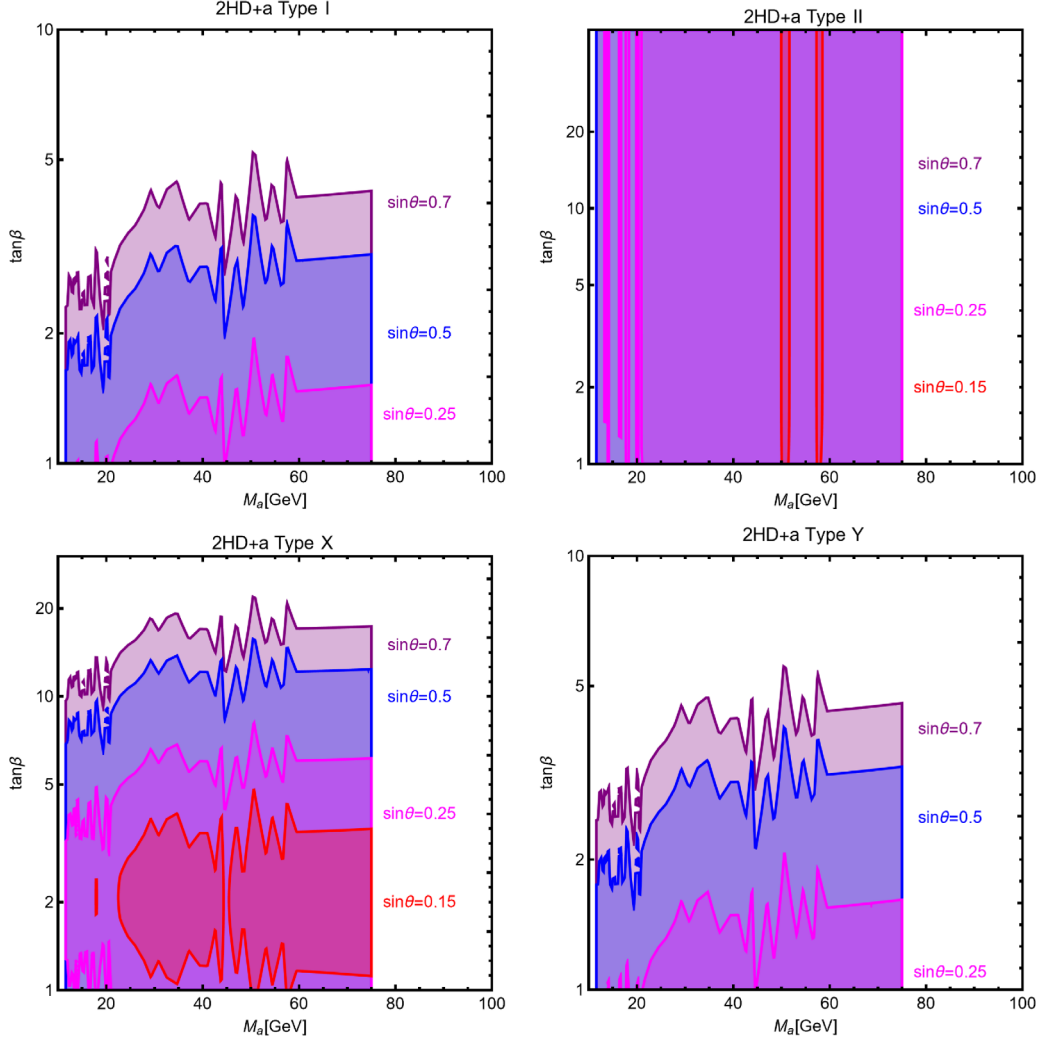FIG. 8. Excluded regions in the $[M_a, \tan\beta]$ plane from searches in the process $gg, b\bar{b} \to a \to \mu^+\mu^-$ in the four types of Yukawa configurations. Each colored region corresponds to different assignments of $\sin\theta$ reported in the panels. Note, in particular, that the whole region $M_a \lesssim 75$ GeV is ruled out for the type II configuration.

explicitly considered by the ATLAS and CMS experiments and there is barely a way to set strong limits. One expects, though, that these limits are not stronger than the ones from the $gg \to a \to \mu^+\mu^-$ process that we discussed here.

IV. THE DARK MATTER AND COMBINED CONSTRAINTS

A. The DM relic density

In our $2\text{HD} + a$ scenario, we have introduced a dark matter particle candidate which was assumed to be a Dirac fermion χ that is isosinglet under the SM gauge group (no substantial change of the results is expected in the case in which the DM was of Majorana type). We also introduced a discrete Z_2 symmetry under which the new DM field is odd and transforms as $\chi \to -\chi$ while all other fields are even and transform like $\phi \to +\phi$, making that the χ particle cannot decay into SM particles and is, hence, absolutely

stable as it should be. Because it is not charged under the $SU(2)_L$ group, χ has no couplings to gauge bosons and, by virtue of the Z_2 symmetry, it couples to Higgs bosons only in pairs.

Starting from an initial coupling $iy_\chi a^0 \bar{\chi} i\gamma^5 \chi$ of the χ states with the a^0 boson (the χ states do not couple to the 2HDM bosons), and, after electroweak symmetry breaking, the DM will interact with the two pseudoscalar Higgs bosons according to the following Lagrangian:

$$\mathcal{L}_{\text{DM}} = y_\chi(\cos\theta a + \sin\theta A)\bar{\chi} i\gamma_5\chi. \tag{39}$$

There are no couplings of the DM fermion to the CP-even Higgs bosons at the tree level, a feature which will have major consequences as will be discussed shortly.

The DM fermion will have the correct cosmological relic density, as we will assume the conventional freeze-out
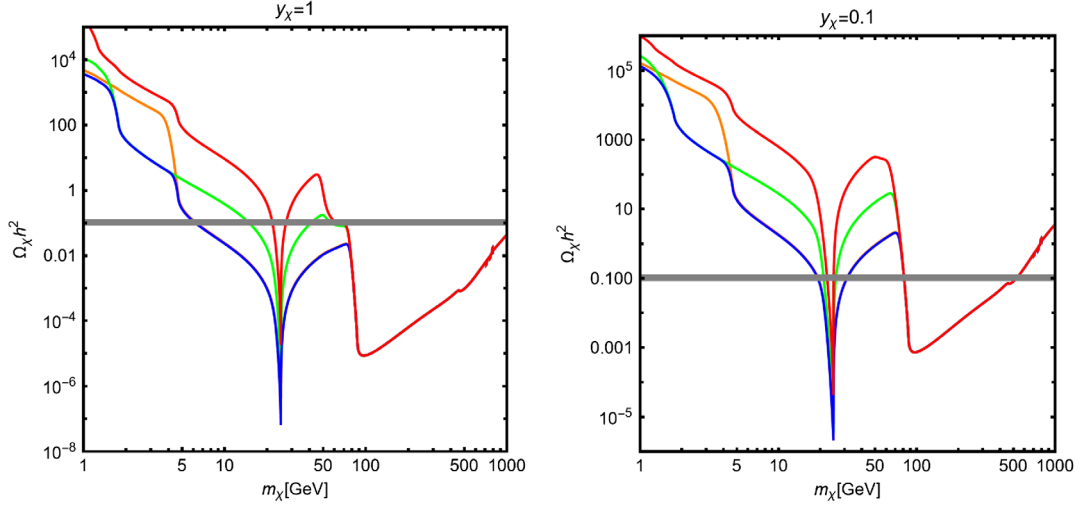
FIG. 9. The DM relic density as a function of the DM mass for $\tan\beta = 5$, $\cos(\beta - \alpha) = 0$, $\theta = \frac{\pi}{4}$, $M_a = 50$ GeV, and $M_{H,A,H^{\pm}} = 800$ GeV. The different colored lines stand for type I (red), II (blue), X (green), and Y (orange), and the left (right) panels refer to $y_\chi = 1$ (0.1). In each panel, we see four distinct curves in the region $m_\chi \lesssim 100$ GeV. This is due to the fact that in this region the main annihilation channel is into SM fermion pairs and the latter is sensitive to the Yukawa configuration. At higher DM mass, the lines overlap, since the relic density is mostly accounted for annihilations with bosonic final states, mostly ha.

mechanism in which the experimentally favored value measured by the Planck Collaboration [12],

$$\Omega_\chi h^2 = 0.12 \pm 0.0012, \qquad (40)$$

is achieved if the DM thermally averaged pair annihilation cross section has a value in the appropriate range. For the scenario that we are interested in here, the most relevant DM annihilation channels are the following final states that occur via a/A boson exchange:

$$\chi\chi \to a^*, \qquad A^* \to \tau^+\tau^-, b\bar{b}, \quad \text{and} \quad t\bar{t}, \qquad (41)$$

the latter channel occurs only when kinematically accessible, i.e., for $m_\chi \gtrsim 175$ GeV. The weight of the individual channels depends on the type of Yukawa coupling configuration, namely, type I, II, X, and Y, as well as on the value of $\tan\beta$. In addition to annihilation into SM fermion pairs, the following final states could also be relevant:

$$\chi\chi \to a^*, \qquad A^* \to ha, Zh, \quad \text{and} \quad \chi\chi \to aa, \qquad (42)$$

where, in the last case, the aa final state is obtained via t-channel exchange of the DM. In the first channel, a^* exchange should be suppressed for $m_\chi \lesssim \frac{1}{2}M_h$ as the coupling g_{haa} should be very small as to make the decays $h \to aa$ very rare. The second channel with a Zh final state is possible only outside the alignment limit when the coupling g_{hZa} is nonzero.

The numerical determination of the DM relic density is achieved through the implementation of the different 2HD + a scenarios into the package micrOMEGAs

[107–109]. For completeness, the annihilation channels into aA, AA, ZH, and $W^{\pm}H^{\mp}$ final states, which open up only for DM masses above several hundred GeV, have also been included.

A simple illustration of the impact of the relic density constraint is provided by Fig. 9. Here, we have considered the same benchmark for all the four Yukawa configurations, namely, $\cos(\beta - \alpha) = 0$, $\tan\beta = 5$, $\theta = \frac{\pi}{4}$, $M_H = M_A = M_{H^{\pm}} = M = 800$ GeV, and $M_a = 50$ GeV, and computed the relic density as a function of the DM mass for two assignments of the coupling y_χ, namely, $y_\chi = 1$ (left) and $y_\chi = 0.1$ (right). In each panel, the different colored curves represent the different Yukawa configurations, namely, red, blue, green, and orange for type I, II, X, and Y, respectively.[8] As can be seen, the DM relic density is sensitive to the different realizations of the 2HD + a model, in particular, in the $m_\chi \lesssim M_a$ range. Here, the relic density is mostly due to annihilations into SM pairs via s-channel mediation of the a/A states, whose cross section are sensitive to the $\tan\beta$ enhancement or suppression of the Yukawa couplings. Even for $y_\chi = 1$, for the type I and X models, the correct relic density requires the occurrence of

---

[8]Some of the important features of the figure can be understood as follows. For $m_\chi \lesssim 100$ GeV, the relic density is mostly accounted for by annihilations into SM fermion pairs, and, as the corresponding cross sections are sensitive to the Yukawa configuration, four distinct lines are visible in the figures. For $m_\chi \gtrsim 100$ GeV, DM annihilation channels into Higgs boson final states, in particular, the ha final state responsible for the sharp drop of the relic density lines, are dominant; these channels are not sensitive to the Yukawa configuration, and, hence, all the contours overlap into a single curve.

the resonant enhancement of the annihilation cross section for $m_\chi \simeq \frac{1}{2} M_a$. In turn, the type II and Y models can have the correct relic density even outside the pole region. As the DM mass increases, the relic density becomes dominated by the aa and, most importantly, ha channels whose cross sections are essentially the same for all the four $2\mathrm{HD}+a$ model types.

B. Constraints from direct and indirect detection

One of the main experimental probes of a weakly interacting and massive DM candidate is represented by direct detection (DD): namely, the search for the recoil energy deposited in a suitable detector when (elastic) scatterings between the DM particle and the atomic nuclei of the target detector occur. In this regard, the $2\mathrm{HD}+a$ scenario has the very peculiar and interesting property that spin-independent interactions, the ones which are most efficiently probed by present experiments, emerge only at the one-loop level.

The Feynman diagrams responsible for such interactions have two possible topologies shown by the two representative examples given in Fig. 10. The first diagram involves triangle vertices with one CP-even neutral Higgs boson which is coupled with the SM quarks and a pair of pseudoscalar Higgs bosons that couple to the DM state. The second topology is represented by box diagrams involving the exchange of two pseudoscalar states between the lines formed by the SM quarks and the fermionic DM candidate.

We have determined the DM scattering cross section, adopting the computation performed in Refs. [110,111] and slightly refined in Refs. [59,112,113], for instance. We have then compared the results with the strongest exclusion limit as given at the moment by the LZ Collaboration [27] (which superseded the earlier strong XENON1T limits [114]; notice that there is also a dedicated study made by the PANDA-X Collaboration [115]).

Some of the relevant annihilation channels of DM, in particular, the ones into SM fermions pairs via pseudoscalar Higgs exchange, feature an s-wave-dominated cross section; i.e., the values of the cross section at present times and at freeze-out are very close to each other. Consequently, the viable parameter space for the relic density can be probed by indirect detection (ID) experiments as well that search for the clean products of the annihilation processes. In order to account for indirect detection, we have used the limits
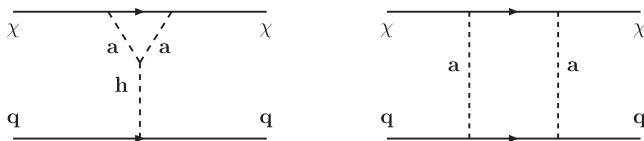

FIG. 10. Generic Feynman diagrams for the loop-induced scattering of the DM particle on quarks in the $2\mathrm{HD}+a$ model.

from searches of continuous γ-ray signals determined by the FERMI-LAT experiment in Refs. [116,117].

Before discussing our main results, obtained via scans of the parameter space, we provide in Figs. 11 and 12 two simplified illustrations of the impact of the DM constraints with some other relevant bounds, namely, the one from the invisible width of the h boson which accounts for possible $h \to aa$ decays and light a boson searches in the $pp \to a \to \mu^+ \mu^-$ mode. The two figures illustrate the limits in the $[M_a, m_\chi]$ plane for all the four flavor-preserving Yukawa configurations for some fixed assignments of the parameters $\cos(\beta - \alpha)$, $\tan\beta$, and θ. For simplicity, we have assumed mass degeneracy for the heavy 2HDM states, $M_H = M_A = M_{H^\pm} = |M|$. The two figures differ only in the assignment of the $a\chi\chi$ coupling, which has been taken to be large $y_\chi = 1$ in Fig. 11 and small $y_\chi = 0.1$ in Fig. 12. In each plot, the correct DM relic density is achieved along the black isocontours while the blue, yellow, green, and red regions are excluded, respectively, by direct detection by LZ, indirect detection by FERMI-LAT, the invisible branching ratio of the SM-like Higgs boson, and LHC searches of light resonances decaying into $\mu^+ \mu^-$ final states.

In summary, the viable parameter space for a given benchmark corresponds to the case in which the black isocontour of the relic density lies outside all the colored regions. As can be seen from Fig. 11, despite of their radiative origin, DM spin-independent interactions can be strongly constrained thanks to the high sensitivity reached by the current generation of multiton detectors. On the other hand, the scattering cross section is strongly sensitive to the DM coupling, as the spin-independent cross section of the DM on protons behaves as $\sigma^{\mathrm{SI}}_{\chi p} \propto y_\chi^4$. Moving from the $y_\chi = 1$ to the $y_\chi = 0.1$ case renders the DM direct detection limits irrelevant while it is still possible to achieve a correct relic density.

One also notices that the region $M_a \lesssim \frac{1}{2} M_h$ is completely ruled out by the bound imposed on the invisible branching ratio of the 125 GeV Higgs, $\mathrm{BR}(h \to \mathrm{inv}) \leq 0.11$. As already pointed out, the latter includes also the decay channel $h \to aa$ which can be evaded only by imposing specific conditions on the parameter of the scalar potential that leads to a very tiny λ_{haa} coupling. This has not been enforced in the benchmark considered in Fig. 12.

As one can easily imagine, it would be very hard to enclose all the features of a rich parameter space, such as the one of the $2\mathrm{HD}+a$ model, into simple bidimensional plots as the ones shown in Figs. 11 and 12. For this reason, we will present in the next section a more general analysis based on a parameter scan. Nevertheless, the results presented above have some general features which would have been only modestly affected if different assignments of the parameters had been adopted. As already pointed out, the bound on the a mass from possible h decays is very general and can be encompassed only at the price of very
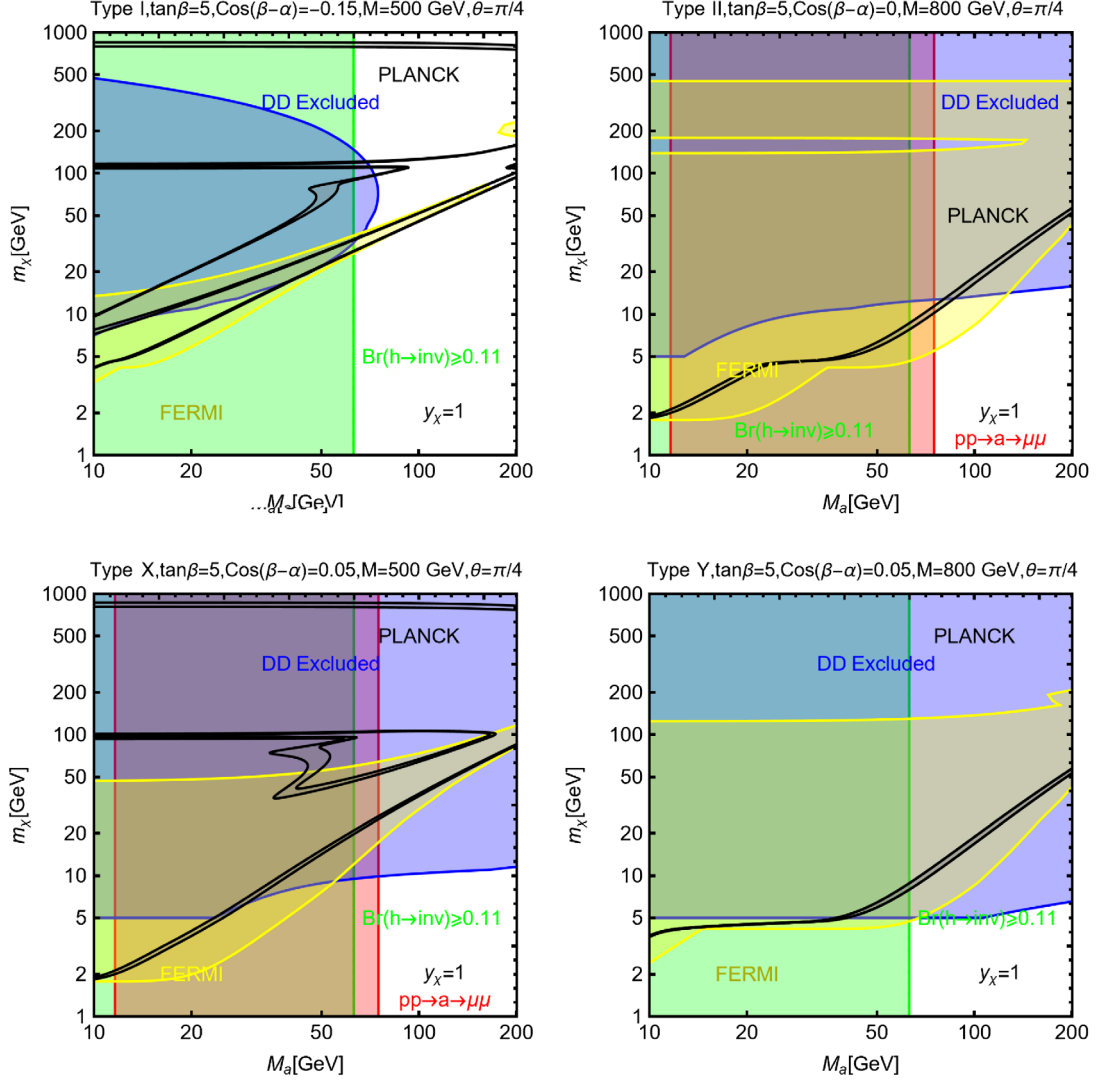
FIG. 11. DM constraints in the $[M_a, m_\chi]$ plane for some benchmark assignments of the 2HD + a model parameters in the four configurations of the Yukawa couplings. In each plot, the black isocontours correspond to the correct DM relic density, while the blue (yellow) regions represent the parameters space excluded by DM direct (indirect) detection. For comparison, the region excluded by the invisible width of the 125 GeV Higgs and by searches of light resonances decaying into $\mu^+\mu^-$ have also been shown, in green and red, respectively.

specific choices of the model parameters. For what concerns the DM relic density, the results for different parameters would be, in general, similar, but a shift of the contours toward higher or lower DM masses could occur in the figure above. In turn, the excluded regions from direct detection searches are strongly sensitive to the assignment of the model parameters. A more detailed discussion of the impact of these constraints is given in the next subsection.

C. Combined constraints

We have now all the ingredients to assess in a more systematic manner the impact of the DM constraints and to combine them with the collider ones. To achieve this task, we have conducted an analogous parameter scan as the one

considered in the previous sections but including also the parameters m_χ and y_χ that appear in the DM context. In summary, the ranges of the parameter scan are the following:

$$\tan\beta \in [1, 60], \qquad |\cos(\beta - \alpha)| < 0.2,$$

$$|M| = M_H = M_A = M_{H^\pm} \in [125 \text{ GeV}, 1 \text{ TeV}],$$

$$M_a \in [10, 400] \text{ GeV}, \qquad \sin\theta \in [0.1, 0.8],$$

$$m_\chi \in [1, 1000] \text{ GeV} \quad \text{and} \quad y_\chi \in [10^{-2}, 10],$$

$$\lambda_{1P} = \lambda_{2P} = 3. \tag{43}$$

We stress again that it is implicitly intended that the mass hierarchy between the two pseudoscalars, $M_a < M_A$, is always respected and that some simplifying assumptions,
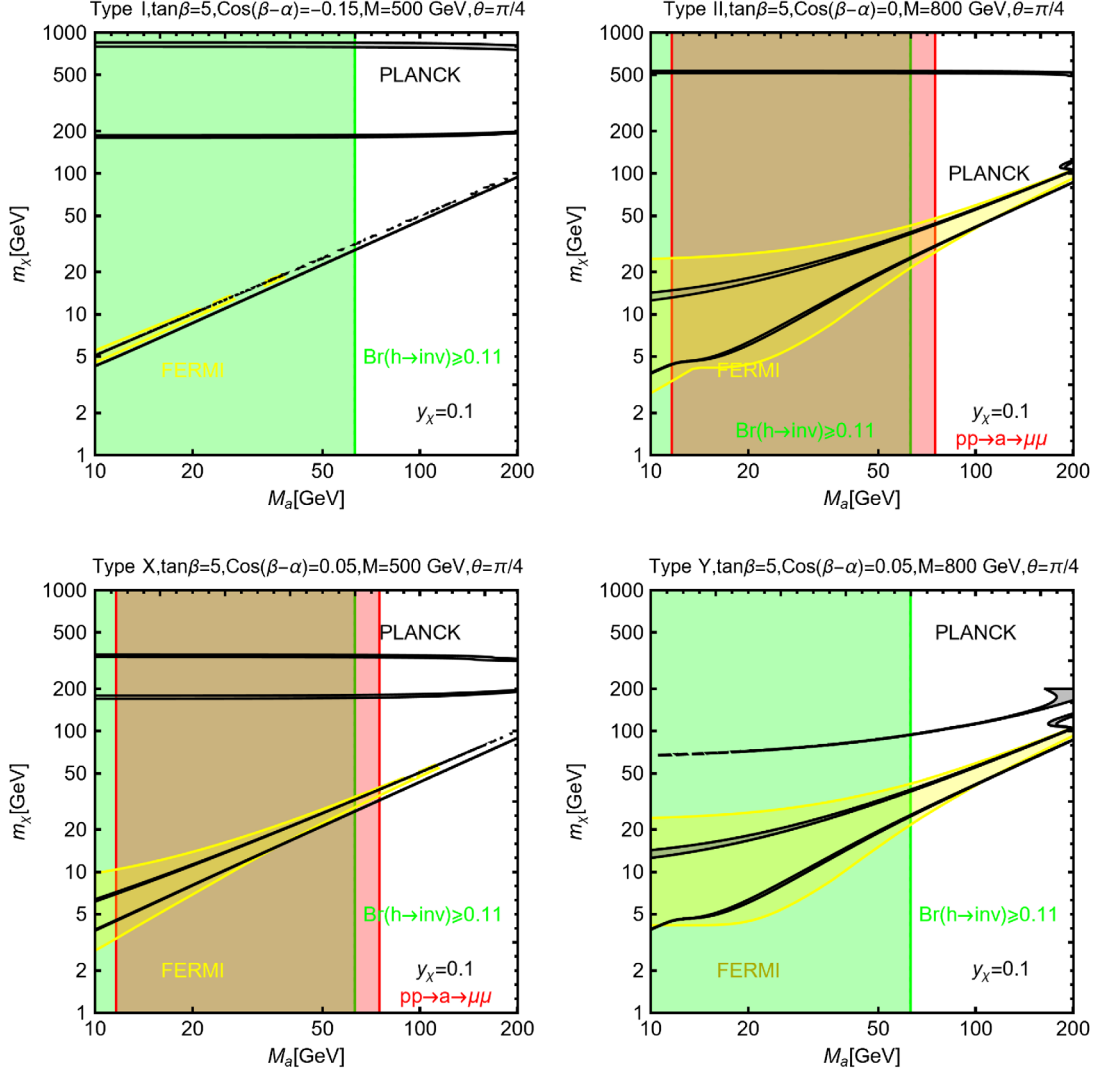
FIG. 12. DM constraints in the $[M_a, m_\chi]$ plane for the four types of the 2HD + a model. Everything is the same as in Fig. 11 but taking $y_\chi = 0.1$ instead of $y_\chi = 1$.

such as, for example, the mass degeneracy for the heavy 2HDM Higgs states, have been made.

A first result of such a parameter scan is shown in Fig. 13, in which each panel reports the model points that satisfy the correct DM cosmological relic density and evade the bounds from DM direct as well as indirect detection. Furthermore, we have applied to the type II and Y models the lower bound $M_{H^\pm} > 800$ GeV from the $b \to s\gamma$ constraint and to all models the LHC bounds from searches of heavy resonances decaying into $\tau^+\tau^-$ and of light resonances decaying into $\mu^+\mu^-$.

The left column of the figure displays the model points in the $\left[\frac{|M_a - 2m_\chi|}{M_a}, \frac{|M_A - 2m_\chi|}{M_A}\right]$ plane, while the right column illustrates the results in the $[m_\chi, y_\chi]$ plane. The distribution of model points in the first column of the plot is mostly sensitive to the relic density constraint. In agreement with

previous findings, one gets very similar results for the four Yukawa configurations. In all cases, the distribution of model points have tails covering the regions in which either $\frac{|M_a - 2m_\chi|}{M_a} \ll 1$ or $\frac{|M_A - 2m_\chi|}{M_A} \ll 1$. This corresponds to the s-channel resonance regions $m_\chi \simeq \frac{1}{2} M_a$ or $\frac{1}{2} M_A$ for which the correct relic density can be achieved also for very small values of the DM coupling y_χ. We further notice that the bottom-left regions of the panels in the left column are substantially empty. There are essentially two reasons for this. These regions correspond to both $\frac{|M_A - 2m_\chi|}{M_A}$ and $\frac{|M_a - 2m_\chi|}{M_a}$ much lower than 1. In other words, both pseudoscalars should essentially have degenerate masses, close to twice the DM mass. Having the two Higgses degenerate in mass is a difficult condition to achieve in the type of numerical scan we have made. Hence, we expect
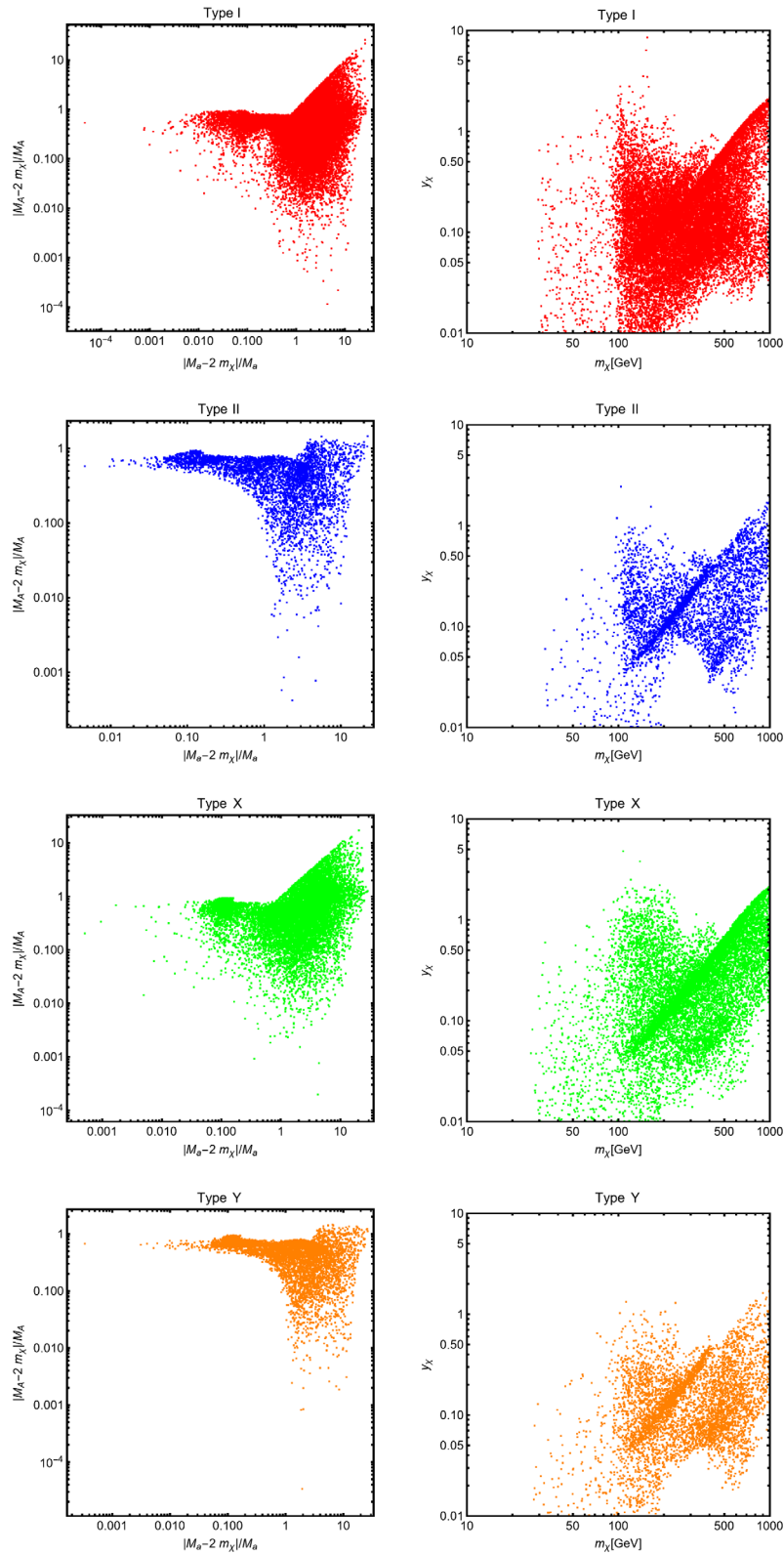
FIG. 13. Outcome of the parameter scan including DM parameters and constraints in the four types of scenarios (see the main text for details). Each plot contains the model points complying with the correct relic density, a spin-independent cross section below the LZ direct limit, and an annihilation cross section complying with indirect constraints. Limits from B-physics and LHC searches (mostly $H/A \to \tau^+\tau^-$ and $a \to \mu^+\mu^-$) are accounted for.
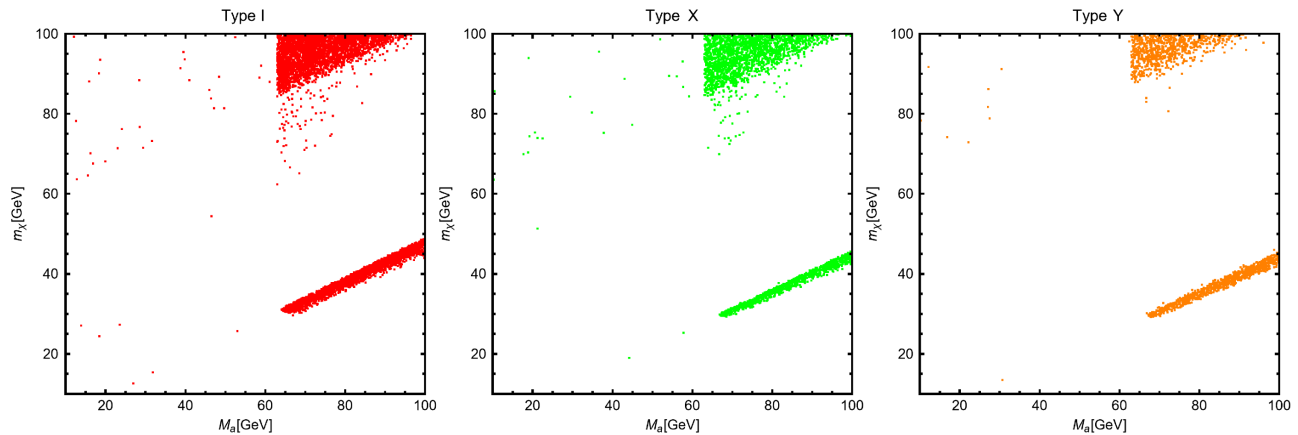
FIG. 14. Accepted model points in the $[M_a, m_\chi]$ plane of a parameter scan focused on the light a region. The figure contains only three panels, relative to the type I, type X, and type Y configurations, as the type II 2HD + a scenario is almost entirely ruled out by LHC searches of light resonances.

this region to be poorly populated regardless of the applied constraints. In addition, Feynman diagrams corresponding to s-channel exchange of two pseudoscalars in the DM annihilation cross section into SM fermions tend to have destructive interference. If the masses are very similar, this would cause a suppression of the cross section, rendering hard to achieve the viable relic density.

Besides the M_a and M_A s-channel poles, the other favored regions of the parameter space correspond to the case in which the DM is heavier than one or both the pseudoscalar Higgs bosons. As already pointed out, in this regime, the relic density constraint has as analogous impact in the four Yukawa configurations. The most notable difference is in the value of $|M_A - 2m_\chi|/M_A$ which does not exceed $\mathcal{O}(1)$ for the type II and Y scenarios. This is due to the strong bounds from the LHC searches and B-physics observables together with the chosen ranges for the scanned parameters.

The impact of constraints from direct and indirect DM searches can be more clearly appreciated by looking to the $[m_\chi, y_\chi]$ planes. As already mentioned, to evade direct detection constraints, one needs to require $y_\chi \lesssim 1$. DM indirect detection, instead, rules out most of the viable parameters space for $m_\chi \lesssim 100$ GeV. The residual points for light DM masses still present in Fig. 13 correspond to DM annihilation in the $m_\chi \simeq \frac{1}{2}M_a$ pole. This is because there is not any longer matching between the DM annihilation cross section at thermal freeze-out and present times in the case of an s-channel resonant enhancement [118].[9]

Figure 14 shows a further illustration of the DM constraints focusing on the $M_a < 100$ GeV region. We

have repeated the previous parameter scan and selected the viable model points in the $[M_a, m_\chi]$ plane, by considering this low-M_a range and keeping fixed the masses $M_H = M_A = M_{H^\pm}$ to $|M| = 500$ GeV in the case of the type I and type X scenarios and to $|M| = 800$ GeV in the type Y case. The type II model has been not included in this analysis, since most of the low-M_a region is already ruled out by searches of light resonances decaying into muon pairs as has been discussed earlier.

As can be seen from the figure, the distributions of the model points are rather similar for the three Yukawa configurations. First, one notices the almost sharp cut of the viable parameter space for $M_a \lesssim 60$ GeV which is essentially due to the bound on the invisible h boson width which can be evaded only by choosing fine-tuned blind spot configurations for the model parameters to suppress or forbid $h \to aa$ decays. Low values of M_a are also subject to the bounds from searches of light resonances, for instance, decaying into muon pairs. For this reason, the type I scenario features more viable model points for $M_a \lesssim 60$ GeV, since it is the least subject to the latter bounds.

Moving to the range $M_a \gtrsim 60$ GeV, the viable model points occupy two very specific regions, the pole $m_\chi \simeq \frac{1}{2}M_a$ region and the $m_\chi \geq M_a$ area. This outcome is mostly due to the constraints from DM indirect detection. A DM state lighter than $\mathcal{O}(100)$ GeV and annihilating into SM fermion pairs is generally strongly disfavored. In the 2HD + a case, this problem can be circumvented by being either in the pole region, as a consequence of the fact that there is not exact matching between the DM annihilation cross section at the time of thermal freeze-out and at present times, or in the $m_\chi > M_a$ regime such that the $\chi\chi \to aa$ process is kinematically allowed. This process, indeed, features a p-wave-dominated cross section for which indirect detection constraints are irrelevant.

---

[9]This mismatch is due to the so-called thermal broadening of the resonance; see, e.g., Ref. [119] for a detailed discussion including some useful analytical approximations.

As already pointed out before, Figs. 13 and 14 show the results of parameter scans performed under rather simplifying assumptions, namely, degenerate masses for the additional Higgs bosons except for the a state and fixed values of the couplings λ_{1P}, λ_{2P}, and λ_a. To understand how the latter parameters affect DM phenomenology, we have conducted further parameter scans fixing the DM mass to two values, namely, $m_\chi = 50$ GeV and $m_\chi = 150$ GeV, and assuming nondegenerate masses for the heavy Higgs bosons while varying freely the quartic couplings of the scalar potential.

As evidenced, in particular, by Fig. 13, for what DM phenomenology is concerned, the type I and type II configurations have a very similar behavior as the type X and type Y configurations, respectively. Hence, without loss of generality, we have restricted ourselves to the type I and type II configurations, the results of which are illustrated in Figs. 15 and 16, respectively.

Each figure shows two series of panels, corresponding to the two chosen values of the DM mass. Each one of these series shows the model points which comply with all

the constraints considered in this work in the $[M_a, M_A]$, $[M_H, M_A]$, and $[M_H, M_{H^\pm}]$ planes (results in the $[M_A, M_{H^\pm}]$ plane are more or less similar to those obtained in the $[M_H, M_{H^\pm}]$ plane). By looking at the distribution of the model points, we notice that the DM constraints, namely, having the correct relic density and complying with the bounds from direct and indirect detection, do not substantially modify the allowed parameter space regions with respect to the LHC and theoretical bounds discussed in the previous sections.

The only exception concerns the mass of the light pseudoscalar boson a. Indeed, for $m_\chi < M_a \lesssim 100$ GeV, the correct DM cosmological relic density is achieved while being compatible with the other constraints, only in the pole $m_\chi \sim \frac{1}{2} M_a$ region. In the case $m_\chi = 50$ GeV, the mass of a is consequently constrained to lie around 100 GeV. This is the reason why in the upper panels in both Figs. 15 and 16 the model points are concentrated in the regions $M_a \simeq 100$ GeV.

This ends the discussion on the combined collider and astroparticle physics constraints on the 2HD + a parameter
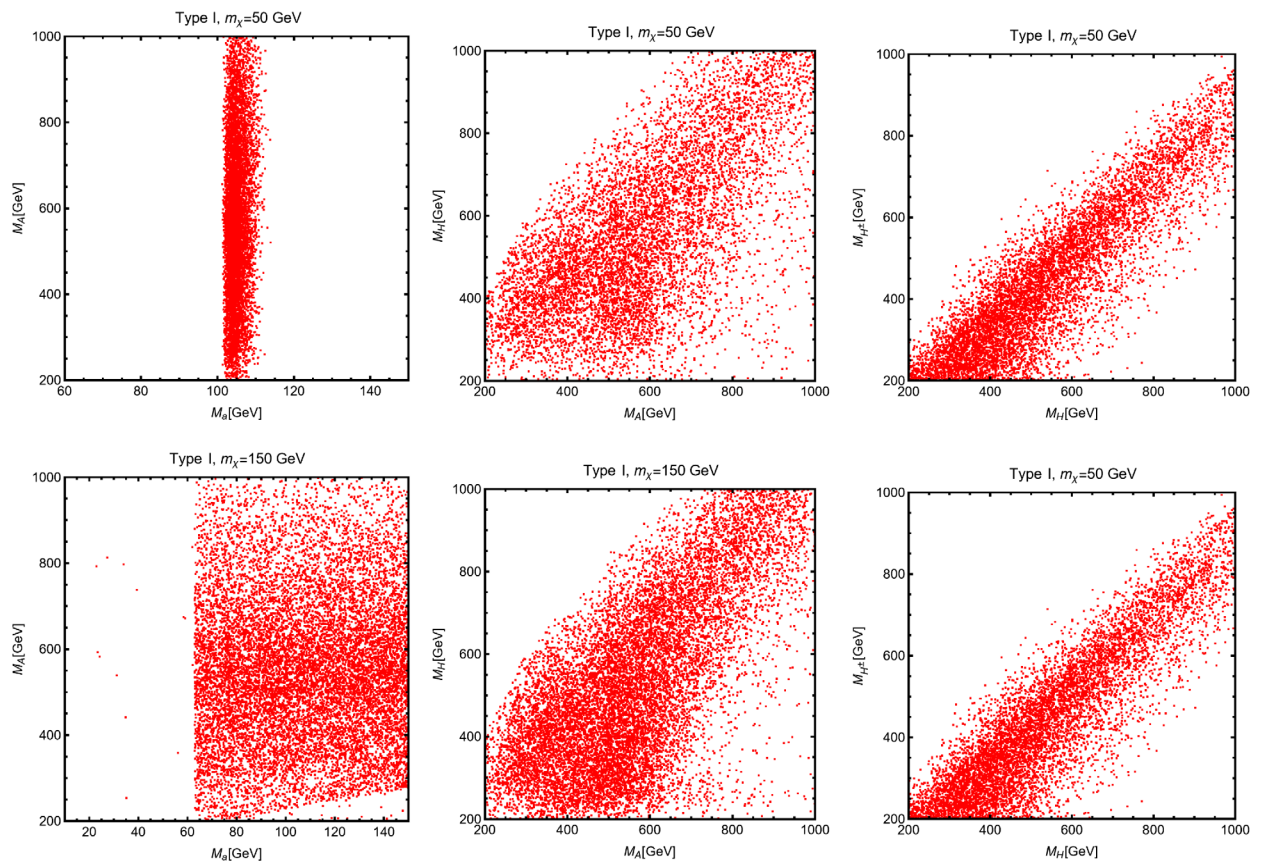

FIG. 15. Outcome of a parameter scan in which all the model parameters are varied but the DM mass, which has been fixed to two values, namely, $m_\chi = 50$ GeV and $m_\chi = 150$ GeV. All the points shown in the panels comply with constraints from DM phenomenology, LHC searches, and theoretical constraints. The type I configuration has been assumed for the Yukawa couplings of the additional Higgs bosons. The concentration of the model points, in the upper left plot, in the region around $M_a \simeq 100$ GeV is due to the fact that the DM relic density is achieved essentially in the $m_\chi \simeq \frac{1}{2} M_a$ pole region.
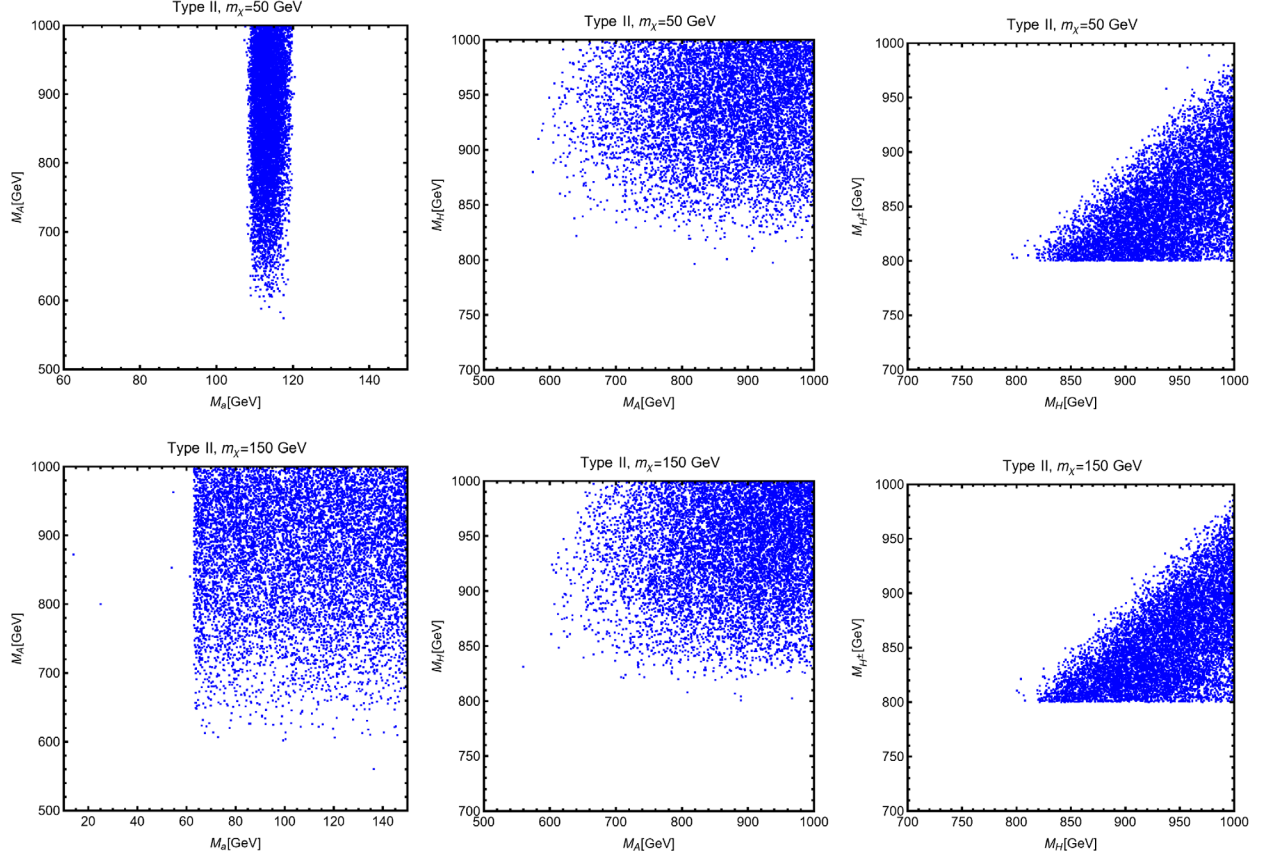
FIG. 16. The same as in Fig. 15 but considering the type II scenario. Note the different scales on the x and y axes for the heavy Higgs boson masses compared to the previous case. Similarly to what occurred in the upper left panel in Fig. 15, the correct relic density for $m_\chi = 50$ GeV requires that $M_a \simeq 2m_\chi \simeq 100$ GeV to meet the condition for an s-channel resonant enhancement of the DM annihilation cross section.

space. From this, one concludes that the constraints are rather strong, in particular, in the type II scenario. They nevertheless leave significant regions in which the model is still viable, in particular, if it does not have to explain the anomalous $(g-2)_\mu$ result which requires too light a states with too strong couplings to isospin $-\frac{1}{2}$ fermions. Part of these regions could, nevertheless, be challenged in the near future by more sensitive LHC and DM direct detection searches.

V. PHASE TRANSITIONS AND GRAVITATIONAL WAVES

A promising way to probe the 2HD + a model is through the detection of the stochastic gravitational wave background. These gravitational waves, originating from the electroweak first-order cosmic phase transitions, propagate freely, being only redshifted by the expansion of the Universe. They can potentially be detected by future space-based GW detectors such as LISA, BBO, or DECIGO. The aim of this section is to compute the GW signal from the electroweak first-order phase transition (FOPT) within the 2HD + a scenario.

Since the fermionic contributions, except from the top quark (because of its large mass), do not play a significant role in the study of thermal phase transitions,[10] it turns out that it does not matter whether we consider the type I, II, X, or Y configuration (as the top coupling is the same in these four configurations) for our 2HD + a model, and the GW signal will be independent of this choice. When computing the stochastic gravitational wave background, we therefore arbitrarily consider the type II configuration. We have nevertheless explicitly checked that we obtain very similar results in the type I scenario; the type X and Y scenarios will give exactly the same results as in type II and I, respectively, as the only difference comes from the different coupling of the τ lepton which plays a negligible role in this context. At the end of our discussion, we consider the 2HDM limit of our model to underline the impact of the parameters related to the pseudoscalar a boson, namely, its mass, mixing, and couplings.

---

[10]In the high-temperature expansion of the thermal function further defined in Eq. (59), it is shown that, unlike for bosons, the function for fermions is lacking a cubic term, a crucial ingredient to generate a thermal barrier in the effective potential.

A. One-loop thermal effective potential

In order to study the electroweak phase transition, both zero-temperature quantum corrections and thermal effects must be incorporated into the full effective potential needed for the analysis of phase transitions. However, let us first revisit the tree-level potential.

We consider phase transitions occurring in the field space (h^0, H^0), where h^0 and H^0 are the CP-even components of Φ_1 and Φ_2, respectively, which are defined in the gauge basis as

$$\Phi_1 = \frac{1}{\sqrt{2}} \begin{pmatrix} G_1 + iG_2 \\ h^0 + v_1 + iG^0 \end{pmatrix},$$

$$\Phi_2 = \frac{1}{\sqrt{2}} \begin{pmatrix} H_{c_1} + iH_{c_2} \\ H^0 + v_2 + iA_n \end{pmatrix}. \tag{44}$$

The tree-level potential (8) in terms of classical background fields, thus, reduces to

$$V_0 = \frac{m_{11}^2}{2}(h^0)^2 + \frac{m_{22}^2}{2}(H^0)^2 - m_{12}^2 h^0 H^0 + \frac{\lambda_1}{8}(h^0)^4$$
$$+ \frac{\lambda_2}{8}(H^0)^4 + \frac{\lambda_3 + \lambda_4 + \lambda_5}{4}(h^0)^2(H^0)^2. \tag{45}$$

The Hessian matrix of the tree-level potential (8) is a 9×9 matrix (four degrees of freedom or d.o.f. from Φ_1, four from Φ_2, and one from a^0, the CP-odd light pseudoscalar). Then, considering only the fields h^0 and H^0, we obtain a block-diagonal matrix, with four blocks. The first one is the 2×2 matrix m_S^2 of the CP-even states, and the second one is the 3×3 matrix m_P^2 of the CP-odd states, while the two last ones are the 2×2 matrix m_C^2 of the charged states.

One-loop quantum corrections are encoded in the Coleman-Weinberg potential [120]

$$V_{\mathrm{CW}} = \frac{1}{64\pi^2} \sum_i n_i m_i^4 \left(\ln \frac{m_i^2}{\mu^2} - c_i \right) \tag{46}$$

with $i \in \{t, b, \chi, W_T^\pm, W_L^\pm, Z_T, Z_L, \gamma_L\}$ and also runs over the states from the scalar potential (8). The degrees of freedom are encoded in n_i, where $n_t = n_b = -12$, $n_\chi = -2$, $n_{W_T^\pm} = 4$, $n_{W_L^\pm} = n_{Z_T} = 2$, $n_{Z_L} = n_{\gamma_L} = 1$, and the d.o.f. for each of the scalar neutral states is 1 and 2 for the charged states. The renormalization scale μ is set to the VEV $v = \sqrt{v_1^2 + v_2^2}$. The value of constant c_i arising from dimensional regularization in the $\overline{\mathrm{MS}}$ scheme is $3/2$ for fermions, scalars, and longitudinal vector bosons and $1/2$ for transverse vector bosons. Finally, $m_i^2 \equiv m_i^2(h^0, H^0)$ corresponds to the eigenvalues of the field-dependent mass matrix.

In the type II or Y models, which differ only by the contributions of the τ lepton that we ignore as its effects are far too small because of its very small mass, the field-dependent masses for the SM states and the DM candidate χ are

$$m_t^2 = \frac{y_t^2}{2\sin^2\beta}(H^0)^2, \qquad m_b^2 = \frac{y_b^2}{2\cos^2\beta}(h^0)^2,$$

$$M_\chi^2 = m_\chi^2 + y_\chi^2(a^0)^2, \tag{47}$$

$$M_W^2 = \frac{g_2^2}{4}[(h^0)^2 + (H^0)^2],$$

$$M_Z^2 = \frac{g_1^2 + g_2^2}{4}[(h^0)^2 + (H^0)^2], \qquad m_\gamma^2 = 0, \tag{48}$$

with y_t, y_b, g_1, and g_2 the top Yukawa coupling, the bottom Yukawa coupling, the $U(1)_Y$ and $SU(2)_L$ gauge couplings, and y_χ^2 the DM Yukawa coupling to the pseudoscalar a^0, respectively. Since we consider only phase transitions occurring in the (h^0, H^0) field space, $a^0 = 0$ (see Sec. V D), the M_χ^2 term in the effective potential contributes only to the cosmological constant. On the other hand, in the type I or X model, the bottom field-dependent mass is given by $m_b^2 = (y_b^2)/(2\sin^2\beta)(H^0)^2$. The eigenvalues of m_S^2 and m_P^2 yield the field-dependent masses for the neutral states, while those of m_C^2 yield the field-dependent masses of the charged states.

In order to compensate the shift from V_{CW} to the VEVs, masses, and mixing in the electroweak vacuum, we consider the counterterms

$$V_{\mathrm{CT}} = \delta m_{11}^2(h^0)^2 + \delta m_{22}^2(H^0)^2 + \delta m_{12}^2 h^0 H^0$$
$$+ \delta\lambda_1(h^0)^4 + \delta\lambda_2(H^0)^4, \tag{49}$$

where these (finite) counterterms satisfy the following renormalization conditions[11] in the electroweak vacuum (v_1, v_2):

$$\partial_{h^0}(V_{\mathrm{CW}} + V_{\mathrm{CT}})\Big|_{(v_1, v_2)} = 0,$$

$$\partial_{H^0}(V_{\mathrm{CW}} + V_{\mathrm{CT}})\Big|_{(v_1, v_2)} = 0, \tag{50}$$

$$\partial_{(h^0)^2}^2(V_{\mathrm{CW}} + V_{\mathrm{CT}})\Big|_{(v_1, v_2)} = 0,$$

$$\partial_{(H^0)^2}^2(V_{\mathrm{CW}} + V_{\mathrm{CT}})\Big|_{(v_1, v_2)} = 0, \tag{51}$$

$$\partial_{h^0 H^0}^2(V_{\mathrm{CW}} + V_{\mathrm{CT}})\Big|_{(v_1, v_2)} = 0 \tag{52}$$

and are given by

---

[11]Divergences arising from Goldstone contributions are treated with the method described in Ref. [121].

$$\delta\lambda_1 = \frac{1}{8v_1^3}\left(\partial_{h^0}V_{CW} - \partial^2_{(h^0)^2}V_{CW}v_1 - \partial^2_{h^0H^0}V_{CW}v_2\right)\Bigg|_{(v_1,v_2)}, \qquad (53)$$

$$\delta\lambda_2 = \frac{1}{8v_2^3}\left(\partial_{H^0}V_{CW} - \partial^2_{(H^0)^2}V_{CW}v_2 - \partial^2_{h^0H^0}V_{CW}v_1\right)\Bigg|_{(v_1,v_2)}, \qquad (54)$$

$$\delta m_{11}^2 = \frac{1}{4v_1}\left(-3\partial_{h^0}V_{CW} + \partial^2_{(h^0)^2}V_{CW}v_1 + 3\partial^2_{h^0H^0}V_{CW}v_2\right)\Bigg|_{(v_1,v_2)}, \qquad (55)$$

$$\delta m_{22}^2 = \frac{1}{4v_2}\left(-3\partial_{H^0}V_{CW} + \partial^2_{(H^0)^2}V_{CW}v_2 + 3\partial^2_{h^0H^0}V_{CW}v_1\right)\Bigg|_{(v_1,v_2)}, \qquad (56)$$

$$\delta m_{12}^2 = -\partial^2_{h^0H^0}V_{CW}\Big|_{(v_1,v_2)}. \qquad (57)$$

Finally, one must consider thermal effects, since the phase transition occurs in the early Universe and, thus, at very high temperature. These thermal corrections are given by [122]

$$V_T = \frac{T^4}{2\pi^4}\sum_i n_i J\left(\frac{m_i^2}{T^2}\right), \qquad (58)$$

where the thermal function is defined as [122]

$$J(y^2) = \int_0^\infty dx\, x^2 \ln\left(1 + (-1)^B e^{-\sqrt{x^2+y^2}}\right), \qquad (59)$$

with $B = 1(0)$ for bosons (fermions).

In order to avoid infrared divergences from the zero Matsubara modes, one resums the daisy diagrams, which amounts to a shift in the mass parameter m^2 with a leading-order thermal contribution in the propagator: $m^2 \to m^2 + cT^2$, with c a constant depending on dimensionless couplings. This thermal mass resummation is made in the gauge basis and only then are mass matrices diagonalized to obtain the thermal field-dependent eigenvalues $m_i^2(h^0, H^0, T)$.

In addition to the usual Debye mass cT^2 for the SM content, the Debye masses peculiar to the type II or Y $2HD + a$ are given by

$$c_1 = (g_1^2 + 3g_2^2 + 4y_b^2/\cos^2\beta)/16 \\ + (3\lambda_1 + 2\lambda_3 + \lambda_4 + \lambda_{1P})/12, \qquad (60)$$

$$c_2 = (g_1^2 + 3g_2^2 + 4y_t^2/\sin^2\beta)/16 \\ + (3\lambda_2 + 2\lambda_3 + \lambda_4 + \lambda_{2P})/12, \qquad (61)$$

and where, in the case of type I or X $2HD + a$ models, $\cos\beta$ is replaced with $\sin\beta$ in Eq. (60).

The resulting one-loop thermal effective potential is then given by[12]

$$V_{eff}(h^0, H^0, T) = V_0 + V_{CW} + V_{CT} + V_T. \qquad (62)$$

B. Key parameters for phase transitions

Initially, before the electroweak phase transition, the Universe is in the symmetric phase. As the temperature decreases, there appears a new minimum in the scalar potential—a new (broken) phase. With decreasing temperature, this minimum eventually becomes deeper than the one in the symmetric phase, thus making it metastable. This metastable or false vacuum eventually decays into the stable or true vacuum. The cosmic first-order phase transition occurs through the nucleation of bubbles of true vacuum, which expand and collide with each other, converting the symmetric phase into the broken phase. The decay rate of the false vacuum or the bubble nucleation rate per time per volume Γ is given by [125]

$$\Gamma \sim T^4 e^{-S/T}, \qquad (63)$$

where S is the three-dimensional Euclidean action minimized by the *bounce* or O(3) critical bubble.

The nucleation temperature T_n is defined such that the number of nucleated bubbles per Hubble time per Hubble volume is unity: $\Gamma H^{-4} \sim O(1)$ with H the Hubble parameter. The latter is expressed in a radiation-dominated Universe as

---

[12]There could be an additional gauge or renormalization-scale dependency which we do not take into account and that could potentially lower the predicted GW signal strength [123,124]. Moreover, this dependency can potentially influence the nature of phase transitions. However, in our analysis, we consider only strong first-order phase transitions (see Sec. V D); thereby, we expect that the impact of gauge and renormalization-scale dependence is not significant enough to transform a strong first-order phase transition into a second-order phase transition. We, thus, expect these dependences to only potentially influence the strength of the phase transition.

$$H^2 = \frac{8\pi\rho_{\rm rad}}{3M_p^2}, \tag{64}$$

where $\rho_{\rm rad} = \pi^2/30 g_* T^4$ is the energy density of the plasma in the false vacuum, with g_* the effective number of relativistic degrees of freedom at T and where M_p is the Planck mass.

Considering the electroweak scale, one has $T \sim O(100)$ GeV and $g_* \sim O(100)$. Therefore, using Eq. (63), one obtains $S/T \sim 140$ at the nucleation temperature T_n.

The strength of a first-order phase transition is given by [126]

$$\alpha \equiv \frac{\Delta\epsilon}{\rho_{\rm rad}}\bigg|_{T=T_*}, \qquad \Delta\epsilon \equiv \epsilon\bigg|_{\rm false\ vacuum} - \epsilon\bigg|_{\rm true\ vacuum} \tag{65}$$

with $\epsilon = V_{\rm eff} - \frac{T}{4}\frac{\partial V_{\rm eff}}{\partial T}$, the vacuum energy.

Finally, the inverse time duration β of the PT is defined as [127]

$$\frac{\beta}{H_n} = T_n \frac{d(S/T)}{dT}\bigg|_{T_n}, \tag{66}$$

where the parameters are evaluated at the nucleation temperature T_n.

C. Predictions for gravitational wave signals

A single bubble of true vacuum alone cannot be responsible for the generation of gravitational waves because of its spherical symmetry (zero quadrupole moment). A stochastic gravitational wave background, however, is possible when at least two bubbles collide with each other. The resulting gravitational power spectrum $h^2\Omega_{\rm GW}$ mainly comes from three contributions[13] [31]: $h^2\Omega_{\rm GW} \simeq h^2\Omega_{\rm col} + h^2\Omega_{\rm sw} + h^2\Omega_{\rm turb}$.

The contribution from bubble collisions is given in the envelope approximation by [129]

$$h^2\Omega_{\rm col}(f) = h^2\Omega_{\rm col}^{\rm peak} S_{\rm col}(f), \tag{67}$$

with

$$h^2\Omega_{\rm col}^{\rm peak} = 1.67 \times 10^{-5} \left(\frac{H_n}{\beta}\right)^2 \left(\frac{\kappa_{\rm col}\alpha}{1+\alpha}\right)^2$$
$$\times \left(\frac{100}{g_n}\right)^{1/3} \left(\frac{0.11 v_w^3}{0.42 + v_w^2}\right), \tag{68}$$

---

[13]A new contribution, from feebly interacting particles, has been recently studied in Ref. [128]. This contribution is more appropriate for phase transitions in the dark sector; therefore, we omit it in our analysis.

$$S_{\rm col} = \frac{3.8(f/f_{\rm col})^{2.8}}{1 + 2.8(f/f_{\rm col})^{3.8}}, \tag{69}$$

where $\kappa_{\rm col}$ is the efficiency factor for the conversion of the vacuum energy into the gradient energy of the scalar field, v_w is the bubble-wall speed in the rest frame of the plasma far away from the bubble [31], $f_{\rm col}$ is the frequency at the peak of the power spectrum, $h^2\Omega_{\rm col}^{\rm peak}$, and $S_{\rm col}$ is the spectral shape of the GW spectrum $h^2\Omega_{\rm col}$.

The overlap of sound waves yield a contribution given by [130–132]

$$h^2\Omega_{\rm sw}(f) = h^2\Omega_{\rm sw}^{\rm peak} S_{\rm sw}(f), \tag{70}$$

with

$$h^2\Omega_{\rm sw}^{\rm peak} = 1.23 \times 10^{-6} \left(\frac{H_n}{\beta}\right) \left(\frac{\kappa_{\rm sw}\alpha}{1+\alpha}\right)^2 \left(\frac{100}{g_n}\right)^{1/3} v_w \Upsilon, \tag{71}$$

$$S_{\rm sw} = \left(\frac{f}{f_{\rm sw}}\right)^3 \left(\frac{7}{4 + 3(f/f_{\rm sw})^2}\right)^{7/2}, \tag{72}$$

where $\kappa_{\rm sw}$ is the efficiency factor for the conversion of the vacuum energy into the bulk motion of the plasma, $f_{\rm sw}$ is the sound-wave peak frequency, and $S_{\rm sw}$ is the spectral shape of the GW spectrum $h^2\Omega_{\rm sw}$. The suppression factor, accounting for the finite lifetime $\tau_{\rm sw}$ of the GW source from sound waves, is defined in a radiation-dominated Universe as [133,134]

$$\Upsilon = 1 - \frac{1}{\sqrt{2\tau_{\rm sw}H_n + 1}}. \tag{73}$$

The magnetohydrodynamics (MHD)-turbulence contribution is given by [31,135]

$$h^2\Omega_{\rm turb}(f) = h^2\Omega_{\rm turb}^{\rm peak} S_{\rm turb}(f), \tag{74}$$

with

$$h^2\Omega_{\rm turb}^{\rm peak} = 3.35 \times 10^{-4} \left(\frac{H_n}{\beta}\right) \left(\frac{\kappa_{\rm turb}\alpha}{1+\alpha}\right)^{3/2} \left(\frac{100}{g_n}\right)^{1/3} v_w \frac{1}{N_{\rm turb}}, \tag{75}$$

$$S_{\rm turb} = \frac{(f/f_{\rm turb})^3}{[1 + (f/f_{\rm turb})]^{11/3}} \frac{N_{\rm turb}}{1 + 8\pi f/h_n}, \tag{76}$$

$$N_{\rm turb} = 2^{11/3}(1 + 8\pi f_{\rm turb}/h_n), \tag{77}$$

where $\kappa_{\rm turb}$ is the efficiency factor for the conversion of the vacuum energy into turbulent flows, $f_{\rm turb}$ is the MHD-turbulence peak frequency, $S_{\rm turb}$ is the spectral shape of the

GW spectrum $h^2\Omega_{\text{turb}}$, N_{turb} is a normalization factor such that $S_{\text{turb}}(f = f_{\text{turb}}) = 1$, and h_n is the value of the Hubble rate at T_n, redshifted to today.

D. Phase transitions and GW signals in the plane of h^0 and H^0

Considering phase transitions that occur only in the plane (h^0, H^0), we set a^0 to zero. This means that we suppose that the path taken in the field space during the phase transition, to tunnel from the false to the true vacuum, occurs with no excursion only along the a^0 direction. This configuration remains different from the 2HDM model, because a^0 and its associated couplings intervene through loops via Eqs. (46) and (58).

In the following, we consider the type II model in the alignment limit $\alpha = \beta - \pi/2$. As already mentioned in the beginning of this section, the impact of the fermionic sector in this context is rather modest, and we have checked that the results are the same in the type I scenario (as well as in the type X and Y cases, as we neglect the impact of the τ lepton). We perform a random sampling in the following parameter space:

$$M_H, M_A, M_{H^\pm} \in [500, 1250] \text{ GeV}, \qquad M_a \in [10, 200] \text{ GeV},$$
$$\tan\beta \in [0.1, 50], \qquad \sin\theta \in [\sqrt{2}/2, 1],$$
$$\lambda_a \in [0, 4\pi], \qquad \lambda_{1P}, \lambda_{2P} \in [-\pi, 4\pi], \qquad (78)$$

where we have fixed the additional parameter m_{12} to $m_{12}^2 = \frac{1}{2}M_H^2 \sin(2\beta)$ ($|M| = M_H$). The resulting points satisfy the constraint of perturbative unitarity Eq. (16) and stability of the potential Eq. (18) and allow a moderate mass splitting between the heavy scalar particles so that it satisfies constraints from electroweak precision observables.

We then scan this region of the parameter space with the package COSMOTRANSITIONS [136] and consider only strong FOPT, that is, with $v_n/T_n \geq 1$ [137], with $v_n \equiv \sqrt{(\langle h^0 \rangle_{\text{sym}} - \langle h^0 \rangle_{\text{brok}})^2 + (\langle H^0 \rangle_{\text{sym}} - \langle H^0 \rangle_{\text{brok}})^2}$ evaluated at the nucleation temperature T_n, in order to avoid any ambiguity about the kind of the phase transition [29,30]. Finally, regarding the GW spectrum, we consider that the bubbles run away and consider $v_w = 1$ for the velocity of the bubble wall.

The points that give rise to strong FOPT are shown in a series of two-dimensional projected spaces. Figure 17 shows these points with the value of the mass of the heavy scalar particles, color coded by $\tan\beta$. One can see from the three panels that the largest value is found for M_A, which reaches the upper limit of 1250 GeV in Eq. (78). As for M_H and $M_{H^\pm}$, their values remain below 1 TeV.

In Fig. 18, the same parameters as in the previous figure are involved, but this time the color code measures the mass splitting between two of the three heavy scalar states, the third one being on the abscissa. In this plot, one more clearly sees the allowed range of values for the masses. In the middle panel, one can see that a zero mass splitting
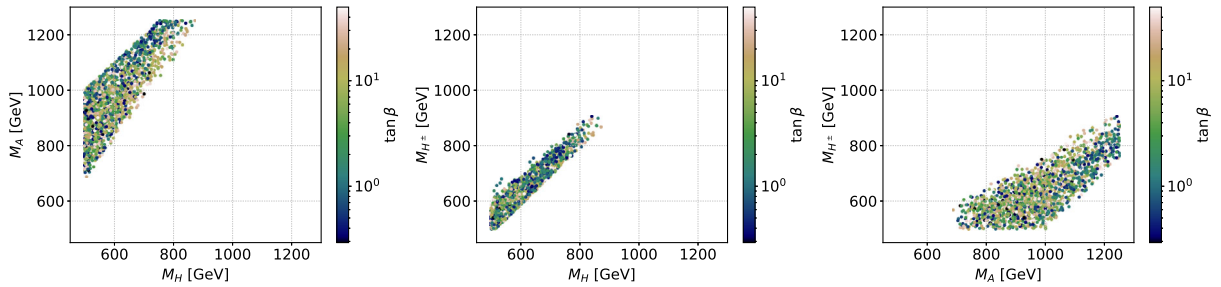

FIG. 17. Points, from the scanned parameter space, giving rise to strong FOPTs that generate a GW signal. Left: M_A vs M_H. Middle: $M_{H^\pm}$ vs M_H. Right: $M_{H^\pm}$ vs M_A. The color code indicates values of $\tan\beta$. Shades of blue characterize points with $0.1 \leq \tan\beta < 1$, and shades of green characterize points with $1 \leq \tan\beta < 10$, while yellow to white shows points with $10 \leq \tan\beta < 50$.
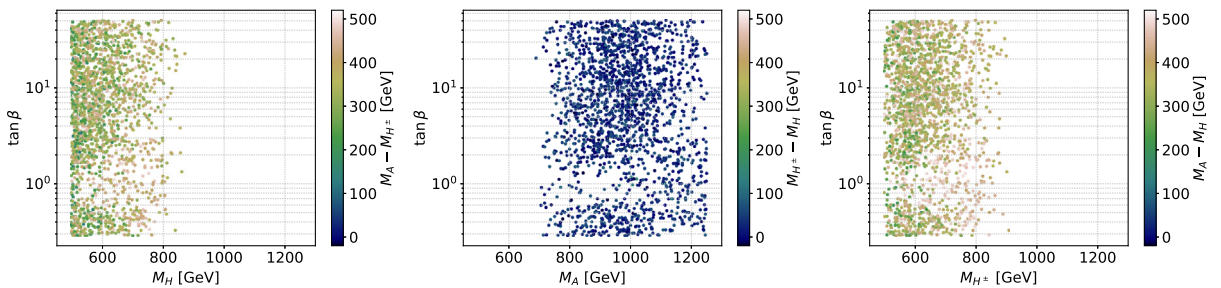

FIG. 18. Parameter space with strong FOPTs. Left: $\tan\beta$ vs M_H. Middle: $\tan\beta$ vs M_A. Right: $\tan\beta$ vs $M_H^\pm$. The color code quantifies the mass splitting between two of the three heavy scalar states. Only the middle panel presents a zero mass splitting.
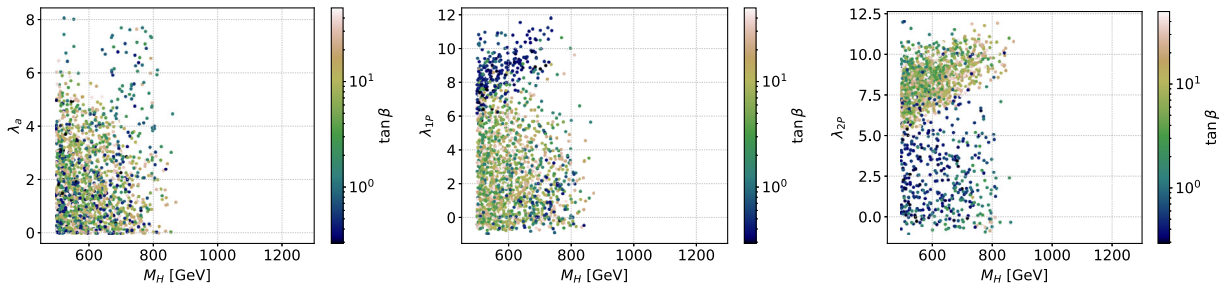
FIG. 19. Parameter space with strong FOPTs. Left: λ_a vs M_H. Middle: λ_{1P} vs M_H. Right: λ_{2P} vs M_H. The color code indicates values of $\tan\beta$.

between $M_{H^\pm} - M_H$ is allowed, while it is not the case for the two other combinations.

For each panel in Fig. 19, we show on the ordinate one of the quartic couplings associated to the light pseudoscalar. Similarly to Fig. 17, the color code represents the value of $\tan\beta$. This color code clearly indicates two regions in both the middle and right panels. In the middle panel, it shows that large values of λ_{1P} are found with small values of $\tan\beta$ and vice versa. On the other hand, in the right panel, λ_{2P} and $\tan\beta$ are positively correlated: When λ_{2P} is small, $\tan\beta$ is small, and vice versa. Regarding the phase-transition parameters, the left panel in Fig. 22 shows the usual correlation between β/H and α: The slower the phase

transition, the stronger it is. The color code represents the value of $\tan\beta$.

Let us now investigate the impact of the parameters related to the light pseudoscalar on the strength of the phase transition α. Figure 20 shows that the maximal value for the pseudoscalar self-coupling λ_a is smaller than the maximal value for the portal couplings λ_{1P} or λ_{2P}, and it seems easier to obtain a strong FOPT for smaller λ_a, as beyond $\lambda_a = 5$ the plot is less populated. The range of values for both λ_{1P} and λ_{2P} are quite similar. However, contrary to λ_a, moderately small negative values of these portal couplings are allowed to give rise to strong FOPTs. In Fig. 21, one can see in the left panel that M_a does not seem to impact the PT strength α, while in the right panel, values of $\sin\theta$ from the
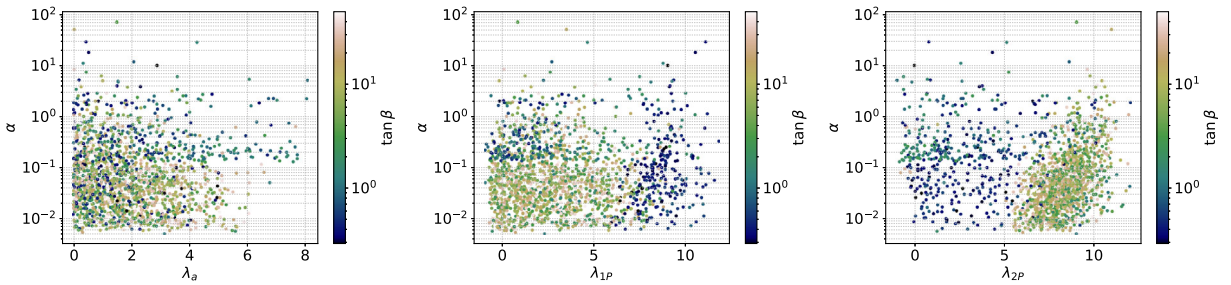

FIG. 20. Parameter space with strong FOPTs. Left: α vs λ_a. Middle: α vs λ_{1P}. Right: α vs λ_{2P}. The color code represents the value of $\tan\beta$.
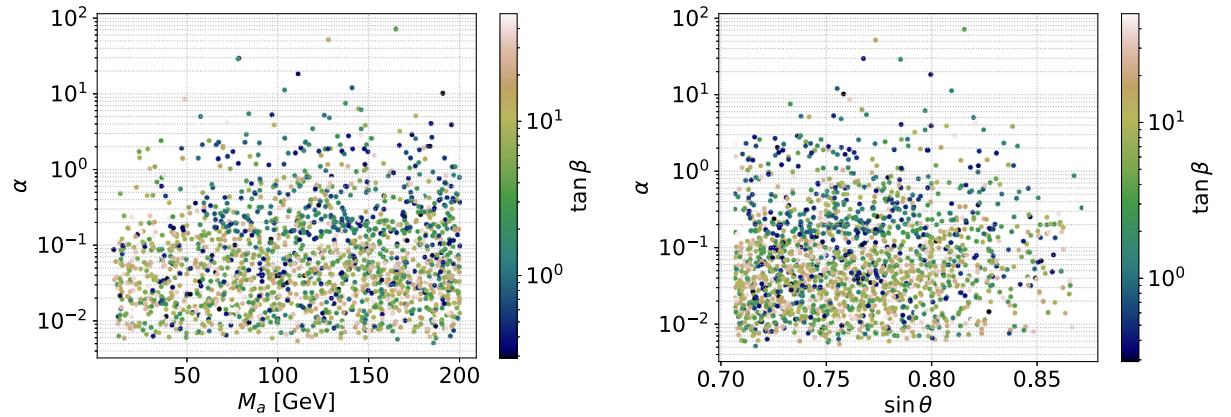

FIG. 21. Parameter space with strong FOPTs. Left: α vs M_a. Right: α vs $\sin\theta$. The color code indicates the value of $\tan\beta$.
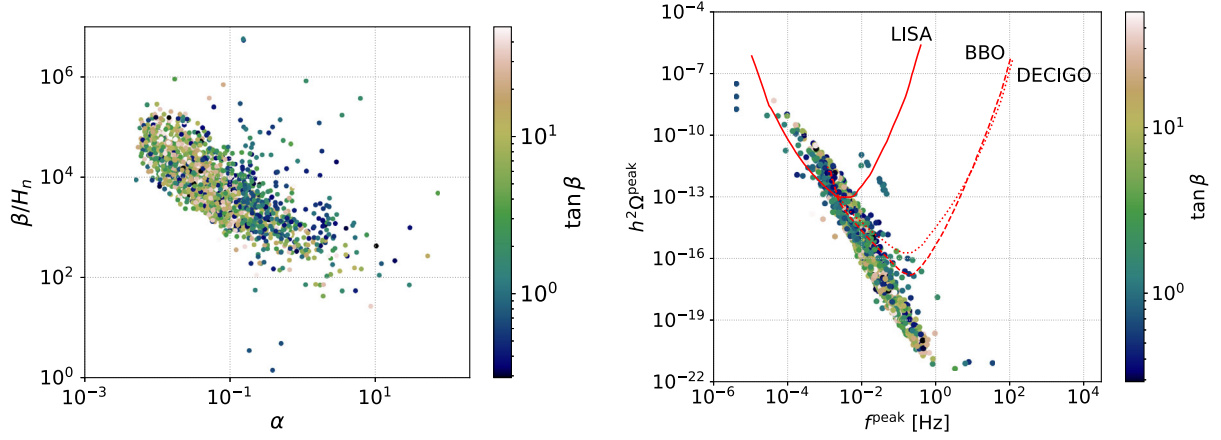
FIG. 22. Parameter space with strong FOPTs. Left: β/H_n vs α. Right: Peak amplitude of the GW signal as a function of the peak frequency. Also shown are the sensitivity curves of future detectors LISA, BBO, and DECIGO.

first half of the scanned range are slightly favored for strong FOPTs.

The right panel in Fig. 22 shows the peak amplitude of the GW signal as a function of the peak frequency. The power-law integrated sensitivity curves for the GW detectors are constructed for an observation time of four years for LISA (solid line), BBO (dashed line), and DECIGO (dotted line), and GWs are considered to be detectable if the signal-to-noise ratio is above 10 [138]. This figure shows points yielding a signal strong enough to be potentially detected by LISA, BBO, or DECIGO.

1. Comparison with the 2HDM

In this section, we consider the 2HDM limit, which means $M_a = \sin\theta = \lambda_a = \lambda_{1P} = \lambda_{2P} = 0$, to put in evidence the impact of these parameters in the 2HD + a model. We again consider the parameter space (78), constrained by perturbative unitarity and the requirement of a potential bounded from below. These constraints can be found in the 2HDM review [8]. In Fig. 23, we can see that the allowed parameter space is narrower than in Fig. 17. Moreover, all the three masses M_H, M_A, and $M_{H^\pm}$ can produce strong FOPTs also for higher values, i.e., beyond
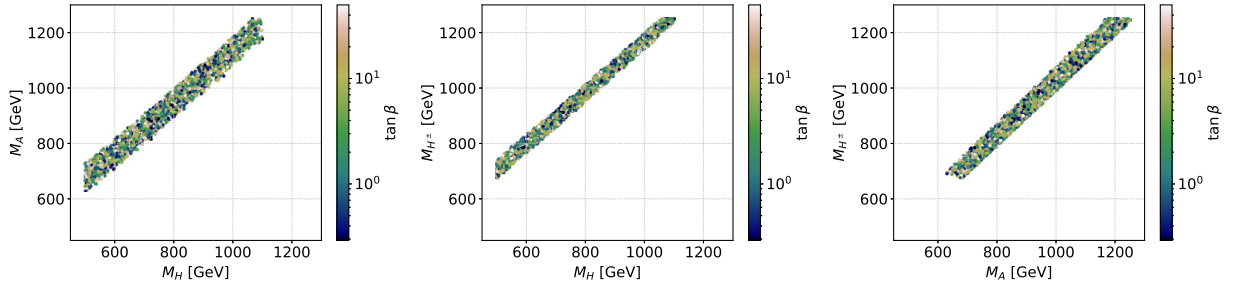

FIG. 23. Parameter space with strong FOPTs for pure 2HDM. Left: M_A vs M_H. Middle: $M_{H^\pm}$ vs M_H. Right: $M_{H^\pm}$ vs M_A. The color code indicates values of $\tan\beta$.
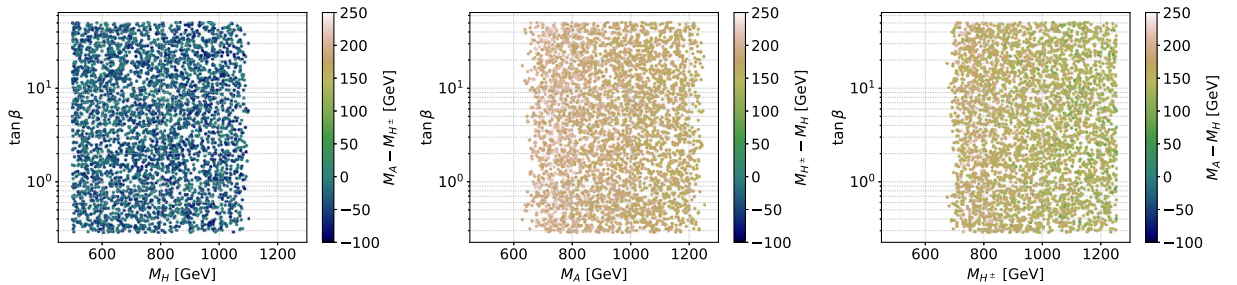

FIG. 24. Parameter space with strong FOPTs for pure 2HDM. Left: $\tan\beta$ vs M_H. Middle: $\tan\beta$ vs M_A. Right: $\tan\beta$ vs $M_{\bar{H}}^\pm$. The color code quantifies the mass splitting between two of the three heavy scalar states. Both the left and right panels present a zero mass splitting.
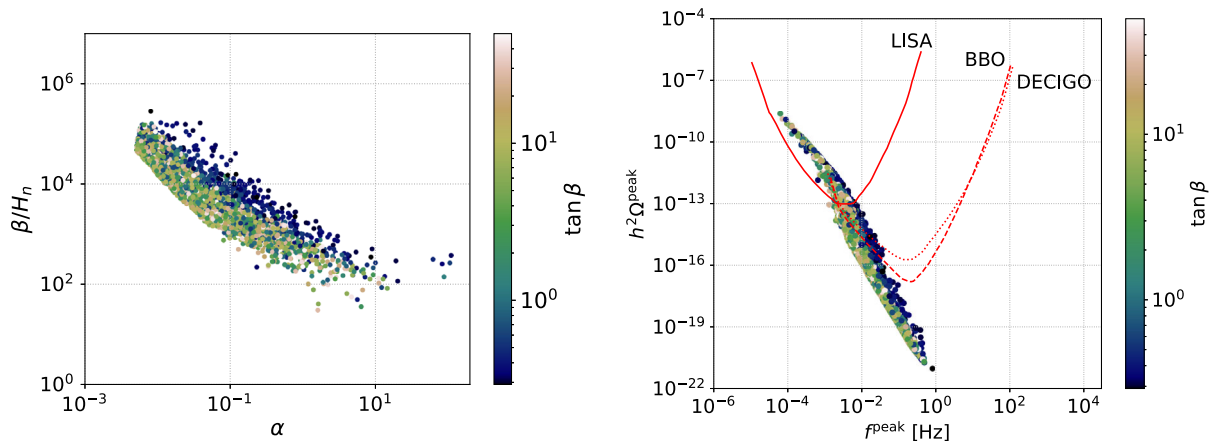
FIG. 25. Parameter space with strong FOPTs for a pure 2HDM. Left: β/H vs α. Right: Peak amplitude of the GW signal as a function of the peak frequency. Also shown are the sensitivity curves of future detectors LISA, BBO, and DECIGO. The GW signal seems correlated with $\tan\beta$, contrary to the 2HD + a case (Fig. 22).

1 TeV. While for the case of strong FOPTs in the 2HD + a model, we find that only the mass splitting $M_{H^\pm} - M_H$ can be zero (Fig. 18), in the 2HDM limit, we find zero splitting only in $M_A - M_{H^\pm}$; see Fig. 24.

The left panel in Fig. 25 shows that, for a fixed value of β/H_n, the phase-transition strength α increases when $\tan\beta$ decreases. As for the GW signal, one can see in the right panel in Fig. 25 that the population of points is a bit narrower than in the right panel in Fig. 22. In terms of the range of values for the GW signal and the frequency, the 2HD + a and 2HDM models are quite similar.

All in all, we see that there is a part of the 2HD + a model parameter space that can be probed by future GW detectors such as LISA, BBO, or DECIGO and that considering a singlet pseudoscalar a state in addition to the usual two Higgs doublets of the 2HDM does, indeed, make a difference.

VI. CONCLUSIONS

The extension of the minimal Higgs sector of the SM to include two Higgs doublet fields, leading to four Higgs bosons A, H, and $H^\pm$ in addition to the already h state observed, and a relatively light pseudoscalar a boson with significant mixing with the A state of the 2HDM, is interesting in many respects. First, when including a cosmologically stable isosinglet fermion, it allows for a nice resolution of the dark matter problem while not conflicting with present data: The correct cosmological relic density is essentially obtained through DM annihilation into SM fermions via s-channel a boson exchange or into a final state involving light a bosons, while elastic DM scattering on the nucleon proceeds through loop diagrams which make the cross sections rather small and, hence, DM detection in direct astrophysical experiments more difficult. Because of its extended particle content, the model has a

very rich phenomenology that can be probed in collider experiments, in particular, at the LHC.

Nevertheless, the model is still subject to severe constraints from both collider and astrophysical data, and the first objective of the present paper was to perform a comprehensive study of all the experimental constraints to which it is subject, in addition to the theoretical ones from perturbativity, unitarity, and the stability of the electroweak vacuum. To this end, we have discussed the impact of the high-precision measurements of the electroweak observables performed mostly at the LEP and Tevatron colliders, the properties of the already observed SM-like Higgs boson at the LHC, in particular, its couplings to fermions and gauge bosons and its invisible decays, and in the flavor sector, with a focus on B-meson physics and the muon $g - 2$. We have also studied the bounds that one can set on the parameter space of the model from the intensive campaign of searches of the heavy Higgs bosons of the 2HDM and the lighter singlet pseudoscalar a boson that has been performed at the 13 TeV LHC with the full dataset, in particular, when they are produced as single resonances in gluon (and eventually bottom-quark) fusion and decay into lepton pairs, $\tau^+\tau^-$ or $\mu^+\mu^-$. We have also studied the impact of the high sensitivity of direct DM detection experiments such as XENON, and very recently LZ, on the mass and couplings of the a boson.

The combined effect of these constraints on the model turns out to be quite severe. While, indeed, one can explain recent anomalies, such as the ones affecting the mass M_W and the muon $(g - 2)_\mu$ and simultaneously satisfying the DM requirements, with a judicious choice of some key parameters or features (such as the mass splitting between the heavy Higgs bosons in the first case and the mass of the a boson and the value of $\tan\beta$ in the second one), these explanations are made rather difficult in some configurations of the model when other constraints, such as those from

Higgs searches at the LHC, are also included. The result strongly depends on the type of configuration which has been chosen for the 2HDM Higgs couplings to fermions in order to avoid flavor-changing neutral couplings at tree level.

The most studied case, the so-called type II configuration which also occurs in supersymmetric theories and in which both the b-quark and charged-lepton Yukawa couplings are enhanced at high $\tan\beta$ values, is the most constrained one, in particular, from searches for single Higgs resonances at the LHC. These searches exclude much of the parameter space that allow for an explanation of the measured value of the $(g-2)_\mu$. The type X configuration, in which only the charged-lepton couplings are proportional to $\tan\beta$, is less constrained by these experiments, but one needs extremely large values of the latter parameter to comply with the $(g-2)_\mu$ deviation. The other scenarios, namely, type I and Y, have suppressed couplings to leptons and are, thus, less severely constrained. All configurations, in turn, allow for an explanation of the recent measurement of M_W performed by the CDF experiment, as one simply needs to allow for a sufficient splitting between the masses of the heavy 2HDM states. Constraints from the signal strengths of the observed light h particle can be easily evaded by enforcing the alignment limit in which the state has SM-like couplings to fermions and gauge bosons, while flavor constraints can be coped with by having a sufficiently heavy charged Higgs and pseudoscalar a bosons. All these constraints still allow for the additional stable fermionic state to be a good DM candidate, namely, to have the correct relic density and to evade the strong bounds from direct detection experiments like XENON and LZ in some areas of the space of the DM and a boson parameters.

In the last part of this work, we have performed a detailed study of the cosmic phase transitions in the 2HD + a model and the corresponding gravitational wave spectrum which is generated. We have calculated the GW signals for phase transitions in the plane of two fields h^0 and H^0 and have shown that they could be observable by near-future experiments such as LISA, BBO, and DECIGO. We have also discussed the differences between the 2HDM and the 2HD + a, which arises from a modified parametrization of quartic couplings and corrections to thermal masses due to couplings with the additional singlet pseudoscalar a^0.

The GW signal frequency and amplitude range in the 2HDM and 2HD + a cases are relatively similar, but there is a larger variation in the signal of the latter model. In some cases, it could potentially help distinguish between the two models.

Our calculation accounts for all four 2HDM configurations for the Higgs couplings to fermions. Because the top and bottom Yukawa couplings dominate over others, we do not have to consider types X and Y separately, since they differ from types I and II, respectively, only in the lepton Yukawa sector. Moreover, also types I and II yield a practically identical parameter space of phase transition patterns and GW signals due to the overall small effect of the fermion contribution in the thermal evolution of the effective potential.

In view of its rather rich phenomenology and the fact that it addresses various important issues and anomalies in high-energy physics and in cosmology, the 2HD + a model is an interesting candidate for physics beyond the SM and can serve as a benchmark in the various searches for it at present-day and future collider and astroparticle physics experiments. It can be further tested at the present and high-luminosity runs of the LHC [139], the DM direct detection experiments like XENONnT [140], and the new and ultimate one DARWIN [141], as well as in future high-precision measurements such as the W mass and muon $(g-2)$. In addition, it is capable of generating gravitational wave signals which can be tested in planned experiments such as LISA [31], BBO [32], and DECIGO [35].

In view of all these features, the 2HD + a model deserves further attention and studies.

ACKNOWLEDGMENTS

[1] Georges Aad *et al.*, Observation of a new particle in the search for the standard model Higgs boson with the ATLAS detector at the LHC, Phys. Lett. B **716,** 1 (2012).

[2] Serguei Chatrchyan *et al.*, Observation of a new boson at a mass of 125 GeV with the CMS experiment at the LHC, Phys. Lett. B **716,** 30 (2012).

[3] Georges Aad *et al.*, Measurements of the Higgs boson production and decay rates and constraints on its couplings from a combined ATLAS and CMS analysis of the LHC pp collision data at $\sqrt{s} = 7$ and 8 TeV, J. High Energy Phys. 08 (2016) 045.

[4] Abdelhak Djouadi, The anatomy of electro-weak symmetry breaking. I: The Higgs boson in the standard model, Phys. Rep. **457,** 1 (2008).

[5] M. Drees, R. Godbole, and P. Roy, *Theory and Phenomenology of Sparticles* (World Scientific, Singapore, 2004), https://doi.org/10.1142/4001.

[6] John F. Gunion, Howard E. Haber, Gordon L. Kane, and Sally Dawson, *The Higgs Hunter's Guide* (Perseus Books, Cambridge, MA, 2000), Vol. 80.

[7] Abdelhak Djouadi, The anatomy of electro-weak symmetry breaking. II. The Higgs bosons in the minimal supersymmetric model, Phys. Rep. **459,** 1 (2008).

[8] G. Branco, P. Ferreira, L. Lavoura, M. Rebelo, Marc Sher, and Joao Silva, Theory and phenomenology of two-Higgs-doublet models, Phys. Rep. **516,** 1 (2012).

[9] Gianfranco Bertone, Dan Hooper, and Joseph Silk, Particle dark matter: Evidence, candidates and constraints, Phys. Rep. **405,** 279 (2005).

[10] Giorgio Arcadi, Maíra Dutra, Pradipta Ghosh, Manfred Lindner, Yann Mambrini, Mathias Pierre, Stefano Profumo, and Farinaldo S. Queiroz, The waning of the WIMP? A review of models, searches, and constraints, Eur. Phys. J. C **78,** 203 (2018).

[11] Giorgio Arcadi, Abdelhak Djouadi, and Martti Raidal, Dark matter through the Higgs portal, Phys. Rep. **842,** 1 (2020).

[12] N. Aghanim *et al.*, Planck 2018 results. VI. Cosmological parameters, Astron. Astrophys. **641,** A6 (2020); **652,** C4 (E) (2021).

[13] S. Ipek, D. McKeen, and A. E. Nelson, A renormalizable model for the Galactic center gamma ray excess from dark matter annihilation, Phys. Rev. D **90,** 055021 (2014).

[14] Dorival Goncalves, Pedro A. N. Machado, and Jose Miguel No, Simplified models for dark matter face their consistent completions, Phys. Rev. D **95,** 055027 (2017).

[15] Martin Bauer, Ulrich Haisch, and Felix Kahlhoefer, Simplified dark matter models with two Higgs doublets: I. Pseudoscalar mediators, J. High Energy Phys. 05 (2017) 138.

[16] Patrick Tunney, Jose Miguel No, and Malcolm Fairbairn, Probing the pseudoscalar portal to dark matter via $\bar{b}bZ(\to \ell\ell) + \not{E}_T$: From the LHC to the Galactic Center excess, Phys. Rev. D **96,** 095020 (2017).

[17] Tomohiro Abe *et al.*, LHC Dark Matter Working Group: Next-generation spin-0 dark matter models, Phys. Dark Universe **27,** 100351 (2020).

[18] Tania Robens, The THDMa revisited, Symmetry **13,** 2341 (2021).

[19] Ulrich Haisch, Jernej F. Kamenik, Augustinas Malinauskas, and Michael Spira, Collider constraints on light pseudo-scalars, J. High Energy Phys. 03 (2018) 178.

[20] Spyros Argyropoulos and Ulrich Haisch, Benchmarking LHC searches for light 2HDM + a pseudoscalars, SciPost Phys. **13,** 007 (2022).

[21] B. Abi *et al.*, Measurement of the Positive Muon Anomalous Magnetic Moment to 0.46 ppm, Phys. Rev. Lett. **126,** 141801 (2021).

[22] Giorgio Arcadi, Abdelhak Djouadi, and Farinaldo da Silva Queiroz, Models with two Higgs doublets and a light pseudoscalar: A portal to dark matter and the possible $(g-2)_\mu$ excess, Phys. Lett. B **834,** 137436 (2022).

[23] G. Arcadi and A. Djouadi, The 2HD plus light pseudo-scalar model for a combined explanation of the possible excesses in the CDF M_W measurement and $(g-2)_\mu$ with dark matter, Phys. Rev. D **106,** 095008 (2022).

[24] T. Aaltonen *et al.*, High-precision measurement of the W boson mass with the CDF II detector, Science **376,** 170 (2022).

[25] ATLAS Collaboration, A detailed map of Higgs boson interactions by the ATLAS experiment ten years after the discovery, Nature (London) **607,** 52 (2022); **612,** E24 (2022).

[26] CMS Collaboration, A portrait of the Higgs boson by the CMS experiment ten years after the discovery, Nature (London) **607,** 60 (2022).

[27] J. Aalbers *et al.*, First Dark Matter Search Results from the LUX-ZEPLIN (LZ) Experiment, Phys. Rev. Lett. **131,** 041002 (2023).

[28] B. P. Abbott *et al.*, Observation of Gravitational Waves from a Binary Black Hole Merger, Phys. Rev. Lett. **116,** 061102 (2016).

[29] K. Kajantie, M. Laine, K. Rummukainen, and Mikhail E. Shaposhnikov, Is There a Hot Electroweak Phase Transition at $m_H \gtrsim m_W$?, Phys. Rev. Lett. **77,** 2887 (1996).

[30] Thomas Biekötter, Sven Heinemeyer, José Miguel No, María Olalla Olea-Romacho, and Georg Weiglein, The trap in the early Universe: Impact on the interplay between gravitational waves and LHC physics in the 2HDM, J. Cosmol. Astropart. Phys. 03 (2023) 031.

[31] Chiara Caprini *et al.*, Science with the space-based interferometer eLISA. II: Gravitational waves from cosmological phase transitions, J. Cosmol. Astropart. Phys. 04 (2016) 001.

[32] Vincent Corbin and Neil J. Cornish, Detecting the cosmic gravitational wave background with the big bang observer, Classical Quantum Gravity **23,** 2435 (2006).

[33] Wen-Hong Ruan, Zong-Kuan Guo, Rong-Gen Cai, and Yuan-Zhong Zhang, Taiji program: Gravitational-wave sources, Int. J. Mod. Phys. A **35,** 2050075 (2020).

[34] Jun Luo *et al.*, TianQin: A space-borne gravitational wave detector, Classical Quantum Gravity **33**, 035010 (2016).

[35] Seiji Kawamura *et al.*, Current status of space gravitational wave antenna DECIGO and B-DECIGO, Prog. Theor. Exp. Phys. **2021**, 05A105 (2021).

[36] S. Davidson and H. Haber, Basis-independent methods for the two-Higgs-doublet model, Phys. Rev. D **72**, 035004 (2005); **72**, 099902(E) (2005).

[37] Lars Fromme, Stephan J. Huber, and Michael Seniuch, Baryogenesis in the two-Higgs doublet model, J. High Energy Phys. 11 (2006) 038.

[38] T. Biekötter, M. Chakraborti, and S. Heinemeyer, A 96 GeV Higgs boson in the N2HDM, Eur. Phys. J. C **80**, 2 (2020).

[39] S. Heinemeyer, C. Li, F. Lika, G. Moortgat-Pick, and S. Paasch, Phenomenology of a 96 GeV Higgs boson in the 2HDM with an additional singlet, Phys. Rev. D **106**, 075003 (2022).

[40] Sheldon L. Glashow and Steven Weinberg, Natural conservation laws for neutral currents, Phys. Rev. D **15**, 1958 (1977).

[41] Shinya Kanemura, Yasuhiro Okada, Eibun Senaha, and C. P. Yuan, Higgs coupling constants as a probe of new physics, Phys. Rev. D **70**, 115002 (2004).

[42] D. Bečirević, E. Bertuzzo, O. Sumensari, and R. Zukanovich Funchal, Can the new resonance at LHC be a *CP*-Odd Higgs boson?, Phys. Lett. B **757**, 261 (2016).

[43] A. Barroso, P. M. Ferreira, I. P. Ivanov, and Rui Santos, Metastability bounds on the two Higgs doublet model, J. High Energy Phys. 06 (2013) 045.

[44] Kristjan Kannike, Vacuum stability conditions from copositivity criteria, Eur. Phys. J. C **72**, 2093 (2012).

[45] D. de Florian *et al.*, Handbook of LHC Higgs cross sections: 4. Deciphering the nature of the Higgs sector, CERN Report No. CERN-2017-002-M, CERN-2017-002, 2017, https://doi.org/10.23731/CYRM-2017-002.

[46] The ATLAS collaboration, Combined measurements of Higgs boson production and decay using up to 139 fb^{-1} of proton-proton data at $\sqrt{s} = 13$ TeV collected with the ATLAS experiment, Report No. ATLAS-CONF-2021-053, Conseil européen pour la recherche nucléaire (CERN), 2021, http://cds.cern.ch/record/2789544.

[47] P. Ferreira, J. Gunion, H. Haber, and R. Santos, Probing wrong-sign Yukawa couplings at the LHC and a future linear collider, Phys. Rev. D **89**, 115003 (2014).

[48] Antonio Pich and Paula Tuzon, Yukawa alignment in the two-Higgs-doublet model, Phys. Rev. D **80**, 091702 (2009).

[49] Nathaniel Craig, Jamison Galloway, and Scott Thomas, Searching for signs of the second Higgs doublet, Report No. RU-NHETC-2013-07, Rutgers University, 2013.

[50] Marcela Carena, Ian Low, Nausheen R. Shah, and Carlos E. M. Wagner, Impersonating the standard model Higgs boson: Alignment without decoupling, J. High Energy Phys. 04 (2014) 015.

[51] Jeremy Bernon, John F. Gunion, Yun Jiang, and Sabine Kraml, Light Higgs bosons in two-Higgs-doublet models, Phys. Rev. D **91**, 075019 (2015).

[52] Pere Arnan, Damir Bečirević, Federico Mescia, and Olcyr Sumensari, Two Higgs doublet models and $b \to s$ exclusive decays, Eur. Phys. J. C **77**, 796 (2017).

[53] A. Abdesselam *et al.*, Measurement of the inclusive $B \to X_{s+d}\gamma$ branching fraction, photon energy spectrum and HQE parameters, in *Proceedings of the 38th International Conference on High Energy Physics* (Sissa Medialab, Trieste, 2016).

[54] Y. Amhis *et al.*, Averages of *b*-hadron, *c*-hadron, and τ-lepton properties as of summer 2016, Eur. Phys. J. C **77**, 895 (2017).

[55] Mikolaj Misiak and Matthias Steinhauser, Weak radiative decays of the B meson and bounds on $M_{H^{\pm}}$ in the two-Higgs-doublet model, Eur. Phys. J. C **77**, 201 (2017).

[56] M. Misiak, Abdur Rehman, and Matthias Steinhauser, Towards $\bar{B} \to X_s\gamma$ at the NNLO in QCD without interpolation in m$_c$, J. High Energy Phys. 06 (2020) 175.

[57] Matthew J. Dolan, Felix Kahlhoefer, Christopher McCabe, and Kai Schmidt-Hoberg, A taste of dark matter: Flavour constraints on pseudoscalar mediators, J. High Energy Phys. 03 (2015) 171; 07 (2015) 103(E).

[58] J. P. Lees *et al.*, Search for a Dark Leptophilic Scalar in e^+e^- Collisions, Phys. Rev. Lett. **125**, 181801 (2020).

[59] Giorgio Arcadi, Manfred Lindner, Farinaldo Queiroz, Werner Rodejohann, and Stefan Vogl, Pseudoscalar mediators: A WIMP model at neutrino floor, J. Cosmol. Astropart. Phys. 03 (2018) 042.

[60] P. A. Zyla *et al.*, Review of particle physics, Prog. Theor. Exp. Phys. **2020**, 083C01 (2020).

[61] M. J. G. Veltman, Second threshold in weak interactions, Acta Phys. Pol. B **8**, 475 (1977), https://cds.cern.ch/record/2792151.

[62] M. Baak, M. Goebel, J. Haller, A. Hoecker, D. Kennedy, K. Moenig, M. Schott, and J. Stelzer, Updated status of the global electroweak fit and constraints on new physics, Eur. Phys. J. C **72**, 2003 (2012).

[63] M. Baak, J. Cúth, J. Haller, A. Hoecker, R. Kogler, K. Mönig, M. Schott, and J. Stelzer, The global electroweak fit at NNLO and prospects for the LHC and ILC, Eur. Phys. J. C **74**, 3046 (2014).

[64] Michael E. Peskin and Tatsu Takeuchi, Estimation of oblique electroweak corrections, Phys. Rev. D **46**, 381 (1992).

[65] Pouya Asadi, Cari Cesarotti, Katherine Fraser, Samuel Homiller, and Aditya Parikh, Oblique Lessons from the *W* mass measurement at CDF II, Report No. MIT-CTP/5420, Massachusetts Institute of Technology (MIT), 2022.

[66] G. W. Bennett *et al.*, Final report of the muon E821 anomalous magnetic moment measurement at BNL, Phys. Rev. D **73**, 072003 (2006).

[67] T. Aoyama *et al.*, The anomalous magnetic moment of the muon in the standard model, Phys. Rep. **887**, 1 (2020).

[68] Sz. Borsanyi *et al.*, Leading hadronic contribution to the muon magnetic moment from lattice QCD, Nature (London) **593**, 51 (2021).

[69] Athanasios Dedes and Howard E. Haber, Can the Higgs sector contribute significantly to the muon anoma-

lous magnetic moment?, J. High Energy Phys. 05 (2001) 006.

[70] A. Djouadi, T. Kohler, M. Spira, and J. Tutas, (e b), (e t) type leptoquarks at e p colliders, Z. Phys. C **46**, 679 (1990).

[71] Stephen M. Barr and A. Zee, Electric Dipole Moment of the Electron and of the Neutron, Phys. Rev. Lett. **65**, 21 (1990); **65**, 2920(E) (1990).

[72] D. Chang, W.-F. Chang, C.-H. Chou, and W.-Y. Keung, Large two loop contributions to g-2 from a generic pseudoscalar boson, Phys. Rev. D **63**, 091301 (2001).

[73] F. Larios, G. Tavares-Velasco, and C. P. Yuan, A very light CP odd scalar in the two Higgs doublet model, Phys. Rev. D **64**, 055004 (2001).

[74] Victor Ilisie, New Barr-Zee contributions to $(g-2)_\mu$ in two-Higgs-doublet models, J. High Energy Phys. 04 (2015) 077.

[75] A. Djouadi, P. M. Zerwas, and J. Zunft, Search for light pseudoscalar Higgs bosons in Z decays, Phys. Lett. B **259**, 175 (1991).

[76] R. Barate et al., Search for the standard model Higgs boson at LEP, Phys. Lett. B **565**, 61 (2003).

[77] G. Aad et al., Search for Heavy Higgs Bosons Decaying into Tau Leptons with the ATLAS Detector Using pp Collisions at $\sqrt{s} = 13$ TeV, Phys. Rev. Lett. **125**, 051801 (2020).

[78] A. Tumasyan et al. (The CMS Collaboration), Searches for additional Higgs bosons and vector leptoquarks in $\tau\tau$ final states in proton-proton collisions at $\sqrt{s} = 13$ TeV, J. High Energy Phys. 07 (2023) 073.

[79] Morad Aaboud et al., Search for heavy particles decaying into top-quark pairs using lepton-plus-jets events in proton–proton collisions at $\sqrt{s} = 13$ TeV with the ATLAS detector, Eur. Phys. J. C **78**, 565 (2018).

[80] Albert M. Sirunyan et al., Search for heavy Higgs bosons decaying to a top quark pair in proton-proton collisions at $\sqrt{s} = 13$ TeV, J. High Energy Phys. 04 (2020) 171; 03 (2022) 187(E).

[81] Morad Aaboud et al., Search for charged Higgs bosons decaying via $H^\pm \to \tau^\pm \nu_\tau$ in the τ + jets and τ + lepton final states with 36 fb^{-1} of pp collision data recorded at $\sqrt{s} = 13$ TeV with the ATLAS experiment, J. High Energy Phys. 09 (2018) 139.

[82] Albert M. Sirunyan et al., Search for charged Higgs bosons in the $H^\pm \to \tau^\pm \nu_\tau$ decay channel in proton-proton collisions at $\sqrt{s} = 13$ TeV, J. High Energy Phys. 07 (2019) 142.

[83] Georges Aad et al., Search for charged Higgs bosons decaying into a top quark and a bottom quark at $\sqrt{s} = 13$ TeV with the ATLAS detector, J. High Energy Phys. 06 (2021) 145.

[84] A. M. Sirunyan et al., Search for charged Higgs bosons decaying into a top and a bottom quark in the all-jet final state of pp collisions at $\sqrt{s} = 13$ TeV, J. High Energy Phys. 07 (2020) 126.

[85] A. Djouadi, L. Maiani, G. Moreau, A. Polosa, J. Quevillon, and V. Riquer, The post-Higgs MSSM scenario: Habemus MSSM?, Eur. Phys. J. C **73**, 2650 (2013).

[86] A. Djouadi, L. Maiani, A. Polosa, J. Quevillon, and V. Riquer, Fully covering the MSSM Higgs sector at the LHC, J. High Energy Phys. 06 (2015) 168.

[87] M. Carena, S. Heinemeyer, O. Stål, C. E. M. Wagner, and G. Weiglein, MSSM Higgs boson searches at the LHC: Benchmark scenarios after the discovery of a Higgs-like particle, Eur. Phys. J. C **73**, 2552 (2013).

[88] Abdelhak Djouadi, John Ellis, Andrey Popov, and Jérémie Quevillon, Interference effects in $t\bar{t}$ production at the LHC as a window on new physics, J. High Energy Phys. 03 (2019) 119.

[89] Morad Aaboud et al., Search for charged Higgs bosons decaying into top and bottom quarks at $\sqrt{s} = 13$ TeV with the ATLAS detector, J. High Energy Phys. 11 (2018) 085.

[90] Giorgio Arcadi, Abdelhak Djouadi, Hong-Jian He, Jean-Loic Kneur, and Rui-Qing Xiao, The hMSSM with a light gaugino/higgsino sector: Implications for collider and astroparticle physics, J. High Energy Phys. 05 (2023) 095..

[91] Francesca Borzumati and A. Djouadi, Lower bounds on charged Higgs bosons from LEP and Tevatron, Phys. Lett. B **549**, 170 (2002).

[92] Robert V. Harlander, Stefan Liebler, and Hendrik Mantler, SusHi: A program for the calculation of Higgs production in gluon fusion and bottom-quark annihilation in the standard model and the MSSM, Comput. Phys. Commun. **184**, 1605 (2013).

[93] Robert V. Harlander, Stefan Liebler, and Hendrik Mantler, SusHi Bento: Beyond NNLO and the heavy-top limit, Comput. Phys. Commun. **212**, 239 (2017).

[94] G. Aad et al. (The ATLAS Collaboration), Search for heavy resonances decaying into a Z or W boson and a Higgs boson in final states with leptons and b-jets in 139 fb^{-1} of pp collisions at $\sqrt{s} = 13$ TeV with the ATLAS detector, J. High Energy Phys. 06 (2023) 016..

[95] Georges Aad et al., Search for heavy resonances decaying into a pair of Z bosons in the $\ell^+\ell^-\ell'^+\ell'^-$ and $\ell^+\ell^-\nu\bar{\nu}$ final states using 139 fb^{-1} of proton–proton collisions at $\sqrt{s} = 13$ TeV with the ATLAS detector, Eur. Phys. J. C **81**, 332 (2021).

[96] Georges Aad et al., Search for a heavy Higgs boson decaying into a Z boson and another heavy Higgs boson in the $\ell\ell bb$ and $\ell\ell WW$ final states in pp collisions at $\sqrt{s} = 13$ TeV with the ATLAS detector, Eur. Phys. J. C **81**, 396 (2021).

[97] Albert M. Sirunyan et al., Search for new neutral Higgs bosons through the $H \to ZA \to \ell^+\ell^- b\bar{b}$ process in pp collisions at $\sqrt{s} = 13$ TeV, J. High Energy Phys. 03 (2020) 055.

[98] Albert M. Sirunyan et al., Search for dark matter produced in association with a leptonically decaying Z boson in proton-proton collisions at $\sqrt{s} = 13$ TeV, Eur. Phys. J. C **81**, 13 (2021); **81**, 333(E) (2021).

[99] Georges Aad *et al.*, Search for dark matter produced in association with a standard model Higgs boson decaying into b-quarks using the full Run 2 dataset from the ATLAS detector, J. High Energy Phys. 11 (2021) 209.

[100] M. Aaboud *et al.* (ATLAS Collaboration), Combination of Searches for Invisible Higgs Boson Decays with the ATLAS Experiment, Phys. Rev. Lett. **122,** 231801 (2019).

[101] Giorgio Arcadi, Giorgio Busoni, Thomas Hugle, and Valentin Tenorth, Comparing 2HDM + scalar and pseudoscalar simplified models at LHC, J. High Energy Phys. 06 (2020) 098.

[102] Albert M. Sirunyan *et al.*, Search for a Narrow Resonance Lighter than 200 GeV Decaying to a Pair of Muons in Proton-Proton Collisions at $\sqrt{s}$ = TeV, Phys. Rev. Lett. **124,** 131802 (2020).

[103] Roel Aaij *et al.*, Searches for low-mass dimuon resonances, J. High Energy Phys. 10 (2020) 156.

[104] Michael Spira, HIGLU: A program for the calculation of the total Higgs production cross-section at hadron colliders via gluon fusion including QCD corrections, Report No. DESY-T-95-05, 1995, http://www-library.desy.de/cgi-bin/showprep.pl?DESY-T-95-05.

[105] A. Djouadi, J. Kalinowski, and M. Spira, HDECAY: A program for Higgs boson decays in the standard model and its supersymmetric extension, Comput. Phys. Commun. **108,** 56 (1998).

[106] Abdelhak Djouadi, Jan Kalinowski, Margarete Muehlleitner, and Michael Spira, HDECAY: Twenty$_{++}$ years after, Comput. Phys. Commun. **238,** 214 (2019).

[107] G. Belanger, F. Boudjema, A. Pukhov, and A. Semenov, MicrOMEGAs: A program for calculating the relic density in the MSSM, Comput. Phys. Commun. **149,** 103 (2002).

[108] G. Belanger, F. Boudjema, A. Pukhov, and A. Semenov, micrOMEGAs2.0.7: A program to calculate the relic density of dark matter in a generic model, Comput. Phys. Commun. **177,** 894 (2007).

[109] G. Belanger, F. Boudjema, A. Pukhov, and A. Semenov, Dark matter direct detection rate in a generic model with micrOMEGAs2.2, Comput. Phys. Commun. **180,** 747 (2009).

[110] Tomohiro Abe, Motoko Fujiwara, and Junji Hisano, Loop corrections to dark matter direct detection in a pseudo-scalar mediator dark matter model, J. High Energy Phys. 02 (2019) 028.

[111] Tomohiro Abe, Motoko Fujiwara, Junji Hisano, and Yutaro Shoji, Maximum value of the spin-independent cross section in the 2HDM + a, J. High Energy Phys. 01 (2020) 114.

[112] Nicole F. Bell, Giorgio Busoni, and Isaac W. Sanderson, Loop effects in direct detection, J. Cosmol. Astropart. Phys. 08 (2018) 017; 01 (2019) E01.

[113] Fatih Ertas and Felix Kahlhoefer, Loop-induced direct detection signatures from *CP*-violating scalar mediators, J. High Energy Phys. 06 (2019) 052.

[114] E. Aprile *et al.*, Dark Matter Search Results from a One Ton-Year Exposure of XENON1T, Phys. Rev. Lett. **121,** 111302 (2018).

[115] Zhou Huang *et al.*, Constraints on the axial-vector and pseudo-scalar mediated WIMP-nucleus interactions from PandaX-4T experiment, Phys. Lett. B **834,** 137487 (2022).

[116] M. Ackermann *et al.*, Searching for Dark Matter Annihilation from Milky Way Dwarf Spheroidal Galaxies with Six Years of Fermi Large Area Telescope Data, Phys. Rev. Lett. **115,** 231301 (2015).

[117] M. Ackermann *et al.*, Updated search for spectral lines from galactic dark matter interactions with pass 8 data from the Fermi LAT, Phys. Rev. D **91,** 122002 (2015).

[118] Kim Griest and David Seckel, Three exceptions in the calculation of relic abundances, Phys. Rev. D **43,** 3191 (1991).

[119] Paolo Gondolo and Graciela Gelmini, Cosmic abundances of stable particles: Improved analysis, Nucl. Phys. **B360,** 145 (1991).

[120] Sidney R. Coleman and Erick J. Weinberg, Radiative corrections as the origin of spontaneous symmetry breaking, Phys. Rev. D **7,** 1888 (1973).

[121] James M. Cline, Kimmo Kainulainen, and Michael Trott, Electroweak baryogenesis in two Higgs doublet models and B meson anomalies, J. High Energy Phys. 11 (2011) 089.

[122] L. Dolan and R. Jackiw, Symmetry behavior at finite temperature, Phys. Rev. D **9,** 3320 (1974).

[123] Djuna Croon, Oliver Gould, Philipp Schicho, Tuomas V. I. Tenkanen, and Graham White, Theoretical uncertainties for cosmological first-order phase transitions, J. High Energy Phys. 04 (2021) 055.

[124] Peter Athron, Csaba Balazs, Andrew Fowlie, Lachlan Morris, Graham White, and Yang Zhang, How arbitrary are perturbative calculations of the electroweak phase transition?, J. High Energy Phys. 01 (2023) 050.

[125] Andrei D. Linde, Decay of the false vacuum at finite temperature, Nucl. Phys. **B216,** 421 (1983); **B223,** 544(E) (1983).

[126] Jose R. Espinosa, Thomas Konstandin, Jose M. No, and Geraldine Servant, Energy budget of cosmological first-order phase transitions, J. Cosmol. Astropart. Phys. 06 (2010) 028.

[127] Christophe Grojean and Geraldine Servant, Gravitational waves from phase transitions at the electroweak scale and beyond, Phys. Rev. D **75,** 043507 (2007).

[128] Ryusuke Jinno, Bibhushan Shakya, and Jorinde van de Vis, Gravitational Waves from feebly interacting particles in a first order phase transition, Report No. DESY-22-172, IFT-UAM/CSIC-22-140, IFT-UAM/CSIC-22-140, MITP-22-095, RESCEU-22/22, Deutsches Elektronen-Synchrotron (DESY), Instituto de Fisica Teorica (IFT), Madrid and Research Center for the Early Universe (RESCEU), Tokyo, 2022.

[129] Stephan J. Huber and Thomas Konstandin, Gravitational wave production by collisions: More bubbles, J. Cosmol. Astropart. Phys. 09 (2008) 022.

[130] Mark Hindmarsh, Stephan J. Huber, Kari Rummukainen, and David J. Weir, Shape of the acoustic gravitational wave

power spectrum from a first order phase transition, Phys. Rev. D **96,** 103520 (2017); **101,** 089902(E) (2020).

[131] Chiara Caprini *et al.*, Detecting gravitational waves from cosmological phase transitions with LISA: An update, J. Cosmol. Astropart. Phys. 03 (2020) 024.

[132] Kai Schmitz, LISA sensitivity to gravitational waves from sound waves, Symmetry **12,** 1477 (2020).

[133] Huai-Ke Guo, Kuver Sinha, Daniel Vagie, and Graham White, Phase transitions in an expanding universe: Stochastic gravitational waves in standard and non-standard histories, J. Cosmol. Astropart. Phys. 01 (2021) 001.

[134] John Ellis, Marek Lewicki, José Miguel No, and Ville Vaskonen, Gravitational wave energy budget in strongly supercooled phase transitions, J. Cosmol. Astropart. Phys. 06 (2019) 024.

[135] Kai Schmitz, New sensitivity curves for gravitational-wave signals from cosmological phase transitions, J. High Energy Phys. 01 (2021) 097.

[136] Carroll L. Wainwright, COSMOTRANSITIONS: Computing cosmological phase transition temperatures and bubble profiles with multiple fields, Comput. Phys. Commun. **183,** 2006 (2012).

[137] Marieke Postma and Graham White, Cosmological phase transitions: Is effective field theory just a toy?, J. High Energy Phys. 03 (2021) 280.

[138] Aleksandr Azatov, Daniele Barducci, and Francesco Sgarlata, Gravitational traces of broken gauge symmetries, J. Cosmol. Astropart. Phys. 07 (2020) 027.

[139] M. Cepeda *et al.*, Higgs physics at the HL-LHC and HE-LHC (2019), https://doi.org/10.23731/CYRM-2019-007 .221.

[140] E. Aprile *et al.*, Projected WIMP sensitivity of the XENONnT dark matter experiment, J. Cosmol. Astropart. Phys. 11 (2020) 031.

[141] J. Aalbers *et al.*, DARWIN: Towards the ultimate dark matter detector, J. Cosmol. Astropart. Phys. 11 (2016) 017.